# Gas Tungsten Arc Welding of Dissimilar Material AISI 304, AISI 316 with AISI 4340 – Experimental Investigation for Mechanical Strength and Metallurgical Study

*A Dissertation Submitted*

In Partial Fulfillment of the Requirements

for the Degree of

**Master of Engineering**

in

**Production Engineering**

By

**SANCHIT SINGLA**

**(Registration No. 801282019)**

THAPAR UNIVERSITY

*to the*

**MECHANICAL ENGINEERING DEPARTMENT**

**THAPAR UNIVERSITY, PATIALA**

JULY, 2014.

# CERTIFICATE

I hereby declare that the thesis entitled **"Gas Tungsten Arc Welding of Dissimilar Material SS304, SS316 with AISI4340 – Experimental Investigation for Mechanical Strength and Metallurgical Study"** is an authentic record of my study carried out as requirements for the award of the degree of **Master of Engineering** in **Production Engineering** at **Thapar University, Patiala** under the supervision of **Anirban Bhattacharya Assistant Professor**, Department of Mechanical Engineering, Thapar University during July 2013 to July 2014. The matter embodied in this report has not been submitted in partial or full to any other university or institute for the award of any degree.

Date: 18/07/2014

**SANCHIT SINGLA**

This is to certify that above declaration made by the student concerned is correct to the best of my knowledge & belief.

**ANIRBAN BHATTACHARYA**
Assistant Professor
Mechanical Engineering Department
Thapar University, Patiala-147004

Countersigned by

**DR. AJAY BATISH**
Professor and Head
Mechanical Engineering Department
Thapar University, Patiala-147004

**DR. S.K. MOHAPATRA**
Dean of Academic Affairs
Thapar University, Patiala-147004

***Dedicated to***

*My Dear Parents*

# ACKNOWLEDGEMENT

With deep sense of gratitude I express my sincere thanks to my guide **Anirban Bhattacharya,** Assistant Professor, Mechanical engineering department, Thapar University, Patiala-147004 for their valuable guidance, proper advice and constant encouragement during period of work which help me in completing my experimental study.

I also feel very much obliged to **Dr. Ajay Batish**, Professor and Head of mechanical Engineering Department.

A very special thanks and reward to non-teaching staff members **Mr. M. Suri, Mr. Surinder, Mr. Rath, Mr. Roshan, Mr. Rajinder, Mr. Narender and other workshop officials** of Central Workshop, Thapar University, Patiala for their help during this period of work.

I am also thankful to my friend **Ramesh Kumar and Kanika Verma** for their help and cooperation.

I am also thankful to **School of Physics** and **Material Science Department** for providing microhardness testing machine for our research work.

I am also wish to record my sincere thanks to the **TEQIP –II** for providing the financial support.

At last but most important I am highly indebted to my dear parents for their love, support and trust.

Sanchit Singla

**SANCHIT SINGLA**

**Registration No. 801282019**

# ABSTRACT

Dissimilar joining of two different metal by welding is the technique to join the two different metals to enhance its mechanical properties as required for some special application. The aim of present study was to investigate the mechanical and metallurgical properties like tensile strength, charpy impact test, microhardness, weld distortion, metallurgical analysis, cracks and dye penetration of dissimilar metal joint stainless steel (AISI 304 & AISI 4340) and (AISI 316 & AISI 4340) during GTAW using the three levels of welding current, shielding gas, gas flow rate, type of filler, pre-heating and post-heating to optimize the process following Taguchi experimental design. Tensile strength of the welded specimens was seen to be dependent on current, filler and post-heating used in various trials in joint of AISI 316 with AISI 4340. Gas type, flow rate and filler are the three influencing parameters which effect the tensile strength of joint AISI 304 and AISI 4340. The maximum tensile strength was seen to be 770 MPa by using current 165 A, gas type Ar + 1.5% He, gas flow rate 12 L/min, filler rod of AISI 304, pre-heating temperature of 175 ºC and post-heating of 650 ºC in joint of AISI 304 with AISI 4340 and 802.40 MPa tensile strength was seen at current 165 A, gas type Ar + 1.5% He, gas flow rate 12 L/min, filler rod of AISI 309, no pre-heating and no post-heating in joint of AISI 316 and AISI 4340. Charpy impact test for toughness results for joint (AISI 304 and AISI 4340) and (AISI 316 and AISI 4340) showed that toughness depends on gas type, filler and post heating. The maximum value of toughness is 147.150 J in case of joint AISI 304 and AISI 4340 and 93.195 J in case of joint AISI 316 and AISI 4340. Dye penetrant test showed that welding was of very good quality and there were negligible amount of defects at corners. Microhardness results for joint AISI 304 and AISI 4340 influenced by current and post-heating having the maximum value of 648.470 and for the joint of AISI 316 and AISI 4340 the maximum value for the micro hardness was found to be 531.00 influenced by gas type, filler rod and post-heating temperature. Weld distortion is found to be minimum of 0.085º in case of joint AISI 304 and AISI 4340 in trial 12 referred from the Table 4.19 and 0.028º in case of joint AISI 316 and AISI 4340 in trial 2 referred from Table 4.22. The surface morphology of the welded plates was characterized by scanning electron microscopy. Microscopy is discussed by considering heat input and flow rate of shielding gas. Dye penetrant test showed that welding was of very good quality. Dye penetration result showed that for both the materials in welded region there is no major flaws and inclusion except a crack observed in a particular sample of dissimilar metal joining of AISI 304 and AISI 316 with AISI 4340.

# Contents

# List of Figures

# List of Tables

# Acronyms

| | |
|---|---|
| GTAW | Gas tungsten arc welding |
| TIG | Tungsten inert gas welding |
| GMAW | Gas metal arc welding |
| SAW | Submerged arc welding |
| ANOVA | Analysis of variance |
| HVN | Vickers hardness number |
| DPT | Dye penetration test |
| AWS | American welding society |
| ISO | International organization for standardization |
| DC | Direct current |
| AC | Alternating current |
| DCEN | Direct current with negatively charged electrode |
| HAZ | Heat affected zone |
| WM | Weld metal |
| BM | Base metal |

# Chapter 1

# Introduction

## 1.1 Introduction

Welding is a fabrication process that joins similar or dissimilar materials of metals. Welding is generally done by fusion of the work pieces by applying heat and putting a filler material to form a pool of molten material (the weld pool) that cools to become a strong joint, with or without pressure, or by themself, to weld. This is entirely different from soldering and brazing, which consider melting between the work pieces to form a bond b/w them, without molten bed the work pieces. Welding also said to be bond which is permanent in between two bodies. Welding prepares its possibility to reconstitute metals between the components to be joined. Components of different material for assembly are easily welded by different welding techniques. The use of different welding techniques for different application of fabrications is extensively in world wide. Welding is used now days in every sector of Engineering. Welding is commonly used in aerospace industries, railways, shipping industries, automobile sector and electronics sector. Actually all welding processes are not applicable at every place so it is the work of an experience welder to decide so many factors like size, shape, material and the most important factor is economical price for fabrication. Welding generally effects the metallurgy of the materials, which could be accomplished by post welding heating treatment to the welded material by seeing the properties of the material used.

## 1.2 Classification of Welding Processes

Generally it is see that welding processes uses heat and pressure for welding joints. By the application and heat sources the process are classified into six different classes. Classification of welding processes is as follows:

## WELDING PROCESSES

### Arc Welding Processes

- Carbon Arc welding
- Shielding Metal Arc welding
- Submerged Arc welding
- Gas Tungsten Arc welding
- Gas Metal Arc welding
- Plasma Arc welding
- Atomic Hydrogen Arc welding
- Electrogas welding
- Electroslag welding
- Stud welding

### Resistance Welding Processes

- Spot welding
- Seam welding
- Projection welding
- Percussion welding
- Resistance butt welding
- Flash butt welding

### Solid State Welding Processes

- Forge welding
- Friction welding
- Explosive welding
- Ultrasonic welding
- Cold pressure welding
- Thermo-compression welding
- Diffusion welding

### Radiant Energy Processes

- Electron Beam Welding
- Laser Beam Welding

**Thermit Welding Processes**

- Thermit Welding
- Pressure Thermit welding

**Oxy-Fuel Gas Welding Processes**

- Gas Welding
- Hot pressure welding

## 1.3 Arc Welding

By the name arc welding it is understood that arc is produced in this process in between the work material and electrode. Through electrode the essential amount of heat is produced to make the two objects to be welded defuse in each other and make a healthy joint. Shielding gas is generally main constituent in these processes which protects the weld pool from the foreign particles in the environment and make a protective layer over the weld pool called slag. Arc welding is mostly done without the applying of pressure. This type of welding can use AC or DC power supply according to the application and availability and also the electrode used may be consumable or non-consumable [Khanna, 2011].

Arc welding is mostly done without the applying of pressure. This type of welding can use AC or DC power supply according to the application and availability and also the electrode used may be consumable or non-consumable. Arc welding can be fully automatic, semi automatic or it can be manually operated. Arc welding is of different types as discussed over a head, from which some of the most important and famous are as follows:

- Shield Metal Arc Welding
- Gas Metal Arc Welding
- Submerged Arc Welding
- Gas Tungsten Arc Welding

### 1.3.1 Shield Metal Arc Welding

Submerged Metal arc welding is an arc welding process within which is produced by heating the work piece with an electric plasma arc set up b/w a flux coated electrode and the work piece. Arc produced by the electrode will melt the electrode end and the workpiece. The drops of material from the electrode are transferred to the workpiece, through arc and transferred material form a joint to be welded. The flux from the electrode will protect molten weld from the atmospheric contamination [Messler, 2004]. The working setup for SMAW is shown in Fig. 1.1.

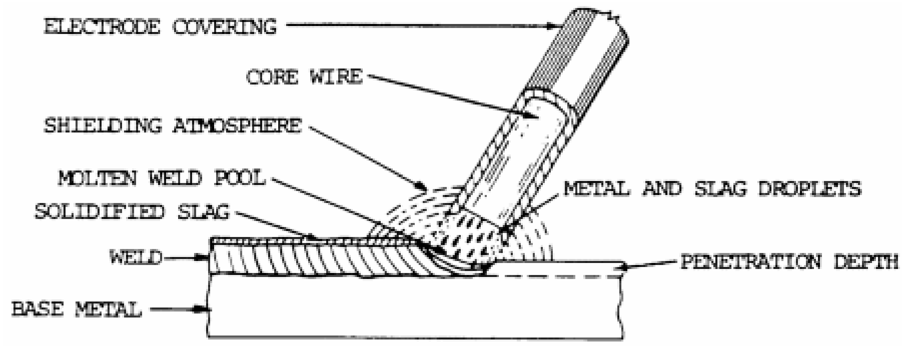


Figure 1.1: Working setup for (SMAW)
[http://www.hotrodders.com]

Generally there are two methods are used to strike the arc one is by touching the tip of electrode to the work piece and momentarily taking it away from the work piece and other is by scratching the electrode on the surface of work piece in the arc of circle. Last method is mostly used by the new operators because this method reduces the sticking of electrode from the work piece.

### 1.3.2 Gas Metal Arc Welding

Gas metal arc welding is an arc welding process. The joint is produced by heating the job with an arc between a continuously supply of spool metal electrode and job. Gas is used as a shield to protect the molten metal by inert gases like argon, helium or mixture of them [Robert, 2004]. The working setup for GMAW is shown in Fig. 1.2.

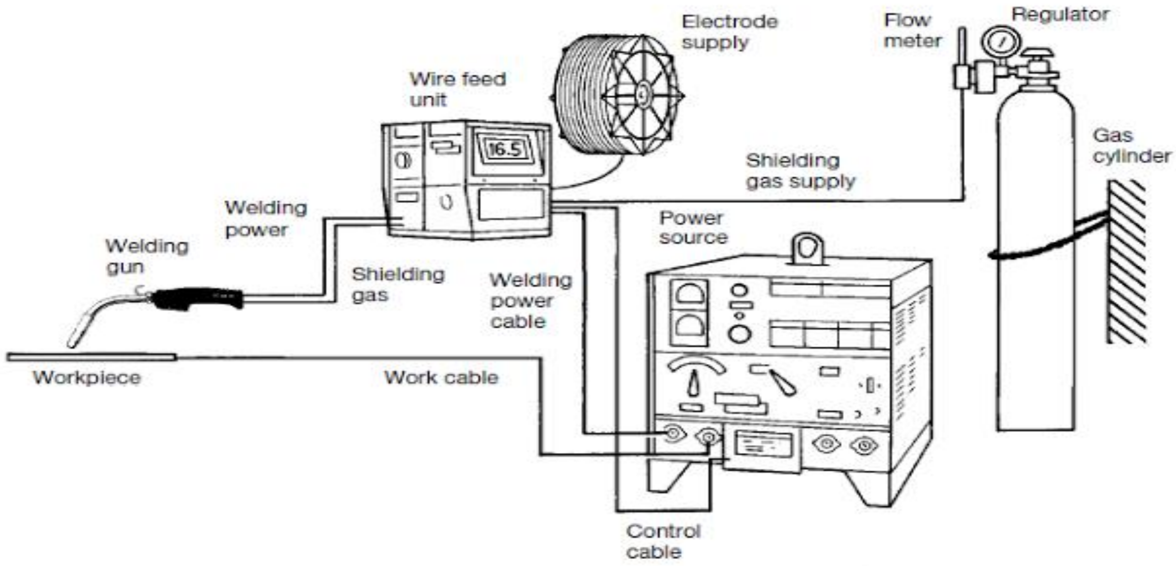


Figure 1.2: Working Setup of (GMAW)
[http://vivesoldando-camilo.blogspot.in]

**Power Source**

GMAW generally uses DC with electrode positive (DCEP) because DCEP leads to a stable arc with smooth metal transfer which gives less spatter and high quality weld.

AC is not recommended for GMAW because arc extinguishes after every half cycle and that can cause partial rectification of welding current and arc gets off completely. DC with electrode negative (DCEN) though gives higher deposition rate is also not recommended as it may cause an unstable arc. However, it vanishes cleaning action on the work piece.

### 1.3.3 Submerged Arc Welding

This arc welding is used for joining thick plates or sheets of metals. The joint is made by heating an arc setup between a bare metal electrode and a work piece. The flux is poured from the hopper on the molten metal just like a blanket on pool by which arc is also hidden within the flux. Flux is generally in the form of granular material. The consumable electrode is continuously fed through a metal spool like in GMAW. Generally these are automatic machines but somewhere semiautomatic machines are used according to the application. The main application is in shipping industries as well as aerospace sectors, pressure vessels, penstocks, boilers, rail road etc where the strength is the main consideration. A laser is also mounted in front of the gun to show the path to the electrode gun. There is separate unit for wire feeding. The weld results by SAW are of very shiny appearance [Robert, 2004]. The general setup for SAW is a shown in Fig. 1.3.

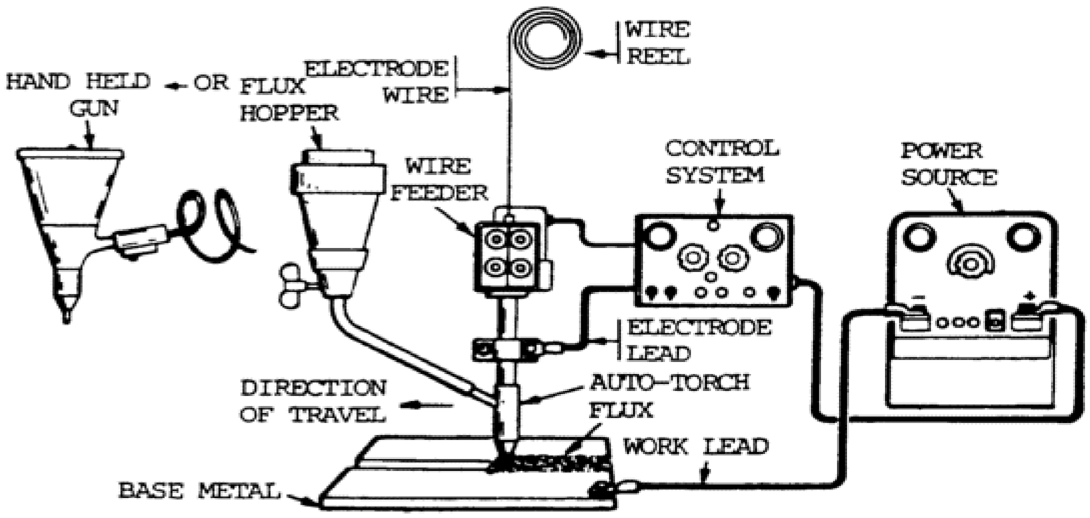


Figure 1.3: General Setup of (SAW)
[http://www.weldguru.com]

### 1.3.4 Gas Tungsten Arc Welding

In the TIG process the arc is produced b/w a pointed tungsten electrode and the WP in an inert atmosphere of Ar or He to protect the weld pool and the electrode from atmospheric contamination. The small arc provided by electrode is of high quality and precision welding. Because the electrode is not consumed during welding, the welder does not have to balance the heat input from the arc as the metal is deposited from the melting electrode. The schematic diagram foe GTAW is as shown in Fig. 1.4.

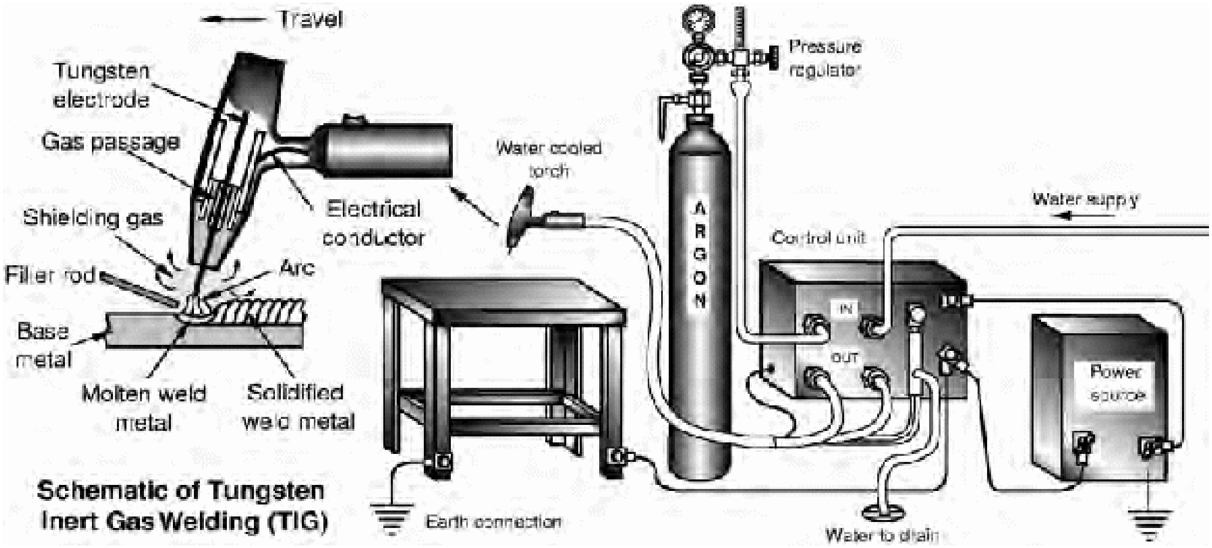


Figure 1.4: The Gas Tungsten Arc welding (GTAW) process [http://www.weldguru.com]

## 1.4 GTAW

### 1.4.1 Overview of GTAW

Gas tungsten arc welding is a fusion welding. The gas tungsten arc welding process also known as tungsten inert gas (TIG) in most of Europe, WIG (wolfram inert gas) in Germany, and still referred to by the original trade names Argonarc or Heliarc welding in some countries. These names are called so because of the use of Argon and Helium gas. TIG welding was introduced in early 1940’s. Initially, the electrode heated quickly, and due to the tungsten's high melting temp., particles of W are transferred to the weld. To address this problem, the polarity of the electrode is transferred from positive to negative, but this made it unsuitable for welding many materials. The development of ac units made it possible to made the arc stable and produce high quality aluminum and magnesium welds.

This process may be applied to the joining of engineering materials, involving stainless steel, aluminum. These features of the process lead to application in the airplane industry, nuclear reprocessing and power sector industries as well as in the fabrication of chemical plant, food processing and brewing equipment.

### 1.4.2 Principle of Operation

Welding current and gas supply were turned on, the arc is struck by using a high frequency unit.

In this method, a high frequency current is superimposed on the welding current. The welding torch is brought nearer to the job. When electrode tip comes within a distance of 3.5 to 2 mm from the job, a spark jumps across the gap b/w the electrode and the job. The air path gets ionized and arc is established. After striking the arc, it is allowed to impinge on the job and a molten weld pool is created. At the end of the job, arc is broken by increasing the length of the arc. The shielding gas is allowed on to the solidifying weld pool for a few seconds even after the arc is extinguished. This avoids atmosphere contamination of the weld metal. The torch and filler are generally kept inclined at an angles of 75 -85 $^{o}$ and 15 -20 $^{o}$ respectively with the flat work piece. A left hand welding technique rod may be used. Filler metal, if required, should be added by dipping the filler rod in the weld pool. When doing so, the tungsten should be taken away from weld pool. During welding operation alternatively filler rod and electrode will taken out and come closer to the weld pool. Introducing and alternating of filler rod into the molten pool may disturb the gas shielding, entrain air, oxidize filler rod end and thus contaminate the weld pool. In order to avoid these problems, it is preferred to keep the heated end of the filler rod always within the inert gas shied even withdrawing the same from weld pool during welding. Table 1.1 shows the parameters for different material.

Table 1.1: TIG parameters for different materials

| No. | Base material | Weld current (A) | Diameter of W-electrode (mm) | Diameter of filler rod (mm) | Flow rate of Ar (L/min) |
|---|---|---|---|---|---|
| 1 | Mild, low alloy and Stainless Steel | 250-350 (DCEN) | 3.0 | 3-4 | 7 |
| 2 | Gray Cast iron | 160 (AC/DCEN) | 3.0 | 5.0 | 8 |
| 3 | Aluminum | 200-350 (AC) | 4.5 | 3-5 | 9 |
| 4 | Copper | 250-375 (DCEN) | 3.0 | 3.0 | 7 |
| 5 | Magnesium | 100-150(AC) | 2.5 | 4.0 | 10 |
| 6 | Silicon bronze | 150-200 (DCEN) | 2.5 | 3-4 | 9 |

## 1.4.3 Basic Set Up

The basic setup for GTAW is as shown in Fig 1.5

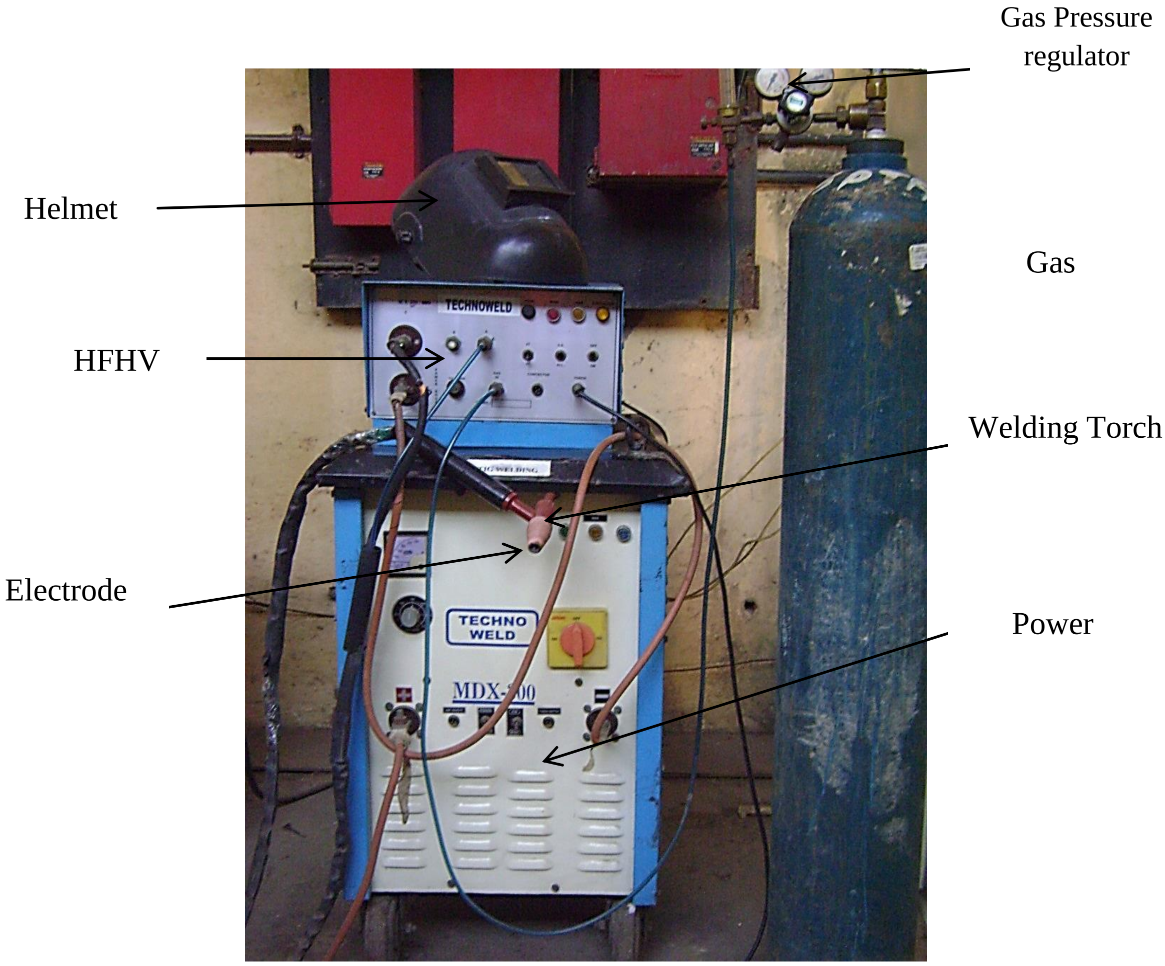


Figure1.5**:** GTAW set up
(Courtesy**:** Central Workshop, Thapar University, Patiala)

## 1.4.4 Basic Equipments of TIG

The basic equipments of TIG welding consist of:

- Welding Torch
- Shielding Gas
- Electrode
- Power Supply

**Welding Torch**

General part of welding torch is as shown in Fig. 1.6.


Figure 1.6: GTAW torch with handle, electrode, ceramic cap, screwed cap and collet
(**Courtesy:** Central Workshop, Thapar University, Patiala)

Welding torch is one of the basic and most important equipment for GTAW. Torch in GTAW welding may be automatic or manually operated. There is no hard and fast difference in the operation of manually operated and automatically operated torch in construction but the difference comes just in the motion or the position of the torch. The torches are connected with cables to the power supply and hoses to the shielding gas source. [Norish, 2006].

The main parts of the manually operated torch are the collet, electrode which is non consumable, Screwed cap, ceramic cap and torch handle. The material used in ceramic cap is ceramic because of its temperature withstand property. Different sizes of caps are used according to the required shielding gas flow. The material of the collet is generally of copper or brass in order to transmit high current and heat effectively. Electrode used is of tungsten, the size of the electrode depend upon the thickness of the material to be welded. The collet is adjustable to some extent. The body of the torch is made of heat-resistant, covering the metal components, providing insulation from electricity to protect the welder.

**Shielding Gases**

The primary functions of the shielding gas in the arc welding processes are to provide a suitable medium for the stable operation of a sustained low voltage arc and to provide shielding from atmospheric contamination. Secondary, important, functions include the control of weld bead geometry and mechanical properties.

**a) Arc Support and Stability**

The arc is maintained by the flow of current in an ionized gas. The ease of ionization of the gas will therefore to initiate and maintain the arc. The ease of ionization is indicated by the ionization potential of the gas and values for the common gases are given in Table 1.2. Argon, in particular, has a low ionization potential and is commonly used in the TIG process. The thermal conductivity of the gas will also influence the arc stability; a high thermal conductivity may result in a reduction in the diameter of the conducting core of the arc and this can lead to an increase in voltage and a reduction in arc stability. Hydrogen, which has a lower ionization potential but a higher thermal conductivity than argon, increases the arc voltage when mixed with argon and may affect both arc stability and arc initiation if more than 8% is added.

Table 1.2: Basic properties of comman shielding gases supplies [Norish, 2006]

| Element | First ionisation potential | Density (kg $m^{-3}$) |
| --- | --- | --- |
| Argon | 15.75 | 1.784 |
| Helium | 24.58 | 0.178 |
| Hydrogen | 13.59 | 0.083 |
| Nitrogen | 14.54 | 1.161 |
| Oxygen | 13.61 | 1.326 |
| Carbon dioxide | (14.0) | 1.977 |

**b) Shielding From Atmospheric Contamination**

The effectiveness of the gas in providing shielding from atmospheric contamination will depend on its chemical reactivity and its physical properties.

In TIG welding, it is necessary to protect the tungsten electrode from oxidation and, for this reason; the inert gases argon or helium is normally used. It is also necessary to protect the weld metal from adverse gas–metal reactions such as the formation of porosity, inclusions, surface oxidation or embrittlement. Common active gases which may cause problems in this respect are oxygen, nitrogen and hydrogen. Most materials form oxides when heated in an oxidizing atmosphere, whereas nitrogen may form insoluble nitrides with reactive metals (Ti, Ta, V and Nb) and soluble compounds with other metals (Fe, Mn, Cr and W). Hydrogen is soluble in most metals, but can form compounds with the reactive metals.

### c) Shielding According to Material

Table 1.3: Shielding gas according to material [Parmar, 2011]

| Sr. No. | Materials | Shielding gases |
|---|---|---|
| 1. | Mild Steel | Argon , Helium , Argon+ Helium |
| 2. | Stainless Steel | Argon, Argon + hydrogen (max 5%) |
| 3. | Aluminium | Argon is preferable for Lower thickness<br>Helium is preferable for higher thickness (deep penetration) |
| 4. | Magnisium | |
| 5. | Copper/Nickel | |
| 6. | Titanium | |

### Electrodes

Electrode used in tungsten arc welding is non consumable and generally of tungsten material because tungsten has the highest melting temperature among pure metals, at 3,422 °C. The tungsten electrodes used in GTAW are usually alloyed with a small amount of thoria or zirconia in order to improve arc starting, by reducing the work function of the tungsten and improving its emission characteristics.

- Tungsten electrodes are general purpose and low cost electrodes. They have poor heat resistance and electron emission. They find limited use in AC of e.g. magnesium and aluminium.
- Thorium oxide alloy electrodes were designed for DC applications and can withstand somewhat higher temperatures while doing many of the benefits of other alloys. Higher % of thorium also makes tungsten more resistant to contamination.
- Electrodes containing zirconium oxide increase the current capacity while improving arc stability and increasing electrode life. Zirconium-tungsten electrodes melt easily than thorium-tungsten.
- In addition, electrode manufacturers may create tungsten alloys with specified metal additions, and these are designated with the classification under the AWS system.

The stable arc operating time (continuous arc operation) may be extended by up to 100% when an electrode with a fine, homogeneous distribution of thoria particles (70 h stable arc operation at 125 A) is substituted for an electrode with a less regular composition (35 h stable operation), whilst re-ignition delays can be reduced from 4% of the total number of arc starts to 1% with the better quality electrode Although thoria (ThO2) is effective in improving arc striking and tip shape retention, it is naturally radioactive. Concern about potential safety implications, in particular in electrode manufacture, has led to the investigation of alternative alloying additions. Oxides of the rare earth elements lanthanum, yttrium and cerium appear to offer similar characteristics to thori [Norish, 2006].

**a) Color coding of tungsten electrode according to AWS**

Figure1.7: Coding of electrode according to AWS [http://www.classictrucks.com]

Table 1.4**:** Different electrode used in TIG

| Electrode | Composition | Color |
|---|---|---|
| EWP | Pure W | Green |
| EW Th-17 | W+1% Thorium | Yellow |
| EW Th-2 | W+2% Thorium | Red |
| EW Zr | W+(0.14-0.4)% Zerconium | Brown |

**b) Shapes of Electrodes**

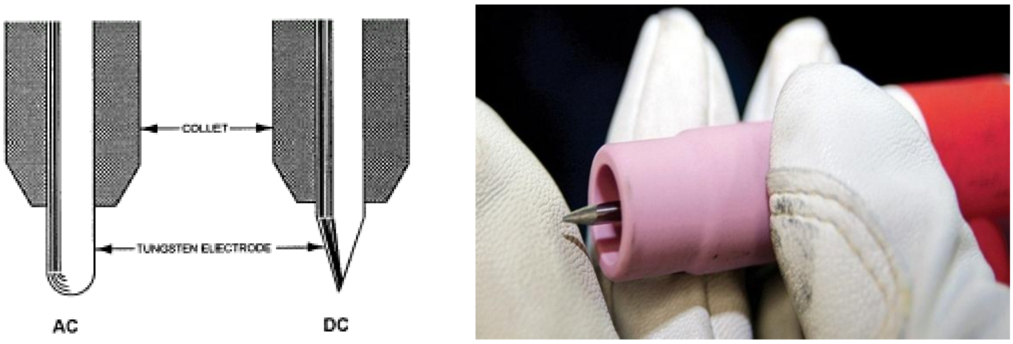


Figure 1.8**:** Electrode shape according to polarity
[http://just122.justhost.com, www.mechanicalengineeringblog.com]

The shapes of the electrode from the tip are according to the current and power supply used in GTAW. Two types of the electrode tips are used sharp ended having diameter on tip and the ball ended tip. Shapes of electrode are as shown in Fig. 1.8.

Table 1.5: Shape of electrode with polarity

| Sr. No. | Power supply to be used | Shape of the electrode |
|---|---|---|
| 1. | DCEP | Sharp ended having diameter on tip. |
| 2. | AC | Ball ended. |

**Power Supply**

- **Arc initiation**

Arc initiation in the GTAW process is a two-stage process consisting of:

- Initial breakdown of the arc gap **(Stage I)**
- Stabilization of the arc **(Stage II)**

**a) Stage-I** Initial breakdown of the arc gap may be achieved by one of the following:

- Touch striking
- High-Voltage DC
- High-Frequency–High-Voltage

- **Touch striking**

Touch striking is probably the simplest technique available. The electrode is brought into contact with the work piece then rapidly withdrawn. The tungsten electrode is heated resistively by the short-circuit current of the power source and the initial arc is established from the heated electrode immediately the electrode is withdrawn. The striking process is assisted by the very small arc length which exists the instant the electrode contact with the work piece is broken and metal vapor is present in this gap. The effectiveness of the technique depends to a large extent on the skill of the operator, but there is always a likelihood of tungsten contamination occurring and this will adversely affect the electrode running performance and weld quality [Norish, 2006].

- **High-voltage DC**

  It has been seen that to obtain reliable arc breakdown at normal arc lengths DC voltages of 10 kV would be required. These voltages would pose serious safety hazards and are not feasible for normal applications. The use of short-duration high-voltage surges has been shown to reduce the danger of lethal electric shock but there is still a risk of injury from reaction to accidental contact with such high pulse voltages. The application of this technique is therefore restricted to automatic systems in which the operator is protected from contact with the high-voltage supply.

- **High-Frequency–High-Voltage**

  High-frequency currents tend to be carried in the outer layers of a conductor and this 'skin' effect can be used to advantage in GTAW arc striking systems. High-frequency–high-voltage supplies (e.g. 3 kV at 5 MHz) are effective in breaking down the arc gap and are non-injurious to the operator. This type of system has been used extensively for arc starting and AC arc stabilization in GTAW and continues to be the main method of striking used in manual GTAW systems. In some cases, arc starting using high-frequency ignition systems becomes inconsistent; this may be due to electrode characteristics or an adverse phase relationship (i.e. lack of synchronization) between the power supply and the arc-starting device. It has also been suggested that a negative space charge may be generated around the end of the electrode and the gas cup. In this case, improved consistency may be obtained by discharging the charge by connecting the gas cup to the positive terminal of the power supply. Where a ceramic gas cup is used, a conductive foil may be wrapped around the nozzle to provide an electrical connection, whereas, with metallic cups, a resistor is inserted between the cup and the positive connection. The main problem with the high-frequency starting technique, however, lies in the use of high-frequency voltage oscillations, which, depending on the design of the oscillator circuit, can cover a wide range of radio frequencies and produce both airborne and mains-borne interference. In the past, this problem has resulted in interference with communication systems and domestic television and radio reception, but it is also likely to create significant problems with electronic control and computing equipment in the welding environment [Norish, 2006].

- **Arc stabilization**

**b) Stage II** Arc initiation or stabilization is largely dependent on the rate at which the power source can supply current to the embryo arc after initial breakdown. Conventional GTAW power sources have been shown to have a current response of around 104 $As^{-1}$ at the optimum settings and with a favorable phase relationship, although much lower rates of rise could be experienced, particularly on single-phase units, when the arc initiation takes place out of phase with the mains supply. It would be expected that this rate of rise of current could lead to striking difficulties especially at low set currents and when long, inductive welding cables are used. In these circumstances effective arc 77 initiation often depends on the use of a capacitor in parallel with the output which can discharge into the arc [Parmar, 2011]

**Control of GTAW and related processes**

GTAW and related processes are capable of producing very high quality welds but, for consistent results, the influence of the welding parameters on weld geometry and quality must be identified and controlled.

Table 1.6: Main control parameters in DC GTAW [Norish, 2006].

| Primary | Secondary |
|---|---|
| Current | Arc length |
| Travel speed | Polarity |
| | Shielding gas |
| | Electrode vertex angle |
| | Filler addition |

The main control parameters in DC GTAW are as follows

- **Current and travel speed**

The mean current normally determines the heating effect of the arc and the arc pressure and stiffness. The penetration and fusion characteristics for a fixed set of secondary parameters are determined by a combination of mean current and travel speed. However, the maximum speed, penetration and fusion area are limited by the onset of unacceptable weld bead profile at high currents. The force generated in the high-current arc displaces the molten weld pool and, at high travel speeds, there is insufficient time for the displaced metal to flow into the joint before solidification. The result is a discontinuous bead or undercut.

- **Arc length**

The arc length in GTAW is the distance between the electrode tip and the work piece. By increasing this distance the heating efficiency, penetration level and fusion level decreases. This reduced efficiency, which is due to radiation losses from the arc column, occurs even though arc voltage increases and the total power may increase. That is why electrode-to-work piece distance should be maintained fixed. The arc voltage gives a useful indication of electrode-to- work piece distance [Norish, 2006].

- **Polarity**

When we are using DCEN polarity the balance b/w the anode and cathode in GTAW is such that 70% of the heat input is absorbed by the anode and 30 % is absorbed at the cathode. Most of the times electrode negative polarity is used since this provides the good heating effects and minimum torch heating. For Al and its alloys, DCEP polarity offers cathodic cleaning of the surface of work piece, but, considering the efficiency of the process, AC is normally used for these materials; this provides plate heating during the electrode negative half cycle and plate cleaning during the electrode positive period [Norish, 2006].

- **Shielding gas**

The shielding gas can have a significant effect on the thermal characteristics of the arc and fusion behavior of GTAW. These effects can be used to extend the operating range of the process and, for example, the maximum speed before the onset of weld bead humping at 400 A may be increased from 7.6 $mms^{-1}$ to 23.3 $mms^{-1}$ by replacing argon with helium as the shielding medium [Norish, 2006].

- **Filler addition**

The addition of cold filler wire will cool the weld pool and reduce the heat available for plate fusion; however, in some circumstances, small traces of elements that alter the surface tension of the weld pool may be added via the filler to improve the fusion characteristics [Norish, 2006].

**Variants in the GTAW process welding are as follows:**

- Pulsed GTAW and High-frequency pulsed GTAW
- Square-wave AC GTAW and plasma
- Cold- and Hot-wire feed additions in GTAW
- Dual-Gas GTAW and plasma welding
- Multi cathode GTAW
- A-TIG welding
- Buried Arc GTAW
- High Current GTAW

### 1.4.5 Applications, Advantages and Disadvantages of GTAW

**Applications of GTAW**

GTAW is one of the best applications in the world wide joining of similar or dissimilar metals. GTAW can be used for depositing metal in all position but the level of skill required is very high. It is extensively used, generally without filler metal, for the welding of longitudinal seams of thin walled stainless steel and alloy steel pressure pipes and tubing in continuous strips mills. GTAW is easily mechanized and gives high quality welds; the process is quite popular for precision welding in the aircraft, atomic energy and instruments industries. Aircraft frame, jet engine casing and rocket motor cases are typically examples can sealing joints are very suitable for mechanized GTAW.

Almost all tube-to-tube sheet welding in heat exchanger is done with automated GTAW equipment, with or without the addition of filler metal. Typical automated equipment employs a welding machine with as extendable rotary quill that allows making welds inside the hole from the face of the tube sheet. High quality welds in aluminum, stainless steel, nimonic alloys (80/20 nickel- chromium) and copper for use in chemical plants, sheet work in aircraft engines and structure are also structure are also accomplished by GTAW. It is also a very useful process for welding die casting.

**Advantages of GTAW**

- No flux is used.
- Due to the clear visibility of the arc and the job, the operator can exercise a better control on the welding process.
- GTAW is used in all positions and produces smooth and sound welds with fewer spatters.
- High quality weld is produced on the material.
- Increased corrosion resistance.
- No slag formation.
- Higher deposition rate.
- Deeper penetration rate.
- Welds all metals including aluminum and stainless steel.

**Disadvantages of GTAW**

- GTAW is slow process as compared to the similar application process MIG.
- Tungsten inclusion is hard and brittle
- Equipment used is costlier and less portable
- Difficult to weld in sharp edges
- Filler rod end if it by chance comes out of the inert gas shield can cause weld metal contamination.

- Less suitable for outdoor work
- Radiations can produce harmful effects to the operator if exposed continuously for long time.
- Non consumable electrode requires frequent grinding.

### 1.4.6 Materials to be Welded by GTAW

GTAW is mostly and commonly used in welding stainless steels, aluminum alloys, magnesium alloys, titanium, copper alloys, nickel alloys and many other mostly all metals except lead and zinc. Mostly it is seen that the carbon steels are welded by GMAW and SMAW processes not by GTAW because of the cheap processes in comparison. GTAW is commonly used for flat position as well as other positions according to the availability of skilled worker.

**Aluminium and Magnesium**

It is seen that Argon is used in welding of aluminum and its alloys in GTAW. For manually operated GTAW of aluminum, argon shielding with AC and HF stabilization is found superior to use of helium shielding with DC.

Aluminum and magnesium are mostly welded by using AC, but the use of DC is also possible, depending on the properties desired. Before welding, the work pieces should be cleaned properly and pre weld heat treatment is given to 175 to 200 °C for aluminum and of 150 °C for thick magnesium workpieces to increase penetration and travel speed. AC current also provides a cleaning effect, removing refractory aluminum oxide layer that forms work piece.

**Steels**

While welding stainless steels by GTAW argon is used for manually operation or hydrogen is added up to 25% in argon or helium for welding the steel alloys. The result of adding hydrogen is to increase the arc voltage and makes the arc hotter. Preheating is generally not necessary for mild steels less than one inch thick, but low alloy steels may require preheating to slow the cooling process and prevent the formation of martensite in the heat-affected zone.

For GTAW of carbon and stainless steels, the selection of a filler material is important to prevent excessive porosity.

**Dissimilar metals**

Generally it is seen in all welding processes the weld material or the base material is always same. But as the application required by the market it is seen that not always the material is same. GTAW is one of the welding processes among the processes which have the wide application on the welding of dissimilar materials. While selection of materials it is very difficult to adjust all the parameters to me taken for both of the materials to be welded. So many factors should be taken under consideration while selection of parameters. Filler material, gas type, gas flow rate, power source, current, voltage and so many other factors have to consider. Preheating and post heating temperatures, position of joint, angle of torch, traveling speed for both the materials for different applications. Dissimilar material is used generally to increase the strength, toughness and other mechanicals properties according to the application where the material is going to be used.

## 1.5 Weldability

Weldability is the capacity of a material to be joined to be welded under the fabrication conditions imposed into a specific suitability designed structure and to perform satisfactory in the intended service. All material is welded by different process by less or more efforts easily or by difficulties. Welding of any material could be done by any method but the main purpose of welding is the quality of weld, ease of weld and the minimum change in metallurgical properties.

Weldability is often hard to define. For instance the International Organization for Standardization (ISO) defines weldability in ISO standard 581-1980 as: "Metallic material is considered to be susceptible to welding to an established extent with given processes and for given purposes when welding provides metal integrity by a corresponding technological process for welded parts to meet technical requirements as to their own qualities as well as to their influence on a structure they form [Blondeau, 2008].

**Stainless steel**

Stainless steels are the iron base alloys in which the 10% or more chromium is added to increase its property of corrosion resistance into it. Chromium as well as other elements are also found in it to increase the manufacturing ability of the steels in the industry for several applications. A type of film is formed of chromium oxide which retards further oxidation, rust or corrosion. Properties of stainless steels:

- Higher resistance to corrosion
- Higher toughness to cryogenic
- Higher hardening work rate
- Higher strength hot
- Higher metal ductility
- Higher hardness and strength
- Appearance is more attractive
- Maintenance free

**Welding of Stainless steel**

During the welding of the stainless steels the temperature of base metal adjacent to the weld reach levels at which microstructure changes occurs. The degree at which these changes occur and their effect on finished weldment, in term of resistance to corrosion and mechanical properties depends upon the content, thickness and filler metal, joint design, weld method and welder skill. Weldability of different grades are easily welded, actually the weldability of various grades depends upon the nature of the family to which it belongs to. Heat conductivity of Cr-Ni steels is about 50 percent less than that of mild steel. Hence concentration of heat is obtained resulting in less heat input for a given job. As a general rule about 10 per cent less current is used with stainless steel electrodes as compared to mild steel.

Melt off rates of stainless steel electrodes are higher than the rates for M.S. electrodes. This is another reason for slightly lower current being used in stainless steel welding. Thermal expansion of Cr-Ni steels is about 50 percent greater than for M.S. This will increase the chance of warping and buckling. Thus suitable fixture must be used while welding stainless steels. Electrical resistance is 6 to 12 times higher than that of M.S. and hence this may cause over heating in the electrodes. So shorter electrodes are normally used to reduce electrode heating [Blondeau, 2008].

**Different types of stainless steels are as follows:**

a) Austenitic stainless steel

b) Ferritic stainless steel

c) Martensitic stainless steel

d) Duplex stainless steel

### 1.5.1 Austenitic Stainless Steel

Austenitic stainless steel has 16% chromium and 6% nickel As a common name for 304 stainless steel is 18 / 8, for 18 % chromium and 8 % nickel.

### 1.5.2 Ferritic Stainless Steel

The ferritic grades do not have good welding properties. The excessive grain growth problem is difficult to overcome, so most grades are only welded in thin gauges. These grades can be welded, but certainly not as readily as the austenitic grades (actually dual-phase ferritic plus some martensite) grade which has a very little carbon content and has the remaining composition and the mill processing route balanced to enable welding.

### 1.5.3 Martenistic Stainless Steel

Martensitic stainless steels can be welded but precaution needs to be exercised as they will make a very hard and brittle zone near to the weld. Cracking of zone can occur unless much care is taken with preheating and with postwelding heat treatment. These steels are often welded with austenitic filler rods to increase the ductility of the deposit. Pre-heating temperature for martenistic stainless steels is 225 $^{o}$C-300 $^{o}$C and post-heating is 725 $^{o}$C and slow cool to remove brittleness.

### 1.5.4 Duplex Stainless Steel

Duplex stainless steels have good weldability, but not quite good as that of the austenitic.. The higher nickel content sures the correct 50/50 (ferrite/austenite) structure in the weld plates, thus maintaining strength, ductility as well as corrosion resistance.

### 1.5.5 AISI 4340 (High Tensile Low Alloy Carbon Steel)

AISI 4340 alloy steel can be welded using fusion or resistance welding methods. Pre-heating and post-heating weld procedures are followed while welding this steel. AISI4340 alloy steel is a heat treatable and low alloy steel containing chromium, nickel and molybdenum.

**Applications**

AISI 4340 high tensile low carbon alloy steel is used in aircraft landing gear, power transmission gears and shafts. Parts exposed to high permanent and fluctuating stresses are the main application of this type of material. Typical components include pinions, bushes and sleeves. 4340 is used where a medium hard, impact resistant weld is required. Also used in die-cast dies, axles, forgings, castings, and buildup under harder weld deposits.

### 1.5.6 Weldability Issues

High electrical resistance, low thermal conductivity and low melting point create a big problem which needs to weld stainless steel at less current. Due to the high current values results in warpage and distortion like defects. Skip welding and back stepping are often indicated procedures for good weldability. Overheating of SS may also result in diffusion of metal.

### 1.5.7 Carbide Precipitation

Austenitic stainless steels are heated within the temperature range 427 $^{o}$C to 870 $^{o}$C or cooled slowly through that range carbon is precipitated from solid solution mainly at the grain boundaries, where it units inter granularly with chromium to form chromium rich carbides. The formation of these carbides effectively eliminates much of the chromium which would otherwise be available to form the protective chromium oxide. It is nature that the areas impoverished in chromium have lower corrosion resistance. Corrosion in stainless steels is generally localized in HAZ adjacent to the welds where carbides are precipitated.

**Carbide precipitation can be controlled by**

- Using stabilized steels by adding columbium and titanium which have greater affinity for carbon than does chromium.
- Rapid quench may minimize the carbide precipitation: however, this may not be possible in all cases, especially in thick sections.
- Limiting the carbon content to a maximum of 0.03 %, known as extra low carbon stainless steel, can help avoiding the harmful carbide precipitation.
- Post weld solution annealing – it puts carbide back into solution and restores corrosion resistance. Austenitic stainless steel stabilized with niobium plus tantalum or titanium and welded with stabilized filler metal gives good strength and corrosion properties.

### 1.5.8 Cracking

Interdendritic cracking in the weld area that occurs before the weld cools to room temperature is known as hot cracking. Metal with fully austenitic structure is more susceptible to micro fissuring that weld metals with a duplex structure of delta ferrite in austenite. Susceptibility can be reduced by a small increase in carbon or nitrogen content or by a substantial increase in manganese content.

Cracking can be avoided: Weld metal should have a ferrite content of atleast 3 to 5 ferrite number (FN) and hence filler metal of suitable composition is to be selected. To determine suitable composition and the corresponding ferrite number the Schaeffler diagram as shown in Fig. 1.9 is made use of which is as shown below:

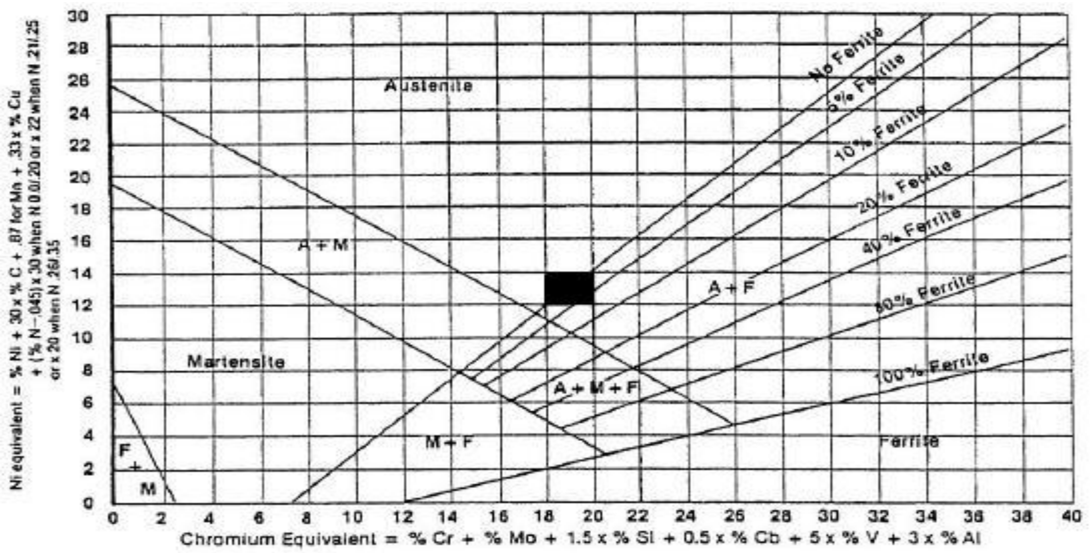


Figure 1.9: Scheffler diagram
[http://www.cartech.com]

Nitrogen acts as a solid solution strengthener and increases the annealed yield strength to approximately twice that of the conventional austenitic steels. Specific attention should be paid to the control of nitrogen when welding these grades. A significant reduction in nitrogen will result in a loss of strength and corrosion resistance. An increase in the nitrogen content is likely to result in weld porosity or weld hot cracking.

### 1.5.9 Pre-heating or Post-heating of Steel

Generally pre heating or post heating of stainless steels is not required. Fully austenitic steel are sometime sensitive to hot cracking thus heat input when welding must be carefully controlled and dilution should be kept minimum. So preheating up to 100 °C is done sometime.

While in the case of duplex no post heating is done if post heating of duplex is done it will lead to the distortion. Sometime pre heating is done up to temperature of 100 °C to remove the moisture from duplex in very cold conditions.

# Chapter 2
# Literature Review

## 2.1 Introduction

Several researchers perform the research work all over the world for predicting the mechanical properties. Different kinds of steel and other materials had been welded by (GTAW) or (TIG) process to find out the effect on properties by changing the various parameters. For a new research work here is a study of few papers on which the work had been done before. A brief review of literature is being presented here. The available literature can be categorized in the following broad areas:

- Effect on microstructure and mechanical properties.
- Effect of shielding gas.
- Effect of Post heating and Pre heating.
- Mechanical properties at cryogenic temperatures.
- Corrosion behavior.

## 2.2 Literature Review

### 2.2.1 Effect on Microstructure and Mechanical Properties.

**Hajiannia et al. [2013]** studied the effect on mechanical properties and micro structure by using two materials AISI 347 under rolled and A335 low alloy steel pipes solution annealed condition. Filler metals, ER 309L and ERNiCr - 3 were taken to weld these metals. Shielding gas used in this GTAW-DCEN was argon gas. Tensile properties, elongation ratio, microhardness and bending tests were conducted to study the effect on microstructure. The results showed that the solidification of ERNiCr - 3 weld metal was similar to the primary austenite, two-phase structure was observed which contains dendritic and interdendritic zones. On welding 347 stainless steel to low alloy steel A335 joints, using ERNiCr-3 filler material a higher value of ultimate tensile strength and elongation but lesser yield strength was observed.

**Arivazhagan et al. [2011]** studied the effect on mechanical properties and microstructure by using two parent metals AISI 304 SS and AISI 4140 low alloy steel. Welding of these metals is done by three different processes GTAW-DCEN, Electron beam welding and continuous drive friction welding. This is seen FW reduces toughness and increase in hardness across the weld. The yield strength weldment made by EBW is higher as compared to GTAW and FRW.

**Ramkumar et al. [2012]** studied out performance of GTAW of two dissimilar materials Monel 400 and AISI 304 by using to different filler materials E309L and ENiCu-7. Higher % of Carbon was found in weld interface while using E309L filler wire but lesser while using ENiCu-7 filler wire. The strength and ductility of ENiCu-7 welds were comparable to those of AISI 304/ Monel 400 base metals. The tensile strength properties of dissimilar metal welds using ENiCu-7 filler wire are better than E309L weldment.

**Ahmad et al. [2007]** studied the microstructure and morphology of different metals Zircaloy-4 and SS304L welded by GTAW using 304L filler metal. Two phase were found in molten state one is Zr $(Cr, Fe)_2$ and another one is $Zr_2Fe$-$Zr_2Ni$ while welding the dissimilar materials by GTAW. The density of Zr2Fe–$Zr_2Ni$ was two times less than that of $Zr(Cr, Fe)_2$. Hardness of $Zr_2Fe$–$Zr_2Ni$ is also three times less than that of $Zr(Cr, Fe)_{2.}$

**Ozdemir et al. [2007]** presented the study by using two dissimilar materials while welding by Friction welding. The two welding materials were AISI 304L and AISI 4340 high tensile low carbon alloy steel. Higher microstructure changes were found in DZ zones.

**Lin et al. [2010]** conducted experimental study using aluminum alloy and austenitic stainless. The filler metal used was 2319 Al–Cu6 welding wire, with a diameter of 2.5 mm and thickness of plate 3 mm. A single-V groove with a bevel angle of $40^o$ in steel side and $30^o$ in aluminum alloy side. The flux suspension (flux powder dissolved in acetone) was spread homogenously in a 0.2–0.5 mm thickness on the groove of the steel in 10 mm width. Aluminum– steel butt TIG welding–brazing was carried out using CLOOS AC-TIG welding source. The aim of this paper is to investigate the microstructures, compositions of IMCs, mechanical properties like micro hardness test and tensile test. The average thickness of IMC layer formed was 3-5 µm which was in welded seam/steel interface and was less than the limited value of 10 µm. The IMC layer was found to be composed of $Fe_4Al_{13}$ and at the bottom Sn diffused into steel matrix and formed the grain boundary filter layer. The tensile strength of butt joint reached 172.5 MPa and the crack initiated from the IMC layer at the bottom of the joint and derived into the welded seam at the upper part of the joint. The joint in this study had higher level than those with coated layer. The average micro-hardness of the layer was 644.7 HV, compared with 104.5 HV in welded seam and 200 HV in steel matrix.

**Yan et al. [2010]** studied the effect on mechanical properties and microstructure by using SS 304 material plates of thickness 3 mm and welded by three welding process TIG welding, Laser welding and laser TIG hybrid welding. Transition zone and HAZ were present in TIG joint but not present in hybrid and laser joints. Size of dendrites in TIG joint is larger as compared to laser and hybrid joints. The laser joint shows the minimum dendrite size in all joints. The tensile strength of TIG, laser and hybrid joints are 560, 733 and 683 MPa, respectively.

**Liu et al. [2013**] studied TIG butt welding joint by using two materials AZ31B Mg Alloy and 6061 Al alloy, Zinc filler metal with and without Al foils, and their thicknesses are 0.1, 0.2, 0.3 and 0.4. The Thermo-Mechanical zone (TZ) and FZ near the Mg base metal are the weak parts of the joints, and these areas are mainly composed of IMCs and a small quantity of MZAS. The quantity of additional 0.2 mm thick Al foil is considered as an appropriate option for the GTA butt welding of AZ31B Mg alloy to 6061 Al alloy filling with Zn filler metal, and the tensile strength of the joint can reach 104 MPa.

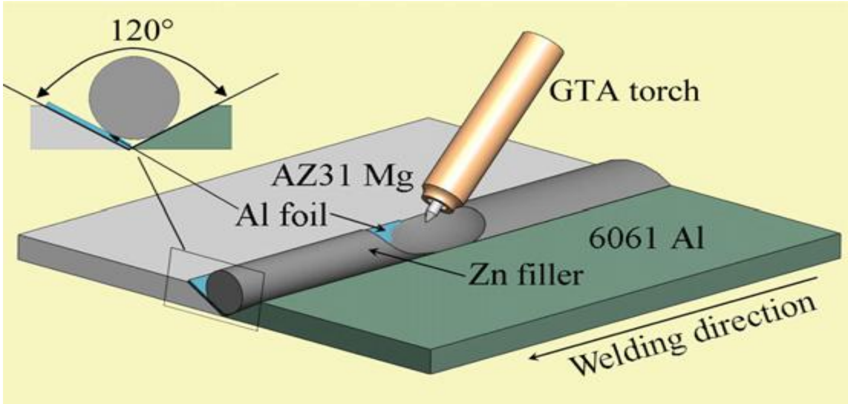


Figure 2.1: The schematic illustration of the GTA butt welding [Liu, 2013]

**Sivashanmugam et al. [2010]** in the present study has compared the microstructure and mechanical properties (tensile strength, hardness and impact strength) on the joints of AA7075 aluminum alloy welded by GTAW and GMAW processes. They found that higher strength was found in welded joints by GTAW as compared to that by GMAW and the improvement in strength value was approximately 28%. Hardness was found lower in the weld metal (WM) region as compared to the HAZ and BM regions. High hardness was recorded in the GTAW (HAZ) and the maximum hardness of 157 VHN was observed in the HAZ as compared to 153 VHN in parent metal. In GMAW (HAZ) also high hardness of 133 VHN was observed as compared to 100.5 VHN in parent metal. In GTAW and GMAW, the values of impact strength by Charpy method were 6 J and 4 J respectively as compared to 12 J of base metal. Fine equated grains were formed in the welding zone and they were uniformly distributed in the microstructure. Mode of fracture was brittle in nature as studied by SEM image.

### 2.2.2 Effect of Shielding Gas

**Durgutlu [2004]** investigated the effect of hydrogen in argon as shielding gas for tungsten inert gas welding of 316L austenitic stainless steel. For tensile strength, the best result is obtained from 1.5% $H_2$–Ar as gas shielding. Mean grain size in the weld metal increases with increasing hydrogen content. More hydrogen content caused deviations in the grain orientation of weld metal. For all shielding media, hardness of weld metal is lower than that of the HAZ and base metal.

**Peasura and Watanapa [2012]** in present study used aluminium AA5083 of thickness 6 mm. Welding current used to weld by GTAW was 100 A – AC taveling speed of 12 mm/sec and the electrode size of 2.4 mm. Shielding gases used in study were argon and helium with flow rate of 6, 10, 14 L/min. The main aim of this study was to find out the effect of shielding gases. Tests performed for this were microstructure examination, microhardness and other mechanical properties on the sample. It was found that hardness at HAZ and fusion zone by using argon with a flow rate of 14 L/min was 74.27 HV and 68.97 HV respectively. The helium having high thermal conductivity result in a large production of heat due to which there was larger grain size, which resulted in decreased hardness. The argon having low thermal conductivity provides smaller grain size resulting in higher hardness both in weld metal and HAZ.

**Lu et al. [2013]** in present study used $Cr_{13}Ni_5Mo$ martensitic stainless steels of dimensions of thickness 12 mm. Welding current used was 160 A, welding speed 2 mm/s, and electrode gap of 3 mm. The nozzle used is shown in Fig. 2.2. Four welding process used were as follows:

| Welding process | Shielding gas (vol.%) and gas flow rate |
|---|---|
| Traditional TIG welding | He, 10 L/min |
| Mixed-gas TIG welding | He + 2% $CO_2$, 10 L/min |
| Double-shielded TIG welding, 2% $CO_2$ | Inner layer He, 10 L/min<br>Outer layer He + 2% $CO_2$, 10 L/min |
| Double-shielded TIG welding, 20% $CO_2$ | Inner layer He, 10 L/min<br>Outer layer He + 20% $CO_2$, 10 L/min |

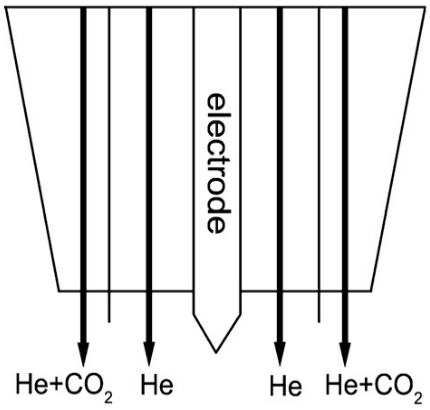


Figure 2.2**:** Double-Shielded TIG welding process

The aim of this study was to investigate the effect of double-shielded TIG welding of welding parameters on the fusion zone profile. In this study it was found that double-shielded TIG welding process controls the weld oxygen content and also controls the convection and fusion zone profile. By using the specified parameters, weld Depth/Width ratio of 0.6–1.0 can be achieved using He-(He + 10% $CO_2$) double shielding with flow rate of 10 L/min for both the outer and inner layer shielding gas. The efficiency of double-shielded TIG welding process is 2 to 4 times greater than that of traditional TIG welding. The weld joint strength of the $Cr_{13}Ni_5Mo$ stainless steel from He-(He + 10% $CO_2$) double shielding was found to be same with the strength of a MAG-welded joint using Ar + 5% $CO_2$ shielding.

### 2.2.3 Effect of Post-heating and Pre-heating

**Dewan et al. [2014]** in present study used plates of AISI-4140 alloy steel with 300 mm × 76 mm × 6.35 mm dimensions are TIG welded with SAE - 4130 chromoly filler rod. To find out the effect of post-weld heat treatment (PWHT) on residual stresses and mechanical properties, the TIG welded specimens were subjected to two different heat treatment processes. Annealing was done in a furnace at 650 °C temperature and Hardening at 500 °C for 1 hour, respectively, followed by air-cooling.

Electrolytic plasma processing (EPP) was also applied on weld and HAZ to study its effect on relieve post-weld residual stresses. The aim of this study was to find out the effect of PWHT and EPP on microstructure and mechanical properties like (micro hardness, residual stress and tensile stress). Parameters used in this study were shielding gas pure argon, welding current 240- 350 A DCSP; electrode used is of 3.2 mm, groove angle of 45 $^{o}$. Loss in ductility, tensile strength and toughness was seen in TIG- welded low alloy steel for martensitic microstructures in HAZ and weld zone. As-welded (AW) specimen showed 39% and 37% decrease in failure strain and toughness values, resp., when compared to the base metal. It was seen that there was 88% hike in toughness values and 12% less yield strength by PWHT at 650 °C compared to AW specimen. The electrolytic plasma process (EPP) was found to improve different properties, like the corrosion resistance. EPP - applied specimens showed 743 MPa and 912 MPa yield and ultimate strength, resp., but the values for as welded specimen were 700 MPa and 839 MPa. Due to the presence of fine martensitic microstructures and surface EPP-treatment about 10 % increase in toughness as compared to as welded samples was seen.

**Temmar et al. [2011]** in present study used 7075 T6 aluminium alloy with thickness of 2.5 mm. Current 100–140 (A), voltage 12.5 (V) and weld speed of 12.7 (mm/s) were taken for experiment. Shielding gas used was pure argon. The post-weld aging treatment was carried out at 140 $^{o}$C for a soaking time of 10 H. This study was done to find out the effect of post weld treatment on mechanical properties and microstructure of differnt zones while using TIG welding. It was found out that strengthening in the TIG weld / Heat Affected zones is correlated to with a balance of dissolution, reversion and precipitation processes across the heat affected zone. By post-weld aging treatment the tensile strength of the welded joint increases. There was decrease in the impact of the 7075 aluminium alloy at fusion zone. Low tensile strength and impact energy properties 7075 aluminium welded alloy were found due to the built of micro-cracks during the welding.

**Shen and Xu [2012]** in this study AZ 61 magnesium alloy of thickness 2 mm and filler wires of AZ91D of diameter 2mm were used. Pre heating temperatures used were 100, 150, 200, 250 and 300 $^{o}$C. parameters used were, current 90 A, speed of 15 mm/sec, argon flow rate of 5 L/min and electrode to work out distance was also set to 2 mm through out the welding. In this study pre heating was applied to improve the microstructure and mechanical properties of the welded material. It was found that microhardness of the fusion zone and the ultimate tensile strength value of the joints were increased by increasing preheating temperature. The elongation % of the joints decreased by increasing volume fraction. High preheating temperature decreased the formation of pores and cracks in the fusion zone of the joint and increased the ultimate tensile strength of the joints.

**Zhu et al. [2011]** in present study used two plates of CLAM steel which were butt-welded by TIG under two conditions (a) using the original CLAM composition filler metal and (b) using the modified composition (9.8 Cr, 2.0 W, 0.5 Ta, 0.35Mn, 0.19 V, and 0.12 C in wt.%, and Fe for the balance). Parameters used were current 64 A, welding voltage of 13 V, shielding gas argon with flow rate of 10 L/min, welding speed of 2 mm/sec. Investigation was carried out to find out the microstructure and mechanical properties on giving post weld heat treatment by using TIG welding. It was found that hardening at weld metal and softening in heat affected zone in the TIG joint. Microhardness of weld joint decreased when the temperature of Post Weld Hear Trearment increases. The tensile strength was found to be decreased when the Post Weld Hear Trearment temperature was increased. Tensile strength of weld metal was higher than that of HAZ and base metal. Absorbed energy increased with increasing PWHT temperature until PWHT was done at 760 $^{o}$C / 30 min, the specimen ductile fractured in local area, but the absorbed energy of each CIT specimen was much lower than that of BM.

**Ahmad et al. [2011]** used 6061 aluminium alloy of thickness of 10 mm and width of 100 mm. Groove angle was of 40 $^{o}$.Gas metal arc welding was done in this study. Filler used was ER 4043 with of diameter 1.2 mm. Parameters used were current 210 A, voltage 24 V, feeding speed 190 mm/sec, heat input 1.4 mm/sec, travel speed 3.6 mm/sec, gas flow 23.6 L/min. Two samples were taken: as-welded and PWHT samples. The PWHTs used were solution heat treatment, water quenching and artificial aging. The samples were solutionized in the induction furnace at 530 $^{o}$C for 1 hand  cooled down rapidly by a water bath. The samples were age hardened at a temperature of 160 $^{o}$C for 20 h. This investigation was performed to found the effect of PWHT on the microstructure and the mechanical properties of material. It was found that by applying PWHT there was 3.8% increase in tensile strength, 25.6% increase in hardness strength and elongation % increase was 21.5%. It was found that by SEM fractographs that small grain size, small gap between the grains and relatively small voids were found for the PWHT joints. This qualitates the superior tensile properties, as compared to the AW joint. It was also found that the elongation or deformation is no longer concentrated in the HAZ. Therefore, the limited elongation capability of the tensile specimen for an as-welded joint is due to the fact that the total elongation of the specimen during testing was concentrated in the HAZ, which was the weakest part of the specimen.

### 2.2.4 Mechanical properties at cryogenic temperatures

**Yuri et al. [2000]** in this study used 304L and 316L austenitic stainless steels. Two filler wires 308 and 316 were used. Thickness of the plate was used was 28 mm. The purpose of this study was to study effect on microstructure and mechanical properties at cryogenic temperature. It was also found that fatigue crack initiation sites of SUS304L weld metals were usually at blowholes with a diameter of 200 ± 700 lm, and those of SUS316L weld metals were at weld pass interface boundaries created during welding. Microvoids, which were undetectable by conventional inspection procedures, cause reduced fatigue resistance.

### 2.2.5 Corrosion Behaviour

**Fahimpour et al. [2012]** studied that 6061 aluminum sheets of thickness 13 mm were welded by two different processes FSW and TIG welding. AISI 4043 alloy was used as filler in TIG welding the thickness of sheets was 13 mm. In FSW shoulder diameter was taken as 20 mm, pin diameter as 7 mm, pin height as 7 mm and tool material was of H13 die steel. Speed of 200 mm/min and rotation speed of 800 rpm was taken for FSW. The study was done to investigate the corrosion behaviour of aluminum  used by using GTAW and FSW to find the microstructure.

## 2.3 Summary of Literature Review

After looking at various research work and studies it is concluded that enough work was done with different parameters on GTAW. Moslty the investigators studied the effects of different parameters to study the microstructure and mechanical properties of the different material according to the applications [Hajiannia et al., 2013; Hajiannia et al., 2011; Ramkumar et al., 2012; Ahmad et al., 2007; Ozdemir et al., 2007]. Some reaserchers had studied effect on microstructure and mechanical properties of dissimilar materials by GTAW process. Effect of pre heating, post heating and shielding gases on microstructures and mechanical properties of weldment and base metals were investigated [Dewan et al., 2013; Temmar et al., 2011; Shen and Xu, 2012; Zhu et al., 2011; Ahmad et al., 2011;]. Gases taken in consideration were of pure inert gas or of mixture of different gases like $H_2$, $CO_2$, Ar, He. Effect on HAZ, FZ, TMAZ and HDAZ on heating at different temperatures also been done by many researches. Some of the investigators also did the work on corrosion behavior of material after using GTAW [Lu et al. 2013, Peasura and Watanapa 2012, Hsieh et al. 1999, Durgutlu, 2004]. It can be concluded from literature review that the main process parameter which affect the properties of welded joints are welding current, shielding gas, voltage, gas type, gas flow rate, electrode type and filler metal.

## 2.4 Scope and Objectives of Present Work

Literature survey reveals that weldability aspects of AISI 4340, high tensile low carbon steel has not been investigated in detail while joining by GTAW although AISI 4340 has lot of application in aerospace and automobile industries. Austenitic stainless steel is one of the most widely used stainless steel however; welding of stainless steels raises many practical issues due cracks formation especially when joined with dissimilar metals. Similarly AISI 316 stainless steel finds many industrial applications including automobile, aerospace, medial etc. However joining of AISI 304 or AISI 316 with AISI 4340 is one of the areas where no work has been reported. Effect of welding process parameters, preheating, post heating, effect of shielding gases while joining dissimilar metals like AISI 304, AISI 316 with AISI 4340 could be studied and optimum process parameters to achieve the best mechanical property of the joint should be investigated. Based on the above scopes the following objectives are decided for the present work.

- To study the effect of process parameters like current, pre-heating, post-heating on the mechanical strength like tensile strength, toughness, micro hardness and metallurgical changes (by SEM study) of the joint, HAZ after GTAW of AISI 304 and AISI 4340.
- To study the effect of shielding gas like pure Ar, Ar and He mixture, Ar and $H_2$, gas flow rate, filler material (304, 308, EN24) while joining AISI 304 and AISI 4340 on tensile strength, toughness, micro hardness and metallurgical changes.
- To investigate the explain effect of process parameters, filler metal (309, 316, EN24) during joining dissimilar metals AISI 316 with AISI 4340 by GTAW.
- Effect of pre-heat and post-heat, gas type (Ar, 70% Ar + 30% He, Ar + 1.5% $H_2$) and flow rate on mechanical properties and metallurgical behavior during joining AISI 316 with AISI 4340.
- To optimize the process parameters that will lead to better joint quality of the welded joints.
- To find the optimum process parameters through proper design of experimental technique and statistical analysis to obtain maximum possible mechanical strength.

# Chapter 3

# Experimental Details

## 3.1 Introduction

In this chapter all the detailed information of experimental data is provided like materials, machine, selection of parameters and measurement setup. Pilot study has also been explained done for selecting the various parameters, setup used for measurements, fabrication of setup.

## 3.2 Welding Setup and Consumables

Before starting of some experiment for welding there is requirement of welding setup and consumables required for welding purpose which are described as:

### 3.2.1 GTAW Machine

TIG welding was carried out on tungsten inert gas welding machine (Make: TECHNO WELD MDX – 300, INDIA) available at Central Workshop, Thapar University, Patiala as shown in the Fig. 3.1. The main parts of the machine are control box panel, electrode gun, gas regulator, gas cylinder. The welding current can be regulated and displayed on control box panel of the welding machine and has a range of 0 – 500 A. The function of electrode gun is to carry the tungsten electrode and direct the supply of shielding gas in the welding region. Gas regulator is used to control the shielding gas flow into the welding area. The machine is totally manual and requires a skilled operator to operate it.


Figure 3.1: TIG welding setup
(**Courtesy:** Central Workshop, Thapar University, Patiala)

Table 3.1: Main technical parameters of welding machine

| Sr. No. | Welding Parameters | Range |
|---|---|---|
| 1. | Welding Current (A) | 0 – 500 A |
| 2. | Diameter of Electrode | 0.5, 1.0, 1.6, 2.4, 3.2, 4.0, 4.8, 6.4 mm |
| 3. | Gas Flow Rate (L/min ) | 0 – 25 l/min |

**Power source**

The setup used for the experimental work will be purely manual. DC power supply sources are used with static volt-ampere (V-I) characteristics of the drooping type, that is, of the constant current type. In this type of power source the change in current with the change in arc length is minimal, thus as inadvertent slight shift in the welder's hand will not have any discernible effect on the performance of the process. That is why the V-I characteristic curve the more satisfactory the power source and this particularly so for manual GTAW. The power source for GTAW is the transformer cum rectifier unit with built-in air flow circuit.

### 3.2.2 Shielding Gas

Shielding gas is the main constituent in TIG welding. Different shielding gases may be used according to the welding materials. Table given below tells us about shielding gases shown in Table 3.2.

Table 3.2: Shielding gases according to the welding material

<table>
<tr><th>Sr. No.</th><th>Materials</th><th>Shielding gases</th></tr>
<tr><td>1.</td><td>Mild Steel</td><td>Argon, Helium, Argon+ Helium</td></tr>
<tr><td>2.</td><td>Stainless Steel</td><td>Argon, Argon + hydrogen (max 5%)</td></tr>
<tr><td>4.</td><td>Magnesium</td><td rowspan="3">Argon is preferable for Lower thickness<br>Helium is preferable for higher thickness (deep penetration)</td></tr>
<tr><td>5.</td><td>Copper/Nickel</td></tr>
<tr><td>6.</td><td>Titanium</td></tr>
</table>

### 3.2.3 Electrode

Non consumable electrodes generally of tungsten material are used in TIG welding of different diameters according to the heat required. The different material of electrode is given in the table below with color coding show in Fig. 3.3.

Table 3.3: Different electrodes to be used in TIG welding

| Electrode | Composition | Color |
|---|---|---|
| EWP | Pure W | Green |
| EW Th-17 | W+1%Thorium | Yellow |
| EW Th-2 | W+2% Thorium | Red |
| EW Zr | W+(0.14-0.4)% Zerconium | Brown |

## 3.3 Workpiece Materials

Materials to be used in this experimental study are Stainless steel AISI 304, Stainless steel AISI 316 and AISI 4340. AISI 304 and AISI 316 both materials are from austenitic group of steels and AISI 4340 is a high tensile low carbon alloy steel. Before the welding of these it is necessary to know about the composition of the materials. Compositions of materials are as written in the Table 3.4.

**AISI 304 and AISI 316**

Austenitic steels: From survey in market it has been concluded that AISI 304 grade steel is mostly used material in industry. Steels of these series are characterized by its chromium and nitrogen content. For welding of austenitic steel filler metal used is same as that of base metal. Chemical compositions listed below in table are obtained by Atomic absorption spectrometer.

Table 3.4: Chemical compositions of AISI 304 and AISI 316 grades metal.

| Metal | Main chemical constituents % | | | | | | | | | |
|---|---|---|---|---|---|---|---|---|---|---|
| | Fe | C | Si | Mn | P | S | Cr | Mo | Ni | Cu |
| AISI 304 | 69.0 | 0.05 | 0.33 | 0.978 | 0.049 | 0.008 | 18.2 | 0.912 | 10.14 | 0.382 |
| AISI 316 | 70.0 | 0.07 | 0.29 | 0.36 | 0.06 | 0.009 | 17.9 | 0.005 | 9.02 | 1.42 |

**AISI 4340 (High Tensile Low Alloy Carbon Steel)**

Chemical composition listed below in Table 3.5 is obtained by Atomic absorption spectrometer.

Table 3.5: Chemical composition of AISI 4340

| Metal | Main chemical constituents % | | | | | | | | | |
|---|---|---|---|---|---|---|---|---|---|---|
| | Fe | C | Si | Mn | P | S | Cr | Mo | Ni | Cu |
| AISI 4340 | 95.4 | 0.39 | 0.250 | 0.789 | 0.035 | 0.040 | 0.800 | 0.270 | 1.577 | 0.152 |

## 3.4 Selection of Parameters

The different parameters taken for welding with TIG are welding current, shielding gas, gas flow rate, gas type, pre-heating temperature and post-heating temperature. The parameters are discussed one by one in details. Before deciding the values of the parameter some pilot experimental and theoretical studies were taken in consideration to conclude.

### 3.4.1 Welding Current

Pilot study was carried out to identify the value of welding current as it is the most important parameter during TIG welding (because TIG welding works on the constant current characteristics). Pilot studies of welding current on AISI 316, AISI 316 and AISI 4340 were done on several current values from 145 A to 190 A shown in Fig. 3.2. Because of the dissimilar material joint it was very difficult to fix the welding current values, so welding current has to be selected in such a way that both the materials with stand at that current values. When the pilot study of AISI 4340 having thickness 5 mm was done, it was seen that cracks were formed on the surface, so it was concluded that AISI 4340 will not withstand 190 A current shown in Fig. 3.3. When same was done with stainless steel materials, there was also overheating, material was burnt out and came out from back side of the plate. By studying all the pilot experimental outputs it was decided to set the values of welding current of **AISI 316 at** 145, 165 and 185 A, **AISI 316 at** 145, 165 and 185 in A and **AISI 4340** at 145, 165 and 185 A for the thickness of 5 mm plate.


Figure 3.2: Pilot experiments at 150 A and 185 A current on AISI 4340 current

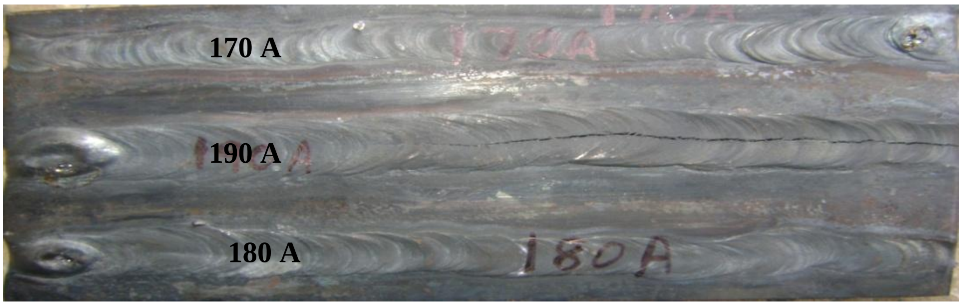


Figure 3.3: Pilot experiments at 170 A, 190 A and 180 A current on AISI 4340

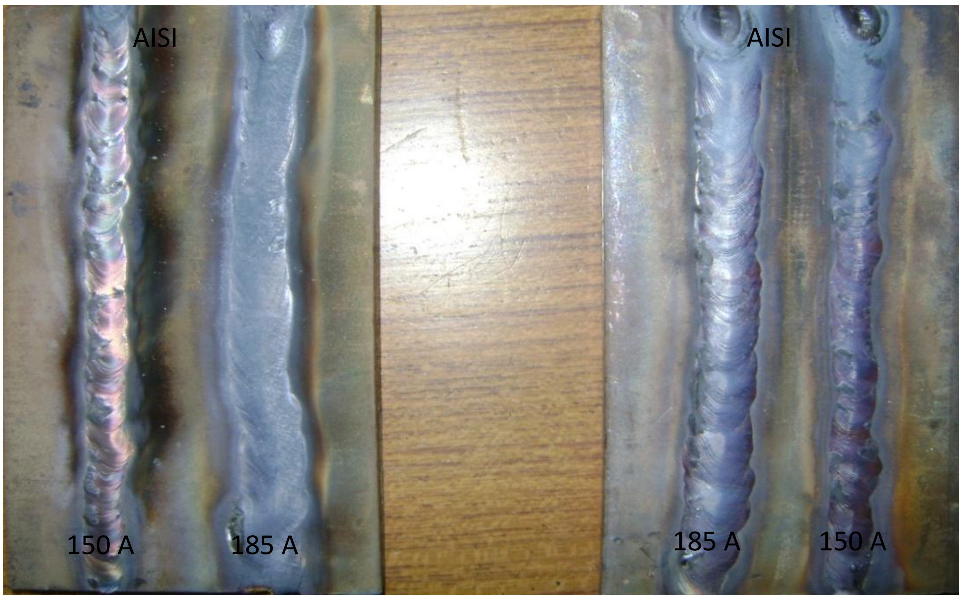


Figure 3.4: Variation in current 150 A and 185 A on both AISI 304 and AISI 316 while doing pilot study.

### 3.4.2 Shielding Gases and Gas Flow Rate

Three shielding gases namely pure argon, mixture of 70% Ar + 30% He and a mixture of argon and hydrogen 1.5% gas will going to be used for welding dissimilar metals to have variations in the welding joints. Gas cylinders of 10 liter capacity containing mixture of 70%

Ar + 30% He and argon-hydrogen 1.5% mixture will be obtained from Dwarka Mai Gases, Jalandhar shown in Fig. 3.5.

Figure 3.5: Cylinder of argon gas, 70% Ar + 30% He gas and argon - hydrogen 1.5% mixture gas

### 3.4.3 Filler Wire

There are five filler wires chosen for welding of (AISI 304 with AISI4340) and (AISI 316 with AISI 4340). Materials of filler wire are 316, 309, 4340 and 304 (ER304L) of size Ø2.4 mm X 1000 mm long and 308 of size 2.4 mm X 500 mm long, as shown in the Fig. 3.6.


(a) Filler 304 (b) Filler 309


(c) EN 24 (d) Filler 316

Figure 3.6: Filler wires

### 3.4.4 Pre-heating and Post-heating Temperature

As it is seen from the past that there is no need to pre heat Austenitic stainless steels. But to improve the mechanical properties pre-heating will be necessarily done for AISI 4340. Figure 3.7 shows effect of welding current at 190 A after preheating at 250 $^{o}$C. From several studies the pre-heating temperatures should be in between 200 $^{o}$C to 300 $^{o}$C. So the temperatures set for pre-heating of AISI 4340 are no preheating, preheating at 175 $^{o}$C and preheating at 250 $^{o}$C. It was seen that the crack formation is less as compared to the crack formation seen in AISI 4340 at 190 A without preheating. Post-heating was also done by three factors no post-heating, post-heating at 500 $^{o}$C and post heating at 650 $^{o}$C. Post-heating helps to relief the stress from the metal and refines the mechanical properties. Baking oven used for pre-heating temperature is as shown in Fig. 3.8


Figure 3.7: Pilot study AISI 4340 having current of 190 A and pre-heating temperature at 250 $^{o}$C

Hot cracking at 250 $^{o}$C preheating


Figure 3.8: Baking oven used for pre-heating temperature.

Infrared thermometer used for the measurement of temperature after post-heating to varify the temperature shown in Fig. 3.9


Figure 3.9: Infrared thermometer used for the measurement of temperature

### 3.4.5 Electrode

Non-consumable tungsten electrode = EWTh-2 (Thoriated tungsten) of 2.4 mm diameter, electrode to work angle 45$^{o}$ and DCEN electrode polarity was used for welding of specimens. Non-consumable electrodes are as shown in Fig. 3.10.

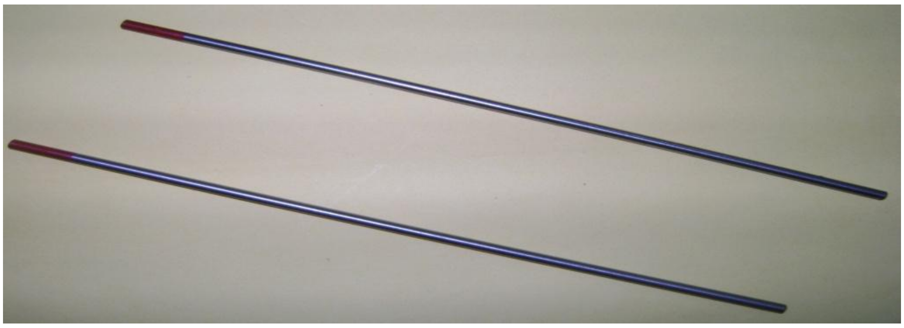

Figure 3.10**:** Non-consumable electrodes of diameter 2.4 mm

## 3.5 Design of Experiment

In any experimental research, when experimental test procedure is time consuming to satisfy the need design objectives with the least number of trials are an important requirement. In this case, Taguchi experimental technique provides an efficient and systematic approach for experiments to determine near optimum value of process parameters for its performance. Taguchi technique involves laying out the experimental conditions using specially constructed tables known as ‘orthogonal arrays’. Orthogonal arrays significantly reduce the number of experimental configurations to be trial. The results given by small scale experimental trial are valid over the entire experimental region spanned by the control factors. The most important stage in Taguchi technique is the design of experiment lies in the selection of the control factors. So, a large number of factors are included initially so that non-significant variables can be excluded at the earliest opportunity. Literature review reveals that parameters viz., current, gas type, gas flow rate, filler, pre-heating and post-heating temperatures largely influence the welding parameters. Thus, the impacts of six process parameters are studied using L27 orthogonal array design. The control factors and the parameter settings for welding are given in Table 3.6 and Table 3.8. Table 3.6 and Table 3.7 presents the selected levels for various control factors. The standard linear graph, as shown in Figure 3.11, is used to assign the factors and interactions to various columns of the orthogonal array.

Table 3.6**:** Process parameters and three levels for the AISI 304 and AISI 4340

| Sr. No. | Parameter | Symbol | Units | Levels | | |
|---|---|---|---|---|---|---|
| | | | | 1 | 2 | 3 |
| 1. | Welding current | *A* | A | 145 | 165 | 185 |
| 2. | Filler type | *B* | | 304 | E24 | 308 |
| 3. | Shielding gas | *C* | | Ar | 70% Ar + 30% He | Ar + 1.5% $H_2$ |
| 4. | Gas flow rate | *D* | L/min | 12 | 14 | 16 |
| 5. | Pre-heating temperature of AISI4340 | *E* | $^oC$ | No | 175 | 250 |
| 6. | Post-heating temperature | *F* | $^oC$ | No | 500 | 650 |

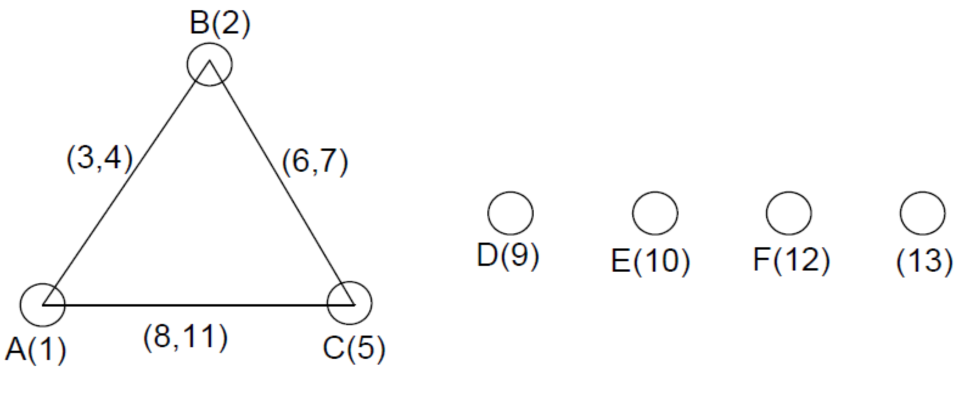


Figure 3.11: Linear graph for L27 orthogonal array

Table 3.7: Process parameters and three levels for AISI 316 and AISI4340

| Sr. no. | Parameter | Symbol | Units | Levels | | |
|---|---|---|---|---|---|---|
| | | | | 1 | 2 | 3 |
| 1. | Welding current | *A* | A | 145 | 165 | 185 |
| 2. | Filler type | *B* | | 316 | EN24 | 309 |
| 3. | Shielding gas | *C* | | Ar | 70% Ar + 30% He | Ar + 1.5% $H_2$ |
| 4. | Gas flow rate | *D* | L/min | 12 | 14 | 16 |
| 5. | Pre heating temperature of AISI 4340 | *E* | $^oC$ | No | 175 | 250 |
| 6. | Post heating temperature | *F* | $^oC$ | No | 500 | 650 |

The selected parameters viz., current, gas type, gas flow rate, filler, pre-heating and post- heating each at three levels, are considered in this study. These six parameters each at three levels would require 36 = 729 runs in a full factorial experiment whereas Taguchi's experimental approach reduces it to 27 runs only offering a great advantage. The plan of the experiments as shown in Table 3.8 is as follows: the first, second, fifth, ninth, tenth and twelfth columns are assigned to current (*A*), gas type (*B*), gas flow rate (*C*), filler (*D*), pre-heating temperature (*E*) and post-heating temperature (*E*) respectively. The third and fourth column are assign interaction between current (*A*) and gas type (*B*), the sixth and seventh column are assigned to estimate interaction between current (*A*) and flow rate (*C*), the eighth and eleventh column are assigned to estimate interaction between the gas type (*B*) and flow rate (*C*) and the remaining columns are used to estimate experimental errors.

**Calculation of DOF**

DOF denotes the number of the independent comparisons that can be made in any experiment. The number of factors considered for experimentation, their respective levels determine the total degree of freedom required for designing OA. Mathematically, DOF for each factor is calculated as,

**DOF= n-1**, where n is the level of each factor

Factors and degree of freedom are shown in Table 3.8

Table 3.8: Factors and degrees of freedom

| Sr. no. | Factors | Unit | Degree of freedom |
|---|---|---|---|
| 1 | Welding current | A | 2 |
| 2 | Gas type | - | 2 |
| 3 | Flow rate | L/min | 2 |
| 4 | Filler | - | 2 |
| 5 | Pre-heating | ºC | 2 |
| 6 | Post-heating | ºC | 2 |

**Orthogonal array**

The experimental layout for the welding parameters using the L27 orthogonal array is shown in Table 3.9 and Table 3.10.

Table 3.9: Orthogonal array for welding of AISI 304 with AISI 4340 grade.

| Exp. No. | Welding current (A) | Gas type | Flow rate (L/min) | Filler | Pre-heating ($^oC$) | Post-heating ($^oC$) |
|---|---|---|---|---|---|---|
| 1 | 145 | Ar | 12 | 304 | No | No |
| 2 | 145 | Ar | 14 | EN24 | 175 | 500 |
| 3 | 145 | Ar | 16 | 308 | 250 | 650 |
| 4 | 145 | 70% Ar + 30% He | 12 | EN24 | 175 | 650 |
| 5 | 145 | 70% Ar + 30% He | 14 | 308 | 250 | No |
| 6 | 145 | 70% Ar + 30% He | 16 | 304 | No | 500 |
| 7 | 145 | Ar + 1.5% $H_2$ | 12 | 308 | 250 | 500 |
| 8 | 145 | Ar + 1.5% $H_2$ | 14 | 304 | No | 650 |
| 9 | 145 | Ar + 1.5% $H_2$ | 16 | EN24 | 175 | No |
| 10 | 165 | Ar | 12 | EN24 | 250 | 500 |
| 11 | 165 | Ar | 14 | 308 | No | 650 |
| 12 | 165 | Ar | 16 | 304 | 175 | No |
| 13 | 165 | 70% Ar + 30% He | 12 | 308 | No | No |
| 14 | 165 | 70% Ar + 30% He | 14 | 304 | 175 | 500 |
| 15 | 165 | 70% Ar + 30% He | 16 | EN24 | 250 | 650 |
| 16 | 165 | Ar + 1.5% $H_2$ | 12 | 304 | 175 | 650 |
| 17 | 165 | Ar + 1.5% $H_2$ | 14 | EN24 | 250 | No |
| 18 | 165 | Ar + 1.5% $H_2$ | 16 | 308 | No | 500 |
| 19 | 185 | Ar | 12 | 308 | 175 | 650 |
| 20 | 185 | Ar | 14 | 304 | 250 | No |
| 21 | 185 | Ar | 16 | EN24 | No | 500 |
| 22 | 185 | 70% Ar + 30% He | 12 | 304 | 250 | 500 |
| 23 | 185 | 70% Ar + 30% He | 14 | EN24 | No | 650 |
| 24 | 185 | 70% Ar + 30% He | 16 | 308 | 175 | No |
| 25 | 185 | Ar + 1.5% $H_2$ | 12 | EN24 | No | No |
| 26 | 185 | Ar + 1.5% $H_2$ | 14 | 308 | 175 | 500 |
| 27 | 185 | Ar + 1.5% $H_2$ | 16 | 304 | 250 | 650 |

Table 3.10: Orthogonal array for welding AISI 316 with AISI 4340 grade.

| Exp. no. | Welding Current (A) | Gas type | Flow rate (L/min) | Filler | Pre-heating ($^oC$) | Post-heating ($^oC$) |
|---|---|---|---|---|---|---|
| 1 | 145 | Ar | 12 | 316 | No | No |
| 2 | 145 | Ar | 14 | EN24 | 175 | 500 |
| 3 | 145 | Ar | 16 | 309 | 250 | 650 |
| 4 | 145 | 70% Ar + 30% He | 12 | EN24 | 175 | 650 |
| 5 | 145 | 70% Ar + 30% He | 14 | 309 | 250 | No |
| 6 | 145 | 70% Ar + 30% He | 16 | 316 | No | 500 |
| 7 | 145 | Ar + 1.5% $H_2$ | 12 | 309 | 250 | 500 |
| 8 | 145 | Ar + 1.5% $H_2$ | 14 | 316 | No | 650 |
| 9 | 145 | Ar + 1.5% $H_2$ | 16 | EN24 | 175 | No |
| 10 | 165 | Ar | 12 | EN24 | 250 | 500 |
| 11 | 165 | Ar | 14 | 309 | No | 650 |
| 12 | 165 | Ar | 16 | 316 | 175 | No |
| 13 | 165 | 70% Ar + 30% He | 12 | 309 | No | No |
| 14 | 165 | 70% Ar + 30% He | 14 | 316 | 175 | 500 |
| 15 | 165 | 70% Ar + 30% He | 16 | EN24 | 250 | 650 |
| 16 | 165 | Ar + 1.5% $H_2$ | 12 | 316 | 175 | 650 |
| 17 | 165 | Ar + 1.5% $H_2$ | 14 | EN24 | 250 | No |
| 18 | 165 | Ar + 1.5% $H_2$ | 16 | 309 | No | 500 |
| 19 | 185 | Ar | 12 | 309 | 175 | 650 |
| 20 | 185 | Ar | 14 | 316 | 250 | No |
| 21 | 185 | Ar | 16 | EN24 | No | 500 |
| 22 | 185 | 70% Ar + 30% He | 12 | 316 | 250 | 500 |
| 23 | 185 | 70% Ar + 30% He | 14 | EN24 | No | 650 |
| 24 | 185 | 70% Ar + 30% He | 16 | 309 | 175 | No |
| 25 | 185 | Ar + 1.5% $H_2$ | 12 | EN24 | No | No |
| 26 | 185 | Ar + 1.5% $H_2$ | 14 | 309 | 175 | 500 |
| 27 | 185 | Ar + 1.5% $H_2$ | 16 | 316 | 250 | 650 |

**Response characteristics**

The response variables are listed below in the Table 3.11.

Table 3.11: Response Characteristics

| Response name | Response type | Unit |
|---|---|---|
| Tensile strength | Higher the better | MPa |
| Toughness | Higher the better | J |
| Hardness | Nominal the better | HRC |
| Distortion | Lower the better | $\theta$ |
| Cracks measurement | Lower the better | |

**Welding of specimens**

As previously decided L27 orthogonal array was chosen and welding on specimens was carried out by using TIG welding machine (Make: TECHNO WELD, INDIA, model MDX-300) available at central workshop Thapar University, Patiala, according to the nine experimental parameter combinations previously decided. All necessary precautions for the operator like hand gloves, helmet with shield, apron etc. were used as shown in the figure 3.12.

Figure 3.12: TIG welding on the specimens

All welded specimens immediately after welding are shown in the Figure 3.13 and 3.14

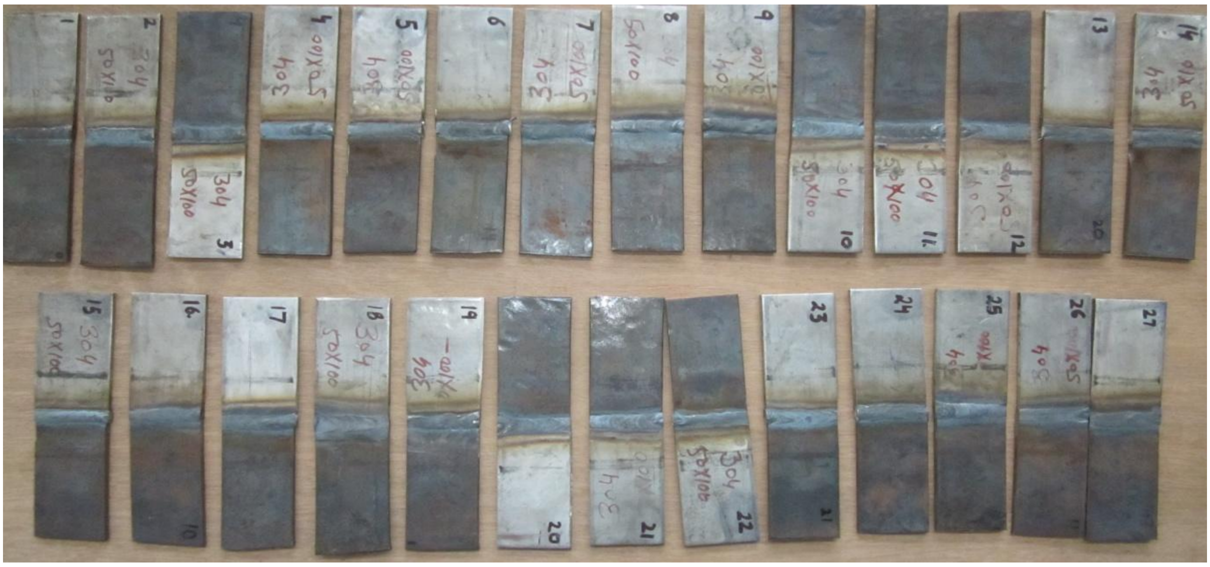

Figure 3.13: Specimens of AISI 304 welded with AISI 4340 grade stainless steel immediately after welding

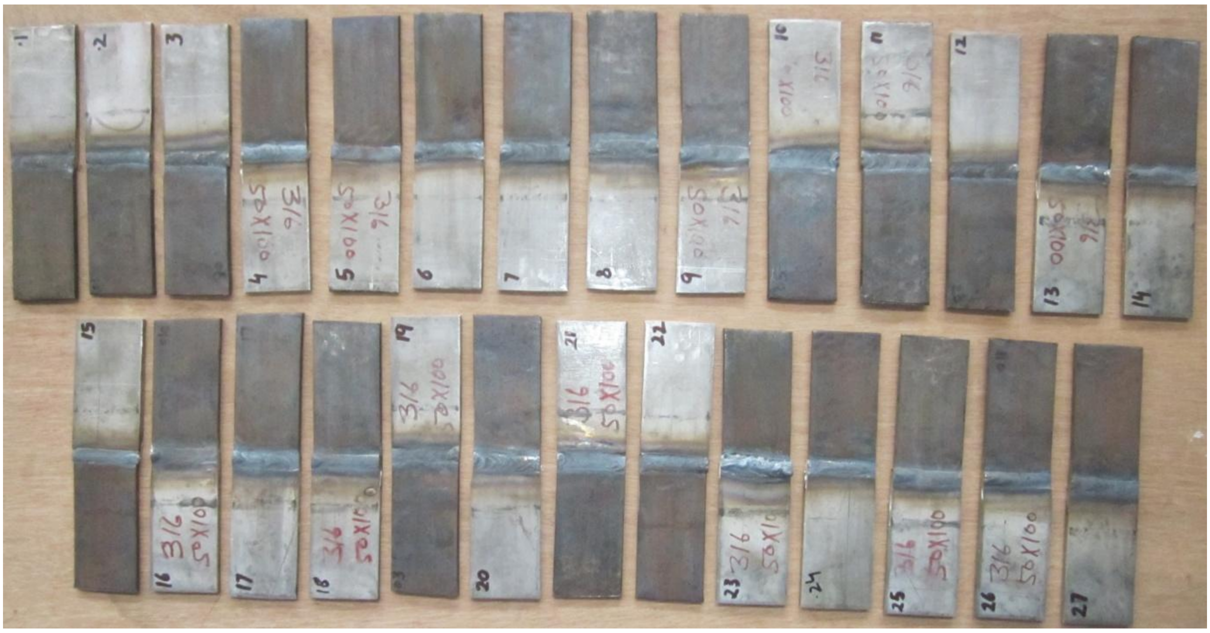

Figure 3.14: Specimens of AISI 316 welded with AISI 4340 grade stainless steel immediately after welding

**Cutting of welded specimens for mechanical testing, microstructure**

For the purpose of testing (mechanical, chemical and optical) of welded joints, cutting was done on the surface grinder machine for various testing (Make: Arvinder Engg. Works, India) as shown in the Fig. 3.15.

Figure 3.15: Surface grinder machine.
(**Courtesy:** Central Workshop, Thapar University, Patiala)

Welded plates were marked for various tests (mechanical and optical) as shown in the Fig. 3.16

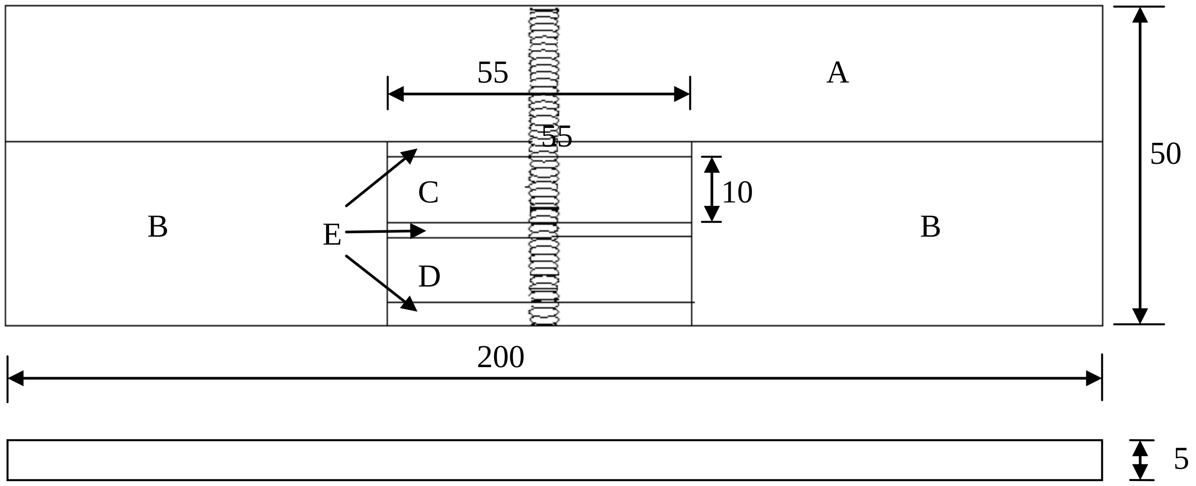


Figure 3.16: Marking and cutting of plates after welding (All dimension are in mm)

Table 3.12: Description of various marked portions in the welded specimens (refer figure 3.16)

| Part name | Use |
|---|---|
| A | Specimen for tensile test |
| B | Rejection at side of plates |
| C | Specimen for impact test |
| D | Specimen for hardness and SEM |
| E | Waste while cutting the specimen |

## 3.6 Measurement Setup

After selecting the parameter for welding it is necessary to investigate the results from these parameters. To calculate or study the results from these parameters measurement setup are required.

**Testing of weld specimen**

Tests to be performed on welded specimens are as follows:

- Tensile strength
- Toughness
- Microhardness
- Weld distortion
- Metallurgical analysis (SEM)
- Dye penetration test

### 3.6.1 Tensile Strength

A ratio of maximum load a material can support without fracture when being stretched to the area of the cross section of the material. When the stresses less than the tensile strength are removed, a material completely or partially returns to its position. As the stress approaches that of the tensile strength, a material that has begun to flow forms of narrow, constricted region is easily fractured. Tensile strength are measured in units of force per unit area.

Universal tensile testing machine is used to carry out tensile strength. Tensile rectangular specimens are prepared according to ASTM E8-04 of dimensions 200 mm×20 mm×5 mm and a uniaxial load is applied from both the ends. Readings of various specimens by using the different type of parameters current, gas type, gas flow rate, fillers, pre-heating and post-heating are taken on UTM. In the present work, this test is performed on the computerized universal testing machine (Make: HEICO Ltd. – New Delhi, India, Load capacity – 60000 N) and the results are used to calculate the tensile strength of metallic samples. Computerized universal testing machine is as shown in Fig.3.17. Sample size for tensile strength is as Shown in Fig. 3.18. Sample specimens are as shown in Fig. 3.19.

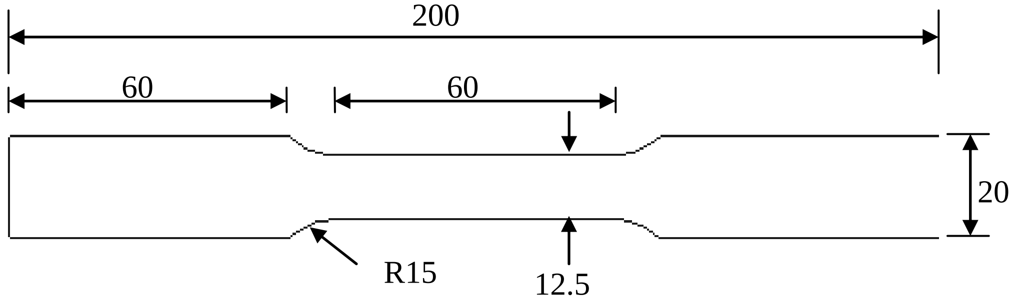

Figure 3.18: All dimension in mm for tensile strength according to ASTM E8-04 (dimension are in mm)

Figure 3.19: Specimen for tensile testing

### 3.6.2 Impact Test

Impact strength of a material is defined as the resistance offered by the material against the suddenly applied load. It is also defined as the maximum amount of energy absorbed by the material when subjected to sudden load. Impact test on the weld specimen is performed on the impact testing machine (Make: Alfred J. Amsler & Co., Switzerland) having a range of 0-30 Kgm or 0-300 joules as shown in the Fig. 3.20 Specimens will be prepared according to ASTM standards A-370 (2010).

Figure 3.20: Impact testing machine
(**Courtesy:** Solid Mechanics Lab, MED, Thapar University, Patiala)

Specimens were prepared according to ASTM standards A-370 (2010) and having size as cross – section of 10 mm × 5 mm × 55 mm shown in Fig. 3.21.

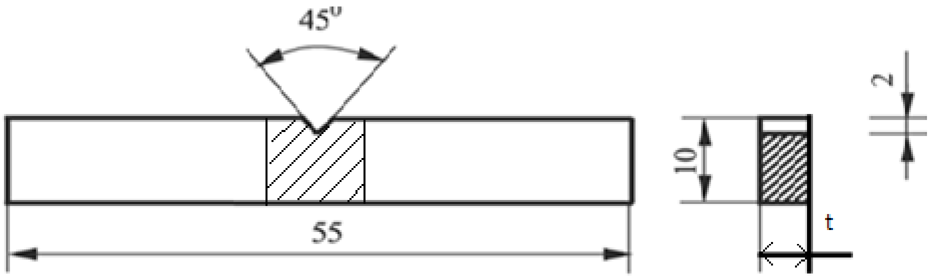


Figure 3.21: Standard size of impact test specimen according to ASTM standard A-370 (dimension in mm)

Fig. 3.22 shows the actual sample ready for impact test.

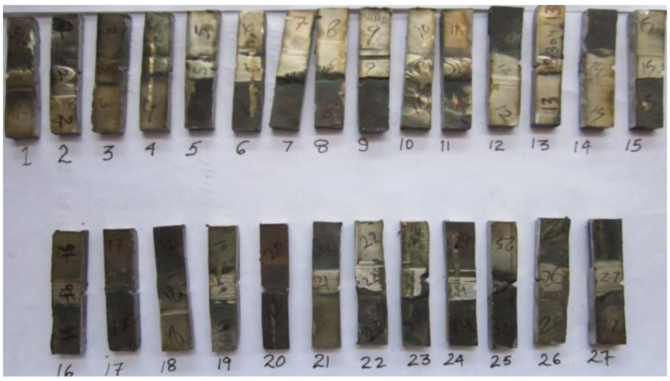

Figure 3.22: Samples prepared for impact strength showing the notch angle and all sizes

### 3.6.3 Microhardness Test

**Indentation Harness Test**

Indentation hardness tests are used to determine the hardness of a material to deformation. Several such tests exist, wherein the examined material is indented until an impression is formed; these tests can be performed on microscopic scale. Microhardness of the weld region was measured by using the manual interfaced microhardness tester (Make: Mitutoyo, optical technologies Ambattur Industrial Estate, Madras) as shown in Fig. 3.23. The measurement was dependent on the size of indentation on the samples. The diagonals of the indents formed by a pyramid- shaped diamond indenter were measured at 40X magnification, which gave a hardness Vickers number (HVN) for micro hardness by putting the average of values in the formula. The hardness values obtained were useful indicators of material properties. The load applied on the indenter was 100 gm. and the dwell time was 20 sec. The samples measuring for micro hardness were firstly ground on the belt grinder, shown in Fig. 3.24 then rubbed with emery paper size no. 400, 600, 800, 1000, 1500 & 2000 and then polished on polishing wheel.


Figure 3.23: Hardness testing machine
(**Courtesy:** Physics Department, Thapar University, Patiala)

Figure 3.24: Belt grinder

### 3.6.4 Distortion Measurement Setup

**To measure the distortion of weld metal the setup is prepared by self**.

In this setup a metallic block is taken from welding shop store room Thapar University, Patiala.

Firstly the block of MS material was taken, after that the first operation for this was to clean up the sides of the block for the orthogonal surface.

Milling operation was done on one of its surface upto the depth of 25 mm to make the groove for holding the welded plate shown in Fig. 3.25. Milling operation was done in Machine shop Thapar University, Patiala.

Figure 3.25: Milling Machine
(**Courtesy:** Machine shop, Thapar University, Patiala)

After milling operation the holes were drilled on Bench drilling machine shown in Fig. 3.26 in fitting shop Thapar University, Patiala having diameter of 2.5 mm.

After the holes are made the threads were made with the help of three tapping keys in Fitting shop Thapar University, Patiala, taping was done manually which was perpendicular to the surface of milling. Nut and bolt arrangement is use to hold the weld piece at the cutting slot. After holding the weld piece a dial gauge indicator is used to measure the setup. This shown in Fig. 3.27 and Fig. 3.28 apparatus is completed


Figure 3.26: Bench drilling machine
(**Courtesy:** Fitting shop, Thapar University, Patiala)

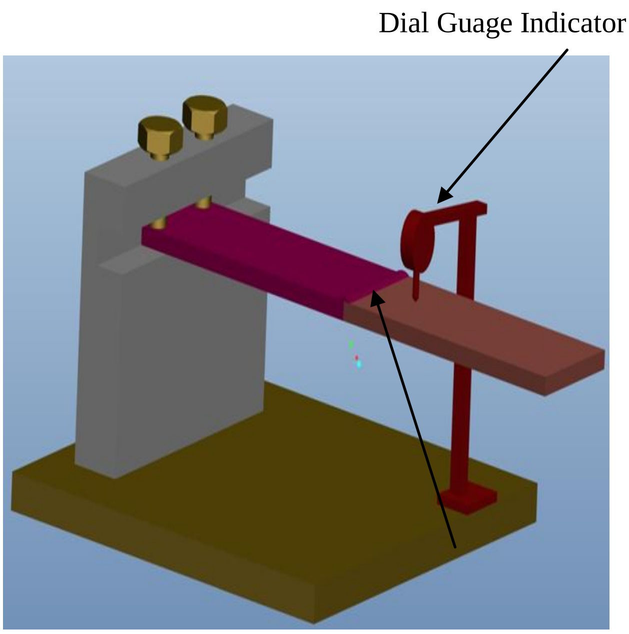

Base Plate

Weld Joint

Figure 3.27: Distortion measurement setup

Figure 3.28: Distortion measurement by fixing the plate by screws.

### 3.6.5 Dye Penetration

DPT (dye penetration test) test will be performed on the welded region to detect the surface cracks and porosity. For performing test, three solutions namely Cleaner CL-96, Pentrant PT-97 and Developer DV-98) were used as shown in the Fig. 3.29.


Figure3.29: Cleaner, penetrant & developer to be used for DPT test of specimen

Steps while performing DPT test were as under:

- Cleaned the test surface for removing the dust, oil, grease, oxide etc. by using the cleaner
- Application of penetrant on the test surface/welded region and allowed penetrant to enter into the weld bead. (approximately 15 minutes waiting)
- Cleaned the surface with a dry and clean cloth.
- Applied of developer on the test surface and allowed the developer to dry out.
- Defect/porosity (if any) appeared on the test surface in the form of colored spot.

### 3.6.6 Scanning Electron Microscope

A scanning electron microscope (SEM) is a type of electron microscope that produces images of a sample by scanning it with a focused beam of electrons. The electrons interact with atoms in the sample, producing various signals that can be detected and that contain information about the sample's surface topography and composition.

Figure 3.30: Scanning Electron Microscope
(**Courtesy:** SAI lab, Thapar University, Patiala)

### 3.6.7 Visual Inspection of Cracks

All the polished specimens prepared above for micro hardness testing were seen under optical (which uses a light beam to view the object) microscope at 200X to find the joint quality in terms of internal defects like crack, porosity, blow hole etc. The optical microscope is as shown in Fig. 3.31.

Figure 3.31: Zeiss optical microscope
(**Courtesy:** Metrology lab, Thapar University, Patiala)

# Chapter 4

# Results and Discussions

## 4.1 Introduction

This chapter deals the effect of selected parameters such as current, type of gas, gas flow rate, type of filler, pre-heating temperature and post-heating temperature on the responses like tensile strength, impact, microhardness, weld distortion, dye penetration, visual inspection of cracks and microstructural observations . Taguchi experimental designs is used to study the effect of different process parameters each varied at three level and their interactions using L27 orthogonal array having 27 trials for the different set of materials. After conducting the experimental study using L27 orthogonal array (OA), various tests are performed such as measurement of tensile test, toughness test, microhardness test, microstructural observation by scanned electron microscopy, weld distortion, dye penetration test and visual inspection of cracks. Besides, the results one analyzed using analysis of variance (ANOVA), response table, main effect plots and best optimal design is obtained. From the analysis of results effect of significant parameters on responses and their behavior are also discussed.

## 4.2 Tensile Strength

Universal tensile testing machine is used to carry out tensile strength. Tensile rectangular specimens are prepared according to ASTM E8-04 of dimensions 200 mm×20 mm×5 mm and a uniaxial load is applied from both the ends. Readings of various specimens by using the different type of parameters current, gas type, gas flow rate, fillers, pre-heating and post-heating are taken on UTM. In the present work, this test is performed on the computerized universal testing machine (Make: HEICO Ltd. – New Delhi, India, Load capacity – 60000 N) and the results are used to calculate the tensile strength of metallic samples. Specimens after tensile test are shown in Fig. 4.1.

Figure 4.1: Specimen after Tensile strength

### 4.2.1 Tensile Strength of Welding Joint AISI 304 with AISI 4340

Results of tensile test of joint AISI 304 and AISI 4340 are shown in Table 4.1. These results are analyzed using analysis of variance ANOVA technique. It helps in identifying the important process parameters affecting the responses.

Table 4.1: Results for tensile strength of joint between AISI 304 and AISI 4340

| Exp. no. | Welding current (A) | Gas type | Flow rate (L/min) | Filler | Pre-heating (°C) | Post-heating (°C) | Tensile strength (MPa) |
|---|---|---|---|---|---|---|---|
| 1 | 145 | Ar | 12 | 304 | No | No | 204.32 |
| 2 | 145 | Ar | 14 | EN24 | 175 | 500 | 373.12 |
| 3 | 145 | Ar | 16 | 308 | 250 | 650 | 196.16 |
| 4 | 145 | 70% Ar +30% He | 12 | EN24 | 175 | 650 | 561.12 |
| 5 | 145 | 70% Ar +30% He | 14 | 308 | 250 | No | 635.84 |
| 6 | 145 | 70% Ar +30% He | 16 | 304 | No | 500 | 392.32 |
| 7 | 145 | Ar + 1.5% $H_2$ | 12 | 308 | 250 | 500 | 587.04 |
| 8 | 145 | Ar + 1.5% $H_2$ | 14 | 304 | No | 650 | 561.12 |
| 9 | 145 | Ar + 1.5% $H_2$ | 16 | EN24 | 175 | No | 204.32 |
| 10 | 165 | Ar | 12 | EN24 | 250 | 500 | 106.40 |
| 11 | 165 | Ar | 14 | 308 | No | 650 | 452.96 |
| 12 | 165 | Ar | 16 | 304 | 175 | No | 122.72 |
| 13 | 165 | 70% Ar +30% He | 12 | 308 | No | No | 492.48 |
| 14 | 165 | 70% Ar +30% He | 14 | 304 | 175 | 500 | 635.84 |
| 15 | 165 | 70% Ar +30% He | 16 | EN24 | 250 | 650 | 278.24 |
| 16 | 165 | Ar + 1.5% $H_2$ | 12 | 304 | 175 | 650 | 770.88 |
| 17 | 165 | Ar + 1.5% $H_2$ | 14 | EN24 | 250 | No | 635.84 |
| 18 | 165 | Ar + 1.5% $H_2$ | 16 | 308 | No | 500 | 732.32 |
| 19 | 185 | Ar | 12 | 308 | 175 | 650 | 271.04 |
| 20 | 185 | Ar | 14 | 304 | 250 | No | 260.00 |
| 21 | 185 | Ar | 16 | EN24 | No | 500 | 197.12 |
| 22 | 185 | 70% Ar +30% He | 12 | 304 | 250 | 500 | 166.24 |
| 23 | 185 | 70% Ar +30% He | 14 | EN24 | No | 650 | 392.32 |
| 24 | 185 | 70% Ar +30% He | 16 | 308 | 175 | No | 470.40 |
| 25 | 185 | Ar + 1.5% $H_2$ | 12 | EN24 | No | No | 492.48 |
| 26 | 185 | Ar + 1.5% $H_2$ | 14 | 308 | 175 | 500 | 734.40 |
| 27 | 185 | Ar + 1.5% $H_2$ | 16 | 304 | 250 | 650 | 557.28 |

**Analysis of variance of tensile strength**

To find out the significance of various factors like current, gas type, gas flow rate, filler type, pre-heating temperature and post-heating on tensile strength. ANOVA is performed at measured data with 90% confidence level. *F*-test is utilized for assess relative significance of each input parameter on the response tensile strenght. The principle of *F*-test is that the greater the *F* value for a particular input parameter, the larger is its effect on the output parameter. ANOVA table for tensile strength of joint between AISI 304 and AISI 4340 is shown in Table 4.2. ANOVA table consists of symbol, sum of squares, variance, *F*- value and percentage contribution for different sources.

Table 4.2: ANOVA table for tensile strength of joint between AISI 304 and AISI 4340

| Sources | Symbol | DF | SS | Variance | *F* - value | PC |
|---|---|---|---|---|---|---|
| Current (A) | *A* | 2 | 28293 | 14147 | 3.69 | 2.63 |
| Gas type | *B* | 2 | 537530 | 268765 | 70.08 | 50.014 |
| Flow rate (L/min) | *C* | 2 | 135314 | 67657 | 17.64 | 12.5 |
| Filler | *D* | 2 | 102649 | 51325 | 13.38 | 9.55 |
| Pre-heating(ºC) | *E* | 2 | 30194 | 15097 | 3.94 | 2.80 |
| Post-heating(ºC) | *F* | 2 | 16738 | 8369 | 2.18 | 1.55 |
| Current × Gas type | *A* × *B* | 4 | 130979 | 32745 | 8.54 | 12.18 |
| Current × Flow rate | *A* × *C* | 4 | 66731 | 16683 | 4.35 | 6.20 |
| Gas Type × Flow rate | *B* × *C* | 4 | 18654 | 4663 | 1.22 | 1.73 |
| Error | | 2 | 7671 | 3835 | | 0.713 |
| Total | | 26 | 1074753 | | | 100 |

(SS= Sum of square, DF= Degree of freedom, F= F factor, PC = Percent contribution)

Figure 4.2 shows the main effect plot of tensile strength for various parameters. In the plot X-axis shows the process parameters and Y-axis shows the tensile strength and center line shows the mean of tensile strength. Main plot shows the trend followed by the output parameter with varying different values of parameters *A*, *B*, *C*, *D*, *E* and *F*. There is large influence of gas type, gas flow rate, filler and interaction current × gas type on tensile strength as compared to other parameters as shown in main effect plot and by observing the *F*- value and percentage contribution from ANOVA table. The tensile strength for gas type increases from Ar to 70% Ar + 30% He and continuously increasing upto Ar + $1.5H_2$ due to the thermal conductivity of gases. In the main effect plot it is seen that the tensile strength increase from gas flow rate 12 L/min to 14 L/min and then decreases from 14 L/min to 16 L/min because at some particular gas flow rate value, the gas shows the shielding effect with moderate cooling effect which diffuses metal properly but as the value of gas flow rate increases from that particular value it increases the cooling effect and readily cool down the heated metal which refuses the diffusion properly leads to the low penetration that why the value of tensile strength decreases when going through14 L/min to 16 L/min gas flow rate. Filler metal has significant contribution seen in ANOVA table as well as in main effect plot shown in Fig. 4.2 in the tensile strength due to its chemical composition. Current has 2.63% percentage contribution in the tensile test as shown. Effect of pre-heating and post-heating is not too much influencing in tensile strength as seen in main effect plot Fig. 4.2 and percentage contribution in ANOVA table (Table 4.2).

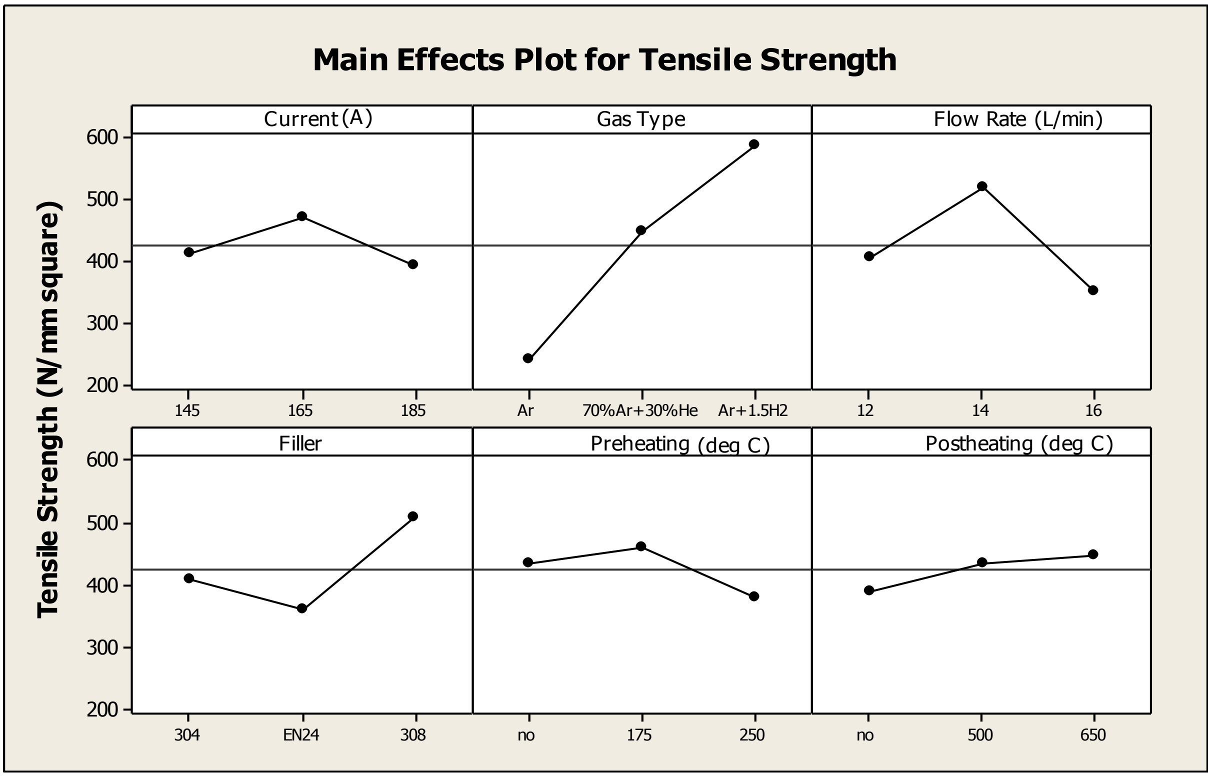


Figure: 4.2: Main Effect Plot of tensile strength for joint AISI 304 with AISI 4340

Figure 4.3 shows the interaction plots for tensile strength correspond to input parameters. Interaction plot tells the combined effect of two parameters which are to be considered. The current × gas interaction has influencing results for tensile strength as seen in ANOVA Table 4.2 and interaction plot in Fig 4.3 as compared to the other parameters. Current individually has not too much significance as seen in ANOVA table but has influencing results when the combined with gas type. Current × gas type gives the combined effect of increases in penetration and thermal conductivity of the different gases.

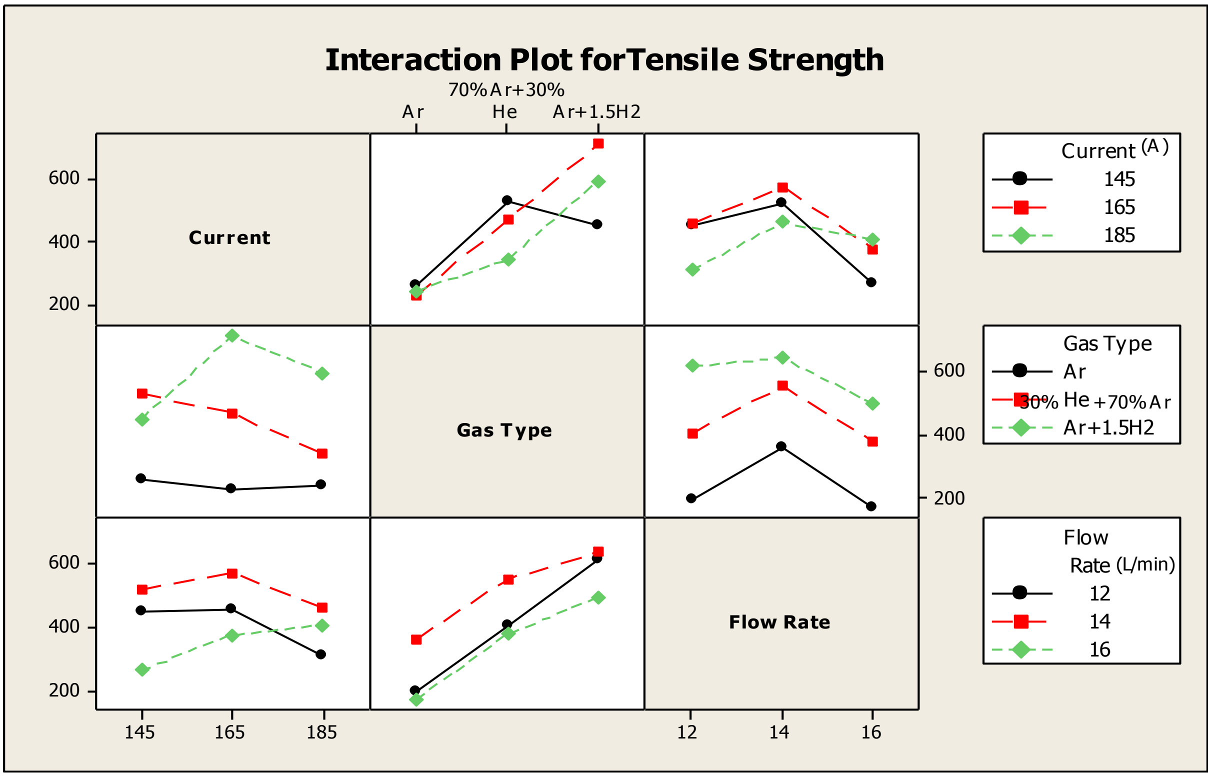


Figure 4.3: Interaction plot of tensile strength for joint AISI 304 with AISI 4340

The various factors are assigned ranks according to their influence on results as shown by ANOVA technique and are listed in Table 4.3. From the response table gas type is the most influencing factor with rank 1 followed by flow rate, filler and other factors. Post-heating parameter is seen to be the most insignificant factor with rank 6.

Table 4.3: Response table for tensile strength joint between AISI 304 and AISI 4340

| Level | Current | Gas type | Flow rate | Filler | Pre-heating | Post-heating |
|---|---|---|---|---|---|---|
| 1 | 412.8 | 242.6 | 405.8 | 407.9 | 435.3 | 390.9 |
| 2 | 469.7 | 447.2 | 520.2 | 360.1 | 460.4 | 436.1 |
| 3 | 393.5 | 586.2 | 350.1 | 508.1 | 380.3 | 449.0 |
| Delta | 76.3 | 343.5 | 170.1 | 148.0 | 80.1 | 58.1 |
| Rank | 5 | 1 | 2 | 3 | 4 | 6 |

**Optimal Design**

The main effect plot and interaction plot in Fig. 4.2 and Fig. 4.3 are used to estimate the maximum tensile strength with optimal design parameters conditions. From Table 4.2 considering higher *F*-value and corresponding percentage contribution gas type, flow rate, filler and interaction between current and gas type are observed significantly influencing the tensile strength. The level of these factors which gives the maximum tensile strength are noted from main effect plot (Fig. 4.2) and the corresponding tensile strength for at these levels of $\overline{B_3}$, $\overline{C_2}$, $\overline{D_3}$ are obtained directly from the Table 4.3. For interactions, levels of current × gas type (A×B) is decided from the interaction plot (Fig. 4.3) and maximum tensile strength is observed at $\overline{A_2 \times B_3}$. To obtain the best estimate of a mean when an interaction is present, the trials that include that treatment condition should be averaged. Average tensile strength for this interaction is obtained by taking the average of three trials (trial 16, 17, 18) for $\overline{A_2 \times B_3}$. Maximum value of gas type, flow rate and filler is selected because tensile strength is 'higher the better' type response. Desired mean value in this case is estimated as:

$$\mu_{B_3,C_2,D_3,A_2\times B_3} = \overline{B_3} + \overline{C_2} + \overline{D_3} + \overline{A_2 \times B_3} - 3\,\overline{T}$$

$$= 586.2 + 520.2 + 508.1 + 713.01 - 3(424.37)$$

$$= 1054.4 \text{ MPa}$$

Confidence interval

$$CI = \sqrt{\frac{F_{\alpha,\nu_1,\nu_2} V_e}{n_{eff}}}$$

Where $F_{\alpha,\nu_1,\nu_2}$ = $F$ ratio

α = 0.1 (risk)

Confidence = 1 – α

$\nu_1$ = DF for mean (always 1)

$\nu_2$ = Total DF (=26)

$\overline{T}$ = Average of an experimental trial

$n_{eff}$ = Number of tests under that condition using the participating factors

$$n_{eff} = \frac{N}{1+DF_{B,C,D,A\times B}} = \frac{27}{1+10} = 2.45$$

N is the number all trials in the experiment

$V_e$ = Variance (of error)

$$CI = \sqrt{\frac{2.91 \times 3835}{2.45}} = \pm 67.49 \text{ MPa}$$

Thus the optimum value of tensile strength is (1054.4 ± 67.49) MPa μ value is 1054.4 MPa which is more than expected value due to influence of some random variable where some parametric combination resulted in very poor joint and low tensile strength (like experiment no. 3, 10, 12). This leads to poor reduction in additivity of interaction terms and in trial average ($\overline{T}$). So optimum value is selected from trial (trials 16, 18, 26) having value above 732 MPa.

### 4.2.2 Tensile Strength of Welding Joint AISI 316 with AISI 4340

Specimens after tensile test are shown in Fig. 4.4

Figure 4.4: Specimen after Tensile strength

Results of tensile test of joint AISI 316 and AISI 4340 are shown in Table 4.4. These results are analyzed using analysis of variance ANOVA technique. It helps in identifying the important process parameters affecting the responses.

Table 4.4: Results for tensile strength of joint between AISI 316 and AISI 4340

| Exp. no. | Welding current (A) | Gas type | Flow rate (L/min) | Filler | Pre-heating ($^oC$) | Post-heating ($^oC$) | Tensile strength (MPa) |
|---|---|---|---|---|---|---|---|
| 1 | 145 | Ar | 12 | 316 | No | No | 559.04 |
| 2 | 145 | Ar | 14 | EN24 | 175 | 500 | 392.96 |
| 3 | 145 | Ar | 16 | 309 | 250 | 650 | 386.72 |
| 4 | 145 | 70% Ar + 30% He | 12 | EN24 | 175 | 350 | 234.40 |
| 5 | 145 | 70% Ar + 30% He | 14 | 309 | 250 | No | 650.40 |
| 6 | 145 | 70% Ar + 30% He | 16 | 316 | No | 500 | 287.20 |
| 7 | 145 | Ar + 1.5% $H_2$ | 12 | 309 | 250 | 500 | 357.60 |
| 8 | 145 | Ar + 1.5% $H_2$ | 14 | 316 | No | 650 | 276.64 |
| 9 | 145 | Ar + 1.5% $H_2$ | 16 | EN24 | 175 | No | 510.72 |
| 10 | 165 | Ar | 12 | EN24 | 250 | 500 | 184.64 |
| 11 | 165 | Ar | 14 | 309 | No | 650 | 112.00 |
| 12 | 165 | Ar | 16 | 316 | 175 | No | 369.60 |
| 13 | 165 | 70% Ar + 30% He | 12 | 309 | No | No | 802.40 |
| 14 | 165 | 70% Ar + 30% He | 14 | 316 | 175 | 500 | 265.44 |
| 15 | 165 | 70% Ar + 30% He | 16 | EN24 | 250 | 650 | 276.64 |
| 16 | 165 | Ar + 1.5% $H_2$ | 12 | 316 | 175 | 650 | 234.40 |
| 17 | 165 | Ar + 1.5% $H_2$ | 14 | EN24 | 250 | No | 248.96 |
| 18 | 165 | Ar + 1.5% $H_2$ | 16 | 309 | No | 500 | 488.96 |
| 19 | 185 | Ar | 12 | 309 | 175 | 650 | 473.60 |
| 20 | 185 | Ar | 14 | 316 | 250 | No | 538.88 |
| 21 | 185 | Ar | 16 | EN24 | No | 500 | 618.88 |
| 22 | 185 | 70% Ar + 30% He | 12 | 316 | 250 | 500 | 538.88 |
| 23 | 185 | 70% Ar + 30% He | 14 | EN24 | No | 650 | 394.40 |
| 24 | 185 | 70% Ar + 30% He | 16 | 309 | 175 | No | 331.04 |
| 25 | 185 | Ar + 1.5% $H_2$ | 12 | EN24 | No | No | 459.20 |
| 26 | 185 | Ar + 1.5% $H_2$ | 14 | 309 | 175 | 500 | 662.88 |
| 27 | 185 | Ar + 1.5% $H_2$ | 16 | 316 | 250 | 650 | 655.52 |

**Analysis of variance of tensile strength**

To find out the significance of various factors like current, gas type, gas flow rate, filler type, pre-heating temperature and post-heating on tensile strength. ANOVA is performed at measured data with 90% confidence level. *F*-test is utilized for assess relative significance of each input parameter on the response tensile strength. The principle of *F*-test is that the greater the *F* value for a particular input parameter, the larger is its effect on the output parameter. ANOVA table for tensile strength of joint between AISI 316 and AISI 4340 is shown in Table 4.5. ANOVA table consists of symbol, sum of squares, variance, *F*- value and percentage contribution for different sources.

Table 4.5: ANOVA table for tensile strength of joint between AISI 316 and AISI 4340

| Sources | Symbol | DF | SS | Variance | *F* - value | PC |
|---|---|---|---|---|---|---|
| Current (A) | *A* | 2 | 160921 | 80460 | 2.56 | 21.00 |
| Gas type | *B* | 2 | 3731 | 1866 | 0.06 | 0.486 |
| Flow rate (L/min) | *C* | 2 | 9038 | 4519 | 0.14 | 1.17 |
| Filler | *D* | 2 | 49930 | 24965 | 0.80 | 6.51 |
| Pre-heating(ºC) | *E* | 2 | 15997 | 7998 | 0.25 | 2.08 |
| Post-heating(ºC) | *F* | 2 | 113078 | 56539 | 1.80 | 14.75 |
| Current × Gas type | *A* × *B* | 4 | 127139 | 31785 | 1.01 | 16.59 |
| Current × Flow rate | *A* × *C* | 4 | 68947 | 17237 | 0.55 | 8.99 |
| Gas Type × Flow rate | *B* × *C* | 4 | 154605 | 38651 | 1.23 | 20.17 |
| Error | | 2 | 62785 | 31393 | | 8.19 |
| Total | | 26 | 766169 | | | |

(SS= Sum of square, DF= Degree of freedom, F= F factor, PC = Percent contribution)

Figure 4.5 shows the main effect plot of tensile strength for various parameters. In the plot X-axis shows the process parameters and Y-axis shows the tensile strength and center line shows the mean of tensile strength. Main plot shows the trend followed by the output parameter with varying different values of parameters *A*, *B*, *C*, *D*, *E* and *F*. There is large influence of current, post-heating, interaction between current × gas type and gas type × flow rate on tensile strength as compared to other parameters as shown in main effect plot in Fig.4.5, interaction plot in Fig. 4.5 and by observing the *F*- value and percentage contribution from ANOVA table. With the increase in the current the tensile strength increases because as more heat input increases penetration increases leads to increase tensile strength. As shown in Fig. 4.5 the tensile strength decreases with the increase in post-heating temperature because with increase in post-heating the residual stresses are reliefied more results in decreases in tensile strength. Filler metal has significant contribution seen in ANOVA table as well as in main effect plot shown in Fig. 4.2 in the tensile strength due to its chemical composition. Gas type has not having any influencing results as its trend is near to the mean line as seen in Fig.4.5. Effect of pre-heating and floe rate are not too much influencing in tensile strength as seen in main effect plot Fig. 4.5 and percentage contribution in ANOVA table (Table 4.5).

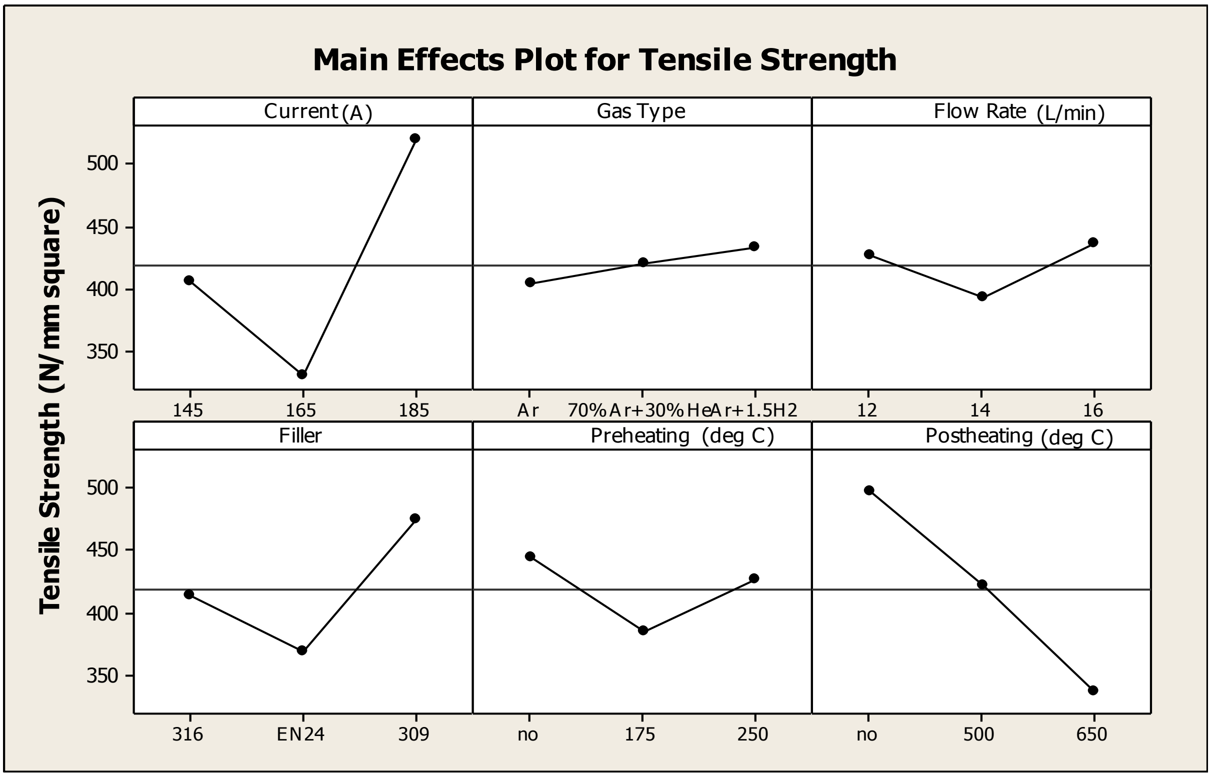


Figure 4.5: Main Effect Plot of tensile strength for joint AISI 316 with AISI 4340

Figure 4.6 shows the interaction plots for tensile strength correspond to input parameters. Interaction plot tells the combined effect of two parameters which are to be considered. The current × gas and gas type × flow rate interactions has influencing results for tensile strength as seen in ANOVA Table 4.5 and interaction plot in Fig 4.6 as compared to the other parameters. Current × gas type gives the combined effect of increases in penetration and thermal conductivity of the different gases which gives the influencing percentage contribution. Similarly gas type × flow rate gives the combined effect of increase in thermal conductivity and cooling input at different values which gives the significant results.

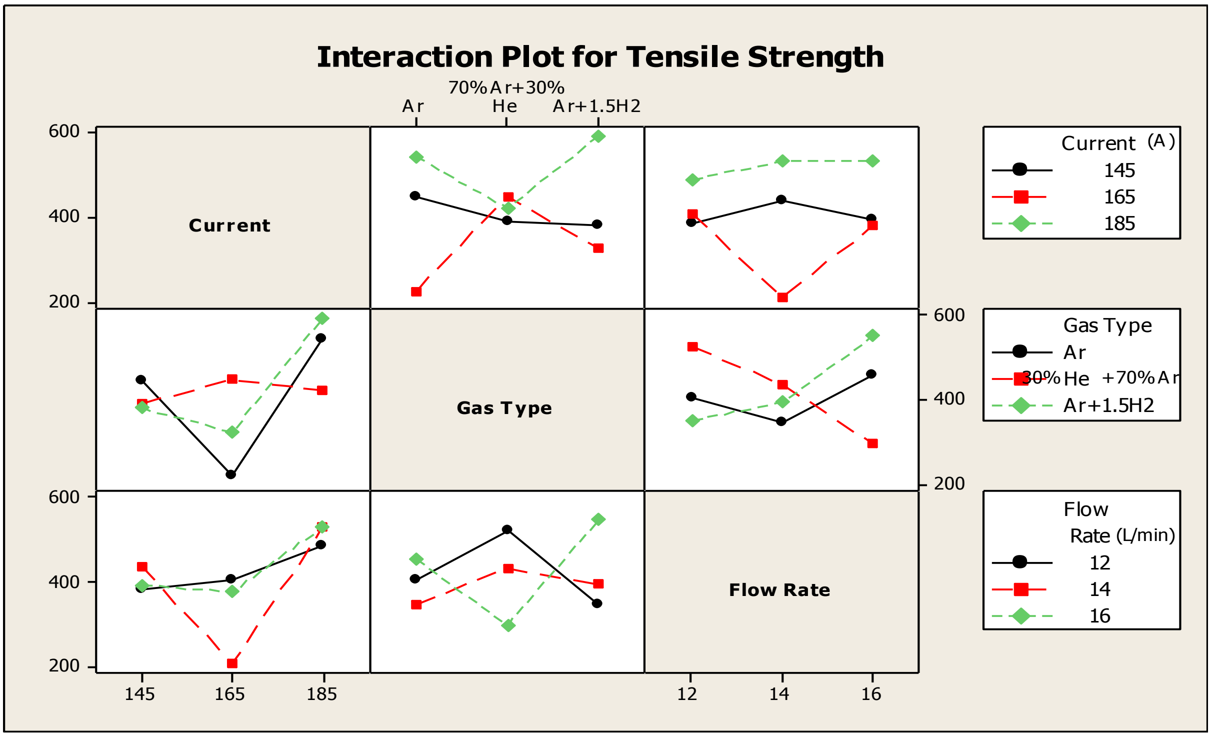


Figure 4.6: Interaction plot of tensile strength for joint AISI 316 with AISI 4340

The various factors are assigned ranks according to their influence on results as shown by ANOVA technique and are listed in Table 4.6. From the response table current is the most influencing factor with rank 1 followed by post-heating, filler, pre-heating and other factors. Gas type parameter is seen to be the most insignificant factor with rank 6.

Table 4.6: Response table for tensile strength joint between AISI 316 and AISI 4340

| Level | Current | Gas type | Flow rate | Filler | Pre-heating | Post-heating |
|---|---|---|---|---|---|---|
| 1 | 406.2 | 404.0 | 427.1 | 414.0 | 444.3 | 496.7 |
| 2 | 331.4 | 420.1 | 393.6 | 369.0 | 386.1 | 421.9 |
| 3 | 519.3 | 435.8 | 436.1 | 474.0 | 426.5 | 338.3 |
| Delta | 187.8 | 28.7 | 42.5 | 105.0 | 58.2 | 158.4 |
| Rank | 1 | 6 | 5 | 3 | 4 | 2 |

### Optimal Design

The main effect plot and interaction plot in Fig. 4.5 and Fig. 4.6 are used to estimate the maximum tensile strength with optimal design parameters conditions. From Table 4.5 considering higher *F*-value and corresponding percentage contribution current, post-heating and interaction between current and gas type, gas type and flow rate are observed significantly influencing the tensile strength. The level of these factors which gives the maximum tensile strength are noted from main effect plot (Fig. 4.5) and the corresponding tensile strength for at these levels of $\overline{A_3}$, $\overline{F_1}$ are obtained directly from the Table 4.6. For interactions, levels of current × gas type (A×B) and gas type × flow rate (B×C) are decided from the interaction plot (Fig. 4.6) and maximum tensile strength is observed at $\overline{A_3 \times B_3}$ and $\overline{B_3 \times C_3}$. To obtain the best estimate of a mean when an interaction is present, the trials that include that treatment condition should be averaged. Average tensile strength for this interaction is obtained by taking the average of three trials (trial 25, 26, 27) for $\overline{A_3 \times B_3}$ and (trial 9, 18, 27) for $\overline{B_3 \times C_3}$. Maximum value of current and post-heating is selected because tensile strength is 'higher the better' type response. Desired mean value in this case is estimated as:

$$\mu_{A_3,F_1,A_3\times B_3,B_3\times C_3} = \overline{A_3} + \overline{F_1} + \overline{A_3 \times B_3} + \overline{B_3 \times C_3} - 3\,\overline{T}$$

$$= 519.3 + 496.7 + 592.53 + 551.73 - 3(418.96)$$

$$= 903.37 \text{ MPa}$$

Confidence interval

$$CI = \sqrt{\frac{F_{\alpha,v_1,v_2} V_e}{n_{eff}}}$$

Where $F_{\alpha,v_1,v_2}$ = $F$ ratio

α = 0.1 (risk)

Confidence = 1 – α

$v_1$ = DF for mean (always 1)

$v_2$ = Total DF (=26)

$\overline{T}$ = Average of all experimental trials

$n_{eff}$ = Number of tests under that condition using the participating factors

$$n_{eff} = \frac{N}{1+DF_{A,F,A\times B,B\times C}} = \frac{27}{1+12} = 2.076$$

N is the number of trial in the experiment

$V_e$ = Variance (of error)

$$CI = \sqrt{\frac{2.91 \times 31393}{2.076}} = \pm 209.77 \text{ MPa}$$

Thus the optimum value of tensile strength is (907.47 $\pm$ 209.77) MPa

μ value is 907.47 MPa which is more than expected value due to influence of some random variable where some parametric combination resulted in very poor joint and low tensile strength (like experiment no. 10, 11, 16). This leads to poor reduction in additivity of interaction terms and in trial average ($\overline{T}$). So optimum value is selected from trial (trials 5, 13, 27) having value above 652 MPa.

## 4.3 Toughness Test

Impact test is used to measure the toughness of the welding joint. The ability of metal to rapidly distribute within itself due to both the stress and strain caused by the suddenly applied load or the ability of the material to withstand shock loading. It is the exact opposite of "brittleness" which carries the implication of sudden failure. The tested specimen after toughness test is shown in Fig. 4.7 for 27 sets of experiment.

Figure 4.7: Specimen after toughness test for welding joint AISI 304 with AISI 4340

### 4.3.1 Toughness test in Welding of AISI 304 with AISI 4340

Results of toughness of joint AISI 304 and AISI 4340 are shown in Table 4.7. These results are analyzed using analysis of variance ANOVA technique. It helps in identifying the important process parameters affecting the responses.

Table 4.7: Results for toughness test of joint between AISI 304 and AISI 4340

| Exp. No. | Welding current (A) | Gas type | Flow rate (L/min) | Filler | Pre-heating (°C) | Post-heating (°C) | Toughness (J) |
|---|---|---|---|---|---|---|---|
| 1 | 145 | Ar | 12 | 304 | No | No | 29.430 |
| 2 | 145 | Ar | 14 | EN24 | 175 | 500 | 29.430 |
| 3 | 145 | Ar | 16 | 308 | 250 | 650 | 34.335 |
| 4 | 145 | 70% Ar + 30% He | 12 | EN24 | 175 | 650 | 9.810 |
| 5 | 145 | 70% Ar + 30% He | 14 | 308 | 250 | No | 9.810 |
| 6 | 145 | 70% Ar + 30% He | 16 | 304 | No | 500 | 4.905 |
| 7 | 145 | Ar + 1.5% $H_2$ | 12 | 308 | 250 | 500 | 132.435 |
| 8 | 145 | Ar + 1.5% $H_2$ | 14 | 304 | No | 650 | 78.480 |
| 9 | 145 | Ar + 1.5% $H_2$ | 16 | EN24 | 175 | No | 22.070 |
| 10 | 165 | Ar | 12 | EN24 | 250 | 500 | 117.720 |
| 11 | 165 | Ar | 14 | 308 | No | 650 | 109.872 |
| 12 | 165 | Ar | 16 | 304 | 175 | No | 9.810 |
| 13 | 165 | 70% Ar + 30% He | 12 | 308 | No | No | 9.810 |
| 14 | 165 | 70% Ar + 30% He | 14 | 304 | 175 | 500 | 9.810 |
| 15 | 165 | 70% Ar + 30% He | 16 | EN24 | 250 | 650 | 63.765 |
| 16 | 165 | Ar + 1.5% $H_2$ | 12 | 304 | 175 | 650 | 4.905 |
| 17 | 165 | Ar + 1.5% $H_2$ | 14 | EN24 | 250 | No | 4.905 |
| 18 | 165 | Ar + 1.5% $H_2$ | 16 | 308 | No | 500 | 34.335 |
| 19 | 185 | Ar | 12 | 308 | 175 | 650 | 93.195 |
| 20 | 185 | Ar | 14 | 304 | 250 | No | 4.905 |
| 21 | 185 | Ar | 16 | EN24 | No | 500 | 58.860 |
| 22 | 185 | 70% Ar + 30% He | 12 | 304 | 250 | 500 | 4.905 |
| 23 | 185 | 70% Ar + 30% He | 14 | EN24 | No | 650 | 4.905 |
| 24 | 185 | 70% Ar + 30% He | 16 | 308 | 175 | No | 9.810 |
| 25 | 185 | Ar + 1.5% $H_2$ | 12 | EN24 | No | No | 19.620 |
| 26 | 185 | Ar + 1.5% $H_2$ | 14 | 308 | 175 | 500 | 147.150 |
| 27 | 185 | Ar + 1.5% $H_2$ | 16 | 304 | 250 | 650 | 4.905 |

**Analysis of variance of toughness**

To find out the significance of various factors like current, gas type, gas flow rate, filler type, pre-heating temperature and post-heating on toughness. ANOVA is performed at measured data with 90% confidence level. *F*-test is utilized for assess relative significance of each input parameter on the response toughness. The principle of *F*-test is that the greater the *F* value for a particular input parameter, the larger is its effect on the output parameter. ANOVA table for toughness test of joint between AISI 304 and AISI 4340 is shown in Table 4.8. ANOVA table consists of symbol, sum of squares, variance, *F* – value and percentage contribution for different sources.

Table 4.8: ANOVA table for toughness test of joint between AISI 304 and AISI 4340

| Sources | Symbol | DF | SS | Variance | *F* - value | PC |
|---|---|---|---|---|---|---|
| Current (A) | *A* | 2 | 18.0 | 9.01 | 0.01 | 0.03 |
| Gas type | *B* | 2 | 8679.2 | 4339.61 | 5.51 | 16.92 |
| Flow rate (L/min) | *C* | 2 | 2112.8 | 1056.41 | 1.34 | 4.11 |
| Filler | *D* | 2 | 10302.5 | 5151.23 | 6.55 | 20.08 |
| Pre-heating(ºC) | *E* | 2 | 99.8 | 49.91 | 0.06 | 0.19 |
| Post-heating(ºC) | *F* | 2 | 10180.1 | 5090.07 | 6.47 | 19.85 |
| Current × Gas type | *A* × *B* | 4 | 10489.8 | 2622.45 | 3.33 | 20.45 |
| Current × Flow rate | *A* × *C* | 4 | 6645.4 | 295.59 | 0.38 | 12.95 |
| Gas Type ×Flow rate | *B* × *C* | 4 | 6645.4 | 1661.35 | 2.11 | 12.95 |
| Error | | 2 | 1573.8 | 786.89 | | 3.06 |
| Total | | 26 | 51283.8 | | | |

(SS= Sum of square, DF= Degree of freedom, F= F factor, PC = Percent contribution)

Figure 4.8 shows the main effect plot of toughness test for various parameters. In the plot X-axis shows the process parameters and Y-axis shows the toughness and center line shows the mean of toughness. Main plot shows the trend followed by the output parameter with varying different values of parameters *A, B, C, D, E* and *F.* There is large influence of gas type, filler, post-heating and interaction between current × gas type on toughness as compared to other parameters as shown in main effect plot in Fig.4.8, interaction plot in Fig. 4.9 and by observing the *F*- value and percentage contribution from ANOVA table. By using different types of gases the penetration increases results in increase in toughness value as shown in main effect plot and influencing value of percentage contribution in ANOVA table. By using different type of filler metal the toughness increases as the nickel content increases. As shown in Fig. 4.8 the toughness increases with the increase in post-heating temperature because with the increase in post-heating temperature the residual stresses are reliefied and results in increase in toughness at some particular value and then start decreasing. There is no influencing percentage contribution of current and pre-heating on toughness as its trend is near to the mean line in main effect plot in Fig. 4.8. Gas flow rate has minute contribution due to cooling effect as the flow rate increases the toughness decreases due to the improper diffusion of metal during welding.

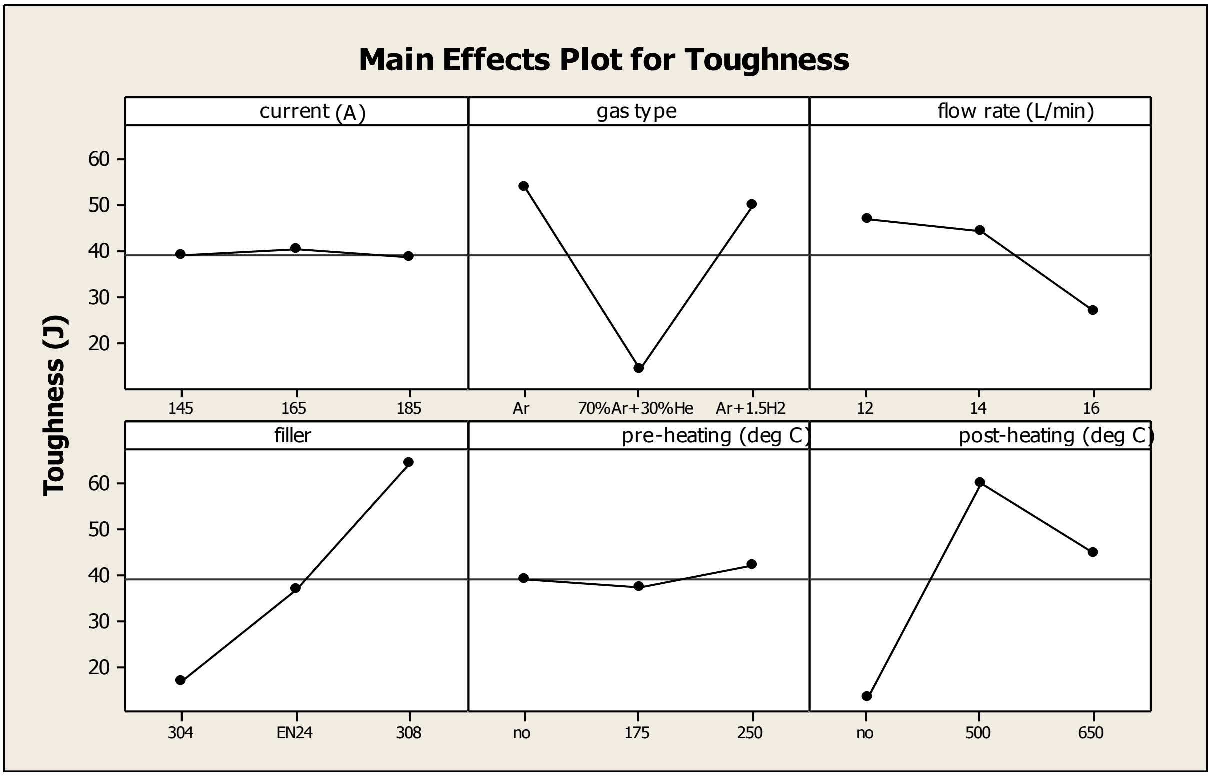


Figure 4.8: Main Effect Plot of toughness for joint AISI 304 with AISI 4340

Figure 4.9 shows the interaction plots for toughness correspond to input parameters. Interaction plot tells the combined effect of two parameters which are to be considered. The current × gas type interaction has influencing results for toughness as seen in ANOVA Table 4.8 and interaction plot in Fig 4.9 as compared to the other parameters. Current individually has not any significant result but by combining with gas type it gives the influencing results. Current × gas type gives the combined effect of increases in penetration and thermal conductivity of the different gases which gives the influencing percentage contribution.

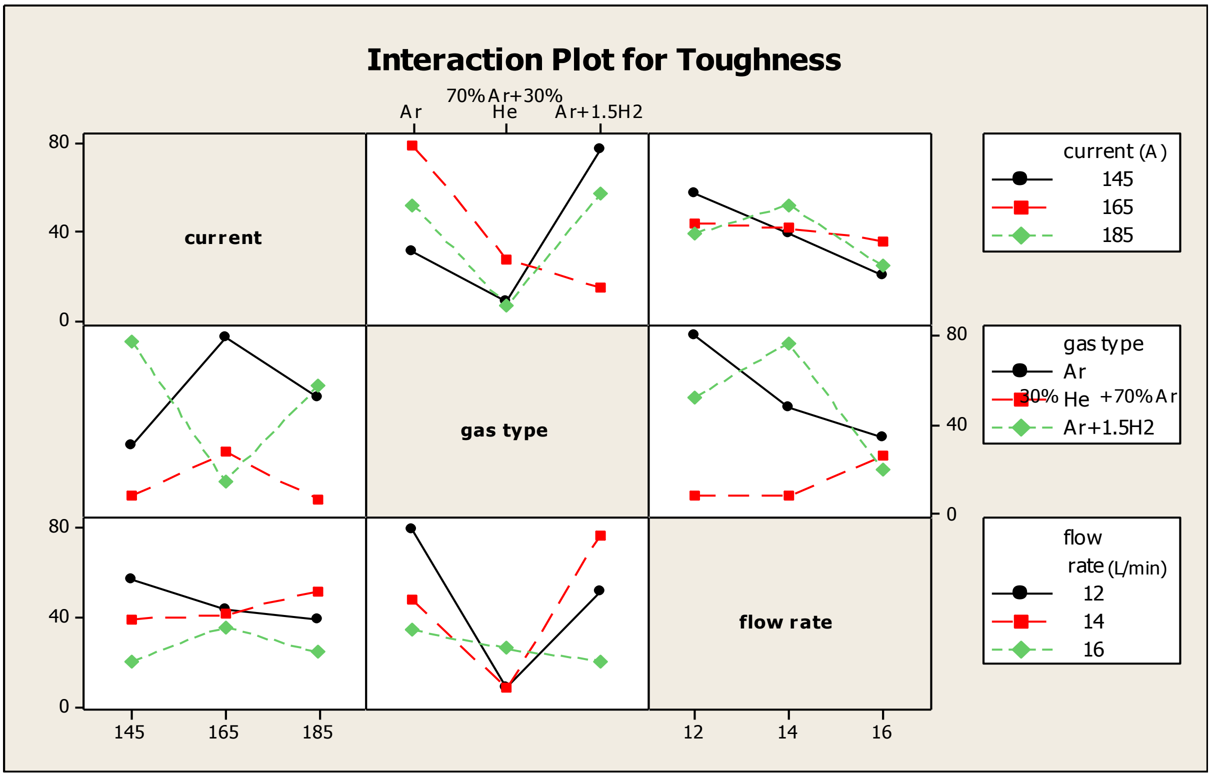


Figure 4.9: Interaction plot of toughness test for joint AISI 304 with AISI 4340

The various factors are assigned ranks according to their influence on results as shown by ANOVA technique and are listed in Table 4.8. From the response table filler is the most influencing factor with rank 1 followed by post-heating, gas type, flow rate and other factors. Current parameter is seen to be the most insignificant factor with rank 6.

Table 4.9: Response table for toughness test joint between AISI 304 and AISI 4340

| Level | Current | Gas type | Flow rate | Filler | Pre-heating | Post-heating |
|---|---|---|---|---|---|---|
| 1 | 38.97 | 54.17 | 46.87 | 16.90 | 38.91 | 13.35 |
| 2 | 40.55 | 14.17 | 44.87 | 36.79 | 37.33 | 59.95 |
| 3 | 38.70 | 49.87 | 26.98 | 64.53 | 41.97 | 44.91 |
| Delta | 1.85 | 40.00 | 19.89 | 47.63 | 4.63 | 46.60 |
| Rank | 6 | 3 | 4 | 1 | 5 | 2 |

**Optimal Design**

The main effect plot and interaction plot in Fig. 4.8 and Fig. 4.9 respectively are used to estimate the maximum toughness with optimal design parameter conditions. From Table 4.8 considering higher *F*-value and corresponding percentage contribution four parameters i.e. gas type, filler, post-heating and interaction current × gas type are significantly influencing the toughness. The level of these factors which gives the maximum toughness are noted from main effect plot (Fig. 4.8) and the corresponding toughness for these levels of $\overline{B_1}$, $\overline{D_3}$, $\overline{F_2}$ are obtained directly from the Table 4.9. For interactions, levels of current × gas type (A×B) is decided from the interaction plot (Fig. 4.9) and maximum toughness is observed at $\overline{A_2 \times B_1}$. To obtain the best estimate of a mean when an interaction is present, the trials that include that treatment condition should be averaged. Average tensile strength for this interaction is obtained by taking the average of three trials (trial 10, 11, 12) for $\overline{A_2 \times B_1}$. Maximum value of gas type, filler and post-heating are selected because toughness is 'higher the better' type response. Desired mean value in this case is estimated as:

$$\mu_{B_1,D_3,F_3,A_2\times B_1} = \overline{B_1} + \overline{D_3} + \overline{F_2} + \overline{A_2 \times B_1} - 3\,\overline{T}$$

$$= 54.17 + 64.53 + 59.95 + 79.134 - 3(39.4034)$$

$$= 139.57 \text{ J}$$

Confidence interval

$$CI = \sqrt{\frac{F_{\alpha,\nu_1,\nu_2} V_e}{n_{eff}}}$$

Where $F_{\alpha,\nu_1,\nu_2}$ = $F$ ratio

$\alpha$ = 0.1 (risk)

Confidence = 1 – $\alpha$

$\nu_1$ = DF for mean (always 1)

$\nu_2$ = Total DF (=26)

$\overline{T}$ = Average of all experimental trials

$n_{eff}$ = Number of tests under that condition using the participating factors

$$n_{eff} = \frac{N}{1+DF_{B,D,F,A\times B}} = \frac{27}{1+10} = 2.4$$

N is the number of trial in the experiment

$V_e$ = Variance (of error)

$$CI = \sqrt{\frac{2.91 \times 786.89}{2.4}} = \pm 30.77 \text{ J}$$

Thus the optimum value of toughness is (139.57 $\pm$ 30.77) J.

μ value is 139.57 MPa which is more than expected value due to influence of some random variable where some parametric combination resulted in very poor joint and low toughness (like experiment no. 4, 6, 25). This leads to poor reduction in additivity of interaction terms and in trial average ($\overline{T}$). So optimum value is selected from trial (trials 10, 11, 12) having value above 109.872 J.

### 4.3.2 Toughness test in Welding of AISI 316 with AISI 4340

Specimens after toughness test are shown in Fig. 4.10

Figure 4.10: Specimen after toughness test for welding joint AISI 316 with AISI 4340

Results of toughness of joint AISI 316 with AISI 4340 are as shown in Table 4.10. These results are analyzed using analysis of variance ANOVA technique. It helps in identifying the important process parameters affecting the responses.

Table 4.10: Results for toughness test of joint between AISI 316 and AISI 4340

| Exp. no. | Welding current (A) | Gas type | Flow rate (L/min) | Filler | Pre-heating ($^oC$) | Post-heating ($^oC$) | Toughness (J) |
|---|---|---|---|---|---|---|---|
| 1 | 145 | Ar | 12 | 316 | No | No | 24.525 |
| 2 | 145 | Ar | 14 | EN24 | 175 | 500 | 4.905 |
| 3 | 145 | Ar | 16 | 309 | 250 | 650 | 44.145 |
| 4 | 145 | 70% Ar + 30% He | 12 | EN24 | 175 | 350 | 4.905 |
| 5 | 145 | 70% Ar + 30% He | 14 | 309 | 250 | No | 19.620 |
| 6 | 145 | 70% Ar + 30% He | 16 | 316 | No | 500 | 4.905 |
| 7 | 145 | Ar + 1.5% $H_2$ | 12 | 309 | 250 | 500 | 12.753 |
| 8 | 145 | Ar + 1.5% $H_2$ | 14 | 316 | No | 650 | 4.905 |
| 9 | 145 | Ar + 1.5% $H_2$ | 16 | EN24 | 175 | No | 27.468 |
| 10 | 165 | Ar | 12 | EN24 | 250 | 500 | 4.905 |
| 11 | 165 | Ar | 14 | 309 | No | 650 | 19.620 |
| 12 | 165 | Ar | 16 | 316 | 175 | No | 9.810 |
| 13 | 165 | 70% Ar + 30% He | 12 | 309 | No | No | 4.901 |
| 14 | 165 | 70% Ar + 30% He | 14 | 316 | 175 | 500 | 14.718 |
| 15 | 165 | 70% Ar + 30% He | 16 | EN24 | 250 | 650 | 4.905 |
| 16 | 165 | Ar + 1.5% $H_2$ | 12 | 316 | 175 | 650 | 4.901 |
| 17 | 165 | Ar + 1.5% $H_2$ | 14 | EN24 | 250 | No | 9.810 |
| 18 | 165 | Ar + 1.5% $H_2$ | 16 | 309 | No | 500 | 93.195 |
| 19 | 185 | Ar | 12 | 309 | 175 | 650 | 9.810 |
| 20 | 185 | Ar | 14 | 316 | 250 | No | 19.620 |
| 21 | 185 | Ar | 16 | EN24 | No | 500 | 4.905 |
| 22 | 185 | 70% Ar + 30% He | 12 | 316 | 250 | 500 | 4.901 |
| 23 | 185 | 70% Ar + 30% He | 14 | EN24 | No | 650 | 9.810 |
| 24 | 185 | 70% Ar + 30% He | 16 | 309 | 175 | No | 13.734 |
| 25 | 185 | Ar + 1.5% $H_2$ | 12 | EN24 | No | No | 4.905 |
| 26 | 185 | Ar + 1.5% $H_2$ | 14 | 309 | 175 | 500 | 63.760 |
| 27 | 185 | Ar + 1.5% $H_2$ | 16 | 316 | 250 | 650 | 4.905 |

**Analysis of variance of toughness**

To find out the significance of various factors like current, gas type, gas flow rate, filler type, pre-heating temperature and post-heating on toughness. ANOVA is performed at measured data with 90% confidence level. *F*-test is utilized for assess relative significance of each input parameter on the response toughness. The principle of *F*-test is that the greater the *F* value for a particular input parameter, the larger is its effect on the output parameter. ANOVA table for toughness test of joint between AISI 316 and AISI 4340 is shown in Table 4.11. ANOVA table consists of symbol, sum of squares, variance, *F*- value and percentage contribution for different sources.

Table 4.11: ANOVA table for toughness test of joint between AISI 316 and AISI 4340

| Sources | Symbol | DF | SS | Variance | *F* - value | PC |
|---|---|---|---|---|---|---|
| Current (A) | *A* | 2 | 52.3 | 26.13 | 0.05 | 0.47 |
| Gas type | *B* | 2 | 1166.4 | 583.19 | 1.07 | 10.69 |
| Flow rate (L/min) | *C* | 2 | 1004.8 | 502.38 | 0.92 | 9.20 |
| Filler | *D* | 2 | 2881.0 | 1440.48 | 2.65 | 26.40 |
| Pre-heating(ºC) | *E* | 2 | 120.3 | 60.13 | 0.11 | 1.10 |
| Post-heating(ºC) | *F* | 2 | 610.0 | 304.98 | 0.56 | 5.59 |
| Current × Gas type | *A* × *B* | 4 | 953.2 | 238.30 | 0.44 | 8.73 |
| Current × Flow rate | *A* × *C* | 4 | 2046.0 | 511.51 | 0.94 | 18.75 |
| Gas Type × Flow rate | *B* × *C* | 4 | 989.7 | 247.43 | 0.46 | 9.07 |
| Error | | 2 | 1086.5 | 543.25 | | 9.95 |
| Total | | 26 | 10910.1 | | | |

(SS= Sum of square, DF= Degree of freedom, F= F factor, PC = Percent contribution)

Figure 4.11 shows the main effect plot of toughness for various parameters. In the plot X-axis shows the process parameters and Y-axis shows the toughenss and center line shows the mean of toughness. Main plot shows the trend followed by the output parameter with varying different values of parameters *A*, *B*, *C*, *D*, *E* and *F*. There is large influence of gas type, filler and interaction between current × flow rate on toughness as compared to other parameters as shown in main effect plot in Fig.4.11, interaction plot in Fig. 4.12 and by observing the *F*- value and percentage contribution from ANOVA table. Different type of fillers has significant contribution to find out the toughness for various parameters, the toughness increases with the increase in the nickel content. There is large influence of gas type on toughness due to thermal conductivity of the gases. Current and pre-heating temperature have minimum amount of contribution on toughness as its graph for toughness is around the mean line. By increasing the gas flow rate the toughness increases proportionally due to the cooling input rate.

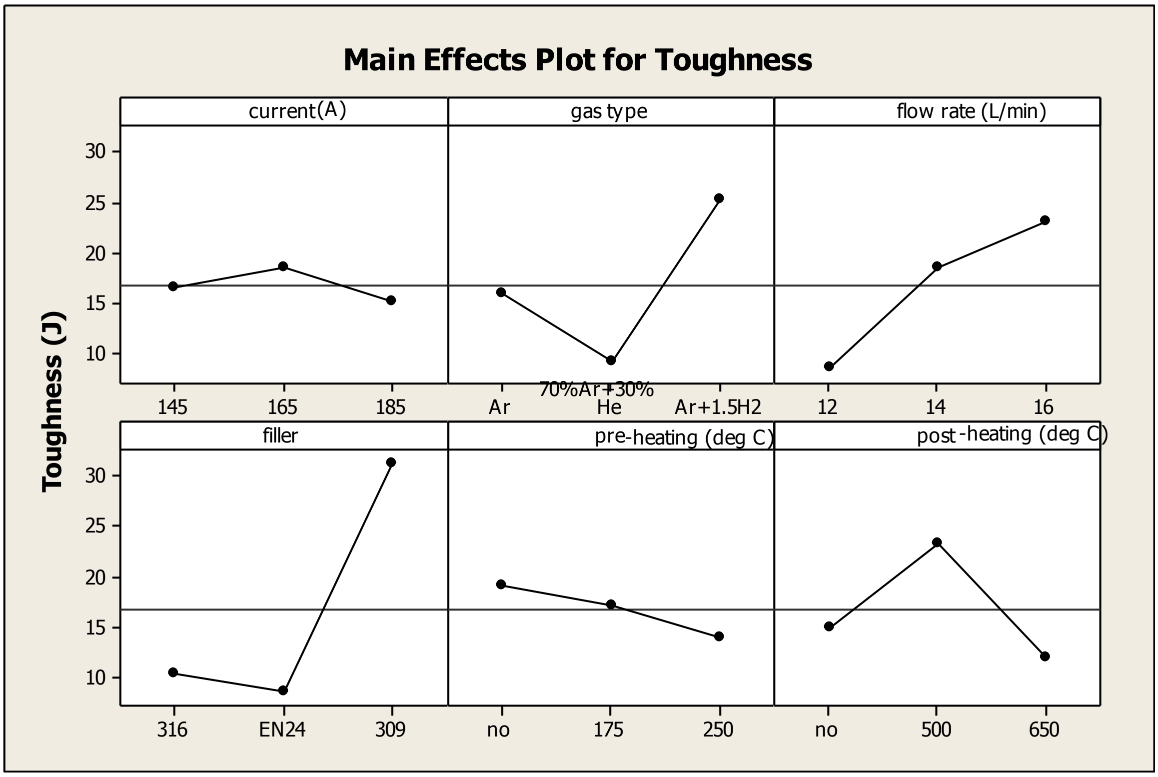


Figure 4.11: Main Effect Plot of toughness for joint AISI 316 with AISI 4340

Figure 4.12 shows the interaction plots for toughness correspond to input parameters. Interaction plot tells the combined effect of two parameters which are to be considered. The current × flow rate interaction has influencing results for toughness as seen in ANOVA Table 4.11 and interaction plot in Fig 4.12 as compared to the other parameters. Current × flow rate gives the combined effect of increases in penetration and the cooling effect at different gas flow rates. A × C gives the influencing percentage contribution for toughness.

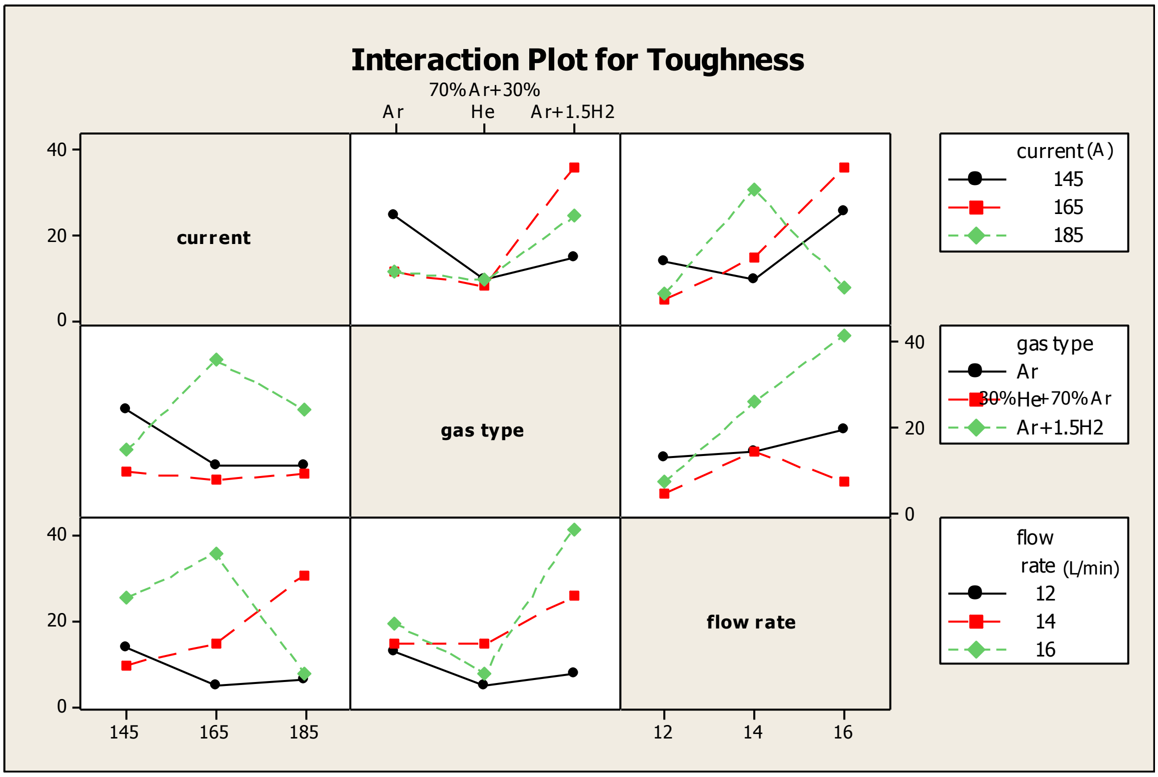


Figure 4.12: Interaction plot of toughness test for joint AISI 316 with AISI 4340

The various factors are assigned ranks according to their influence on results as shown by ANOVA technique and are listed in Table 4.11. From the response table filler is the most influencing factor with rank 1 followed by gas type, flow rate, post-heating and other factors. Current parameter is seen to be the most insignificant factor with rank 6.

Table 4.12: Response table for toughness test joint between AISI 316 and AISI 4340

| Level | Current | Gas type | Flow rate | Filler | Pre-heating | Post-heating |
|---|---|---|---|---|---|---|
| 1 | 16.459 | 15.805 | 8.501 | 10.354 | 19.075 | 14.933 |
| 2 | 18.529 | 9.155 | 18.530 | 8.502 | 17.112 | 23.216 |
| 3 | 15.150 | 25.178 | 23.108 | 31.282 | 13.952 | 11.990 |
| Delta | 3.379 | 16.023 | 14.607 | 22.780 | 5.123 | 11.227 |
| Rank | 6 | 2 | 3 | 1 | 5 | 4 |

**Optimal Design**

The main effect plot and interaction plot in Fig. 4.11 and Fig. 4.12 respectively are used to estimate the maximum toughness with optimal design parameter conditions. From Table 4.11 considering higher *F*-value and corresponding percentage contribution for three parameters i.e. gas type, filler and interaction current × flow rate are significantly influencing the toughness. The level of these factors which gives the maximum toughness are noted from main effect plot (Fig. 4.11) and the corresponding toughness for these levels of $\overline{B_3}$, $\overline{D_3}$ are obtained directly from the Table 4.12. For interactions, levels of current × flow rate (A×C) is decided from the interaction plot (Fig. 4.12) and maximum toughness is observed at $\overline{A_2 \times C_3}$. To obtain the best estimate of a mean when an interaction is present, the trials that include that treatment condition should be averaged. Average tensile strength for this interaction is obtained by taking the average of three trials (trial 12, 15, 18) for$\overline{A_2 \times C_3}$. Maximum value of gas type and filler are selected because toughness is 'higher the better' type response. Desired mean value in this case is estimated as:

$$\mu_{B_3,D_3,A_2\times C_3} = \overline{B_3} + \overline{D_3} + \overline{A_2 \times C_3} - 2\,\overline{T}$$

$$= 25.178 + 31.282 + 35.97 - 2(16.7128)$$

$$= 59.00 \text{ J}$$

Confidence interval

$$CI = \sqrt{\frac{F_{\alpha,\nu_1,\nu_2} V_e}{n_{eff}}}$$

Where $F_{\alpha,\nu_1,\nu_2}$ = $F$ ratio

$\alpha$ = 0.1 (risk)

Confidence = 1 – $\alpha$

$\nu_1$ = DF for mean (always 1)

$\nu_2$ = Total DF (=26)

$\overline{T}$ = Average of all experimental trials

$n_{eff}$ = Number of tests under that condition using the participating factors

$$n_{eff} = \frac{N}{1+DF_{\text{B,D,A×C}}} = \frac{27}{1+8} = 3$$

N is the number of trial in the experiment

$V_e$ = Variance (of error)

$$CI = \sqrt{\frac{2.91 \times 543.25}{3}} = \pm\, 22.95 \text{ J}$$

Thus the optimum value of toughness is (59.00 $\pm$ 22.95) J

## 4.4 Microhardness Test

Microhardness of the weld region was measured by using the computerized interfaced micro hardness tester. The measurement was dependent on the size of indentation on the samples. The diagonals of the indent formed by the pyramid- shaped diamond indenter was measured at 40X magnification, which gave a direct hardness Vicker number (HVN) for microhardness. The load applied on the indenter was 100g and the dwell time was 20 sec. Microhardness being the surface characteristics, gives the value of hardness at micro level. MH value is calculated in terms of Vickers's Hardness Number (VHN).

### 4.4.1 Microhardness of Fusion Zone of welding joint AISI 304 with AISI4340

Results of microhardness test of joint AISI 304 and AISI 4340 at fussion zone are shown in Table 4.13. These results are analyzed using analysis of variance ANOVA technique. It helps in identifying the important process parameters affecting the responses.

Table 4.13: Results for microhardness at fusion zone test of joint between AISI 304 and AISI 4340

| Sr. No. | Welding current (A) | Gas type | Flow rate (L/min) | Filler | Pre-heating ($^oC$) | Post-heating ($^oC$) | Microhardness (HVN) |
|---|---|---|---|---|---|---|---|
| 1 | 145 | Ar | 12 | 304 | No | No | 328.920 |
| 2 | 145 | Ar | 14 | EN24 | 175 | 500 | 322.640 |
| 3 | 145 | Ar | 16 | 308 | 250 | 650 | 282.300 |
| 4 | 145 | 70% Ar + 30% He | 12 | EN24 | 175 | 650 | 580.290 |
| 5 | 145 | 70% Ar + 30% He | 14 | 308 | 250 | No | 338.920 |
| 6 | 145 | 70% Ar + 30% He | 16 | 304 | No | 500 | 648.470 |
| 7 | 145 | Ar + 1.5% $H_2$ | 12 | 308 | 250 | 500 | 370.350 |
| 8 | 145 | Ar + 1.5% $H_2$ | 14 | 304 | No | 650 | 455.000 |
| 9 | 145 | Ar + 1.5% $H_2$ | 16 | EN24 | 175 | No | 324.800 |
| 10 | 165 | Ar | 12 | EN24 | 250 | 500 | 531.760 |
| 11 | 165 | Ar | 14 | 308 | No | 650 | 324.350 |
| 12 | 165 | Ar | 16 | 304 | 175 | No | 408.130 |
| 13 | 165 | 70 %Ar + 30% He | 12 | 308 | No | No | 253.000 |
| 14 | 165 | 70% Ar + 30% He | 14 | 304 | 175 | 500 | 239.950 |
| 15 | 165 | 70% Ar + 30% He | 16 | EN24 | 250 | 650 | 356.450 |
| 16 | 165 | Ar + 1.5% $H_2$ | 12 | 304 | 175 | 650 | 327.129 |
| 17 | 165 | Ar + 1.5% $H_2$ | 14 | EN24 | 250 | No | 392.370 |
| 18 | 165 | Ar + 1.5% $H_2$ | 16 | 308 | No | 500 | 530.525 |
| 19 | 185 | Ar | 12 | 308 | 175 | 650 | 273.170 |
| 20 | 185 | Ar | 14 | 304 | 250 | No | 235.002 |
| 21 | 185 | Ar | 16 | EN24 | No | 500 | 220.995 |
| 22 | 185 | 70% Ar + 30% He | 12 | 304 | 250 | 500 | 345.010 |
| 23 | 185 | 70% Ar + 30% He | 14 | EN24 | No | 650 | 514.170 |
| 24 | 185 | 70% Ar + 30% He | 16 | 308 | 175 | No | 317.531 |
| 25 | 185 | Ar + 1.5% $H_2$ | 12 | EN24 | No | No | 310.460 |
| 26 | 185 | Ar + 1.5% $H_2$ | 14 | 308 | 175 | 500 | 362.186 |
| 27 | 185 | Ar + 1.5% $H_2$ | 16 | 304 | 250 | 650 | 345.941 |

**Analysis of variance of microhardness**

To find out the significance of various factors like current, gas type, gas flow rate, filler type, pre-heating temperature and post-heating on microhardness test. ANOVA is performed at measured data with 90% confidence level. *F*-test is utilized for assess relative significance of each input parameter on the response hardness. The principle of *F*-test is that the greater the *F* value for a particular input parameter, the larger is its effect on the output parameter. ANOVA table for microhardness test of joint between AISI 304 and AISI 4340 is shown in Table 4.14. ANOVA table consists of symbol, sum of squares, variance, *F* – value and percentage contribution for different sources.

Table 4.14: ANOVA table for microhardness test of joint between AISI 304 and AISI 4340

| Sources | Symbol | DF | SS | Variance | *F* - value | PC |
|---|---|---|---|---|---|---|
| Current (A) | *A* | 2 | 29804 | 14902 | 1.20 | 9.60 |
| Gas type | *B* | 2 | 26535 | 13268 | 1.07 | 8.55 |
| Flow rate (L/min) | *C* | 2 | 3495 | 1748 | 0.14 | 1.12 |
| Filler | *D* | 2 | 14047 | 7023 | 0.57 | 4.5 |
| Pre-heating(ºC) | *E* | 2 | 12486 | 6243 | 0.50 | 4.0 |
| Post-heating(ºC) | *F* | 2 | 27932 | 13966 | 1.13 | 9.00 |
| Current × Gas type | $A \times B$ | 4 | 113986 | 28497 | 2.30 | 36.73 |
| Current × Flow rate | $A \times C$ | 4 | 30447 | 7612 | 0.61 | 9.81 |
| Gas Type × Flow rate | $B \times C$ | 4 | 26787 | 6697 | 0.54 | 8.63 |
| Error | | 2 | 24756 | 12378 | | 7.97 |
| Total | | 26 | 310277 | | | 99.91 |

(SS= Sum of square, DF= Degree of freedom, F= F factor, PC = Percent contribution)

Figure 4.13 shows the main effect plot of microhardness test for various parameters. In the plot X-axis shows the process parameters and Y-axis shows the microhardness and center line shows the mean of microhardness. Main plot shows the trend followed by the output parameter with varying different values of parameters *A*, *B*, *C*, *D*, *E* and *F*. There is large influence of current, post-heating and interaction between current × gas type and current × flow rate on microhardness as compared to other parameters as shown in main effect plot in Fig.4.13, interaction plot in Fig. 4.14 and by observing the *F*- value and percentage contribution from ANOVA table. As it is seen as the value of current increases heat input increases result in fast cooling which makes the size of grain larger results in decrease in value of hardness. It is also seen that as the post-heating temperature increases the value of microhardness increases from 0ºC to 500ºC due to the relief in residual stresses and then slightly decreases as the temperature increases from 500ºC to 650ºC. There is no influencing percentage contribution of flow rate on microhardness as its trend is near to the mean line in main effect plot in Fig. 4.14. Filler and pre-heating temperature has minute contribution on microhardness.

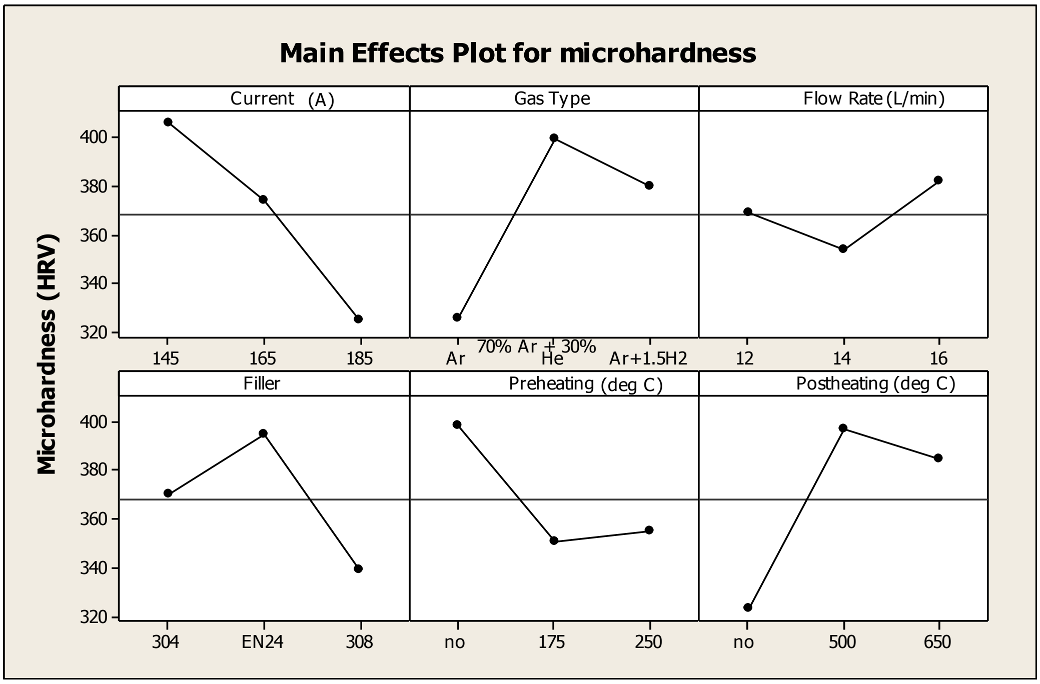


Figure 4.13: Main Effect Plot of microhardness for joint AISI 304 with AISI 4340

Figure 4.14 shows the interaction plots for microhardness correspond to input parameters. Interaction plot tells the combined effect of two parameters which are to be considered. The current × gas type and current × flow rate interactions has influencing results for microhardness as seen in ANOVA Table 4.14 and interaction plot in Fig 4.14 as compared to the other parameters. Current × gas type gives the combined effect of increases in cooling rate at different gas type and heat input. Current × flow rate gives the combined effect of increases in penetration and the cooling effect at different gas flow rates. A × B gives the influencing percentage contribution for microhardness.

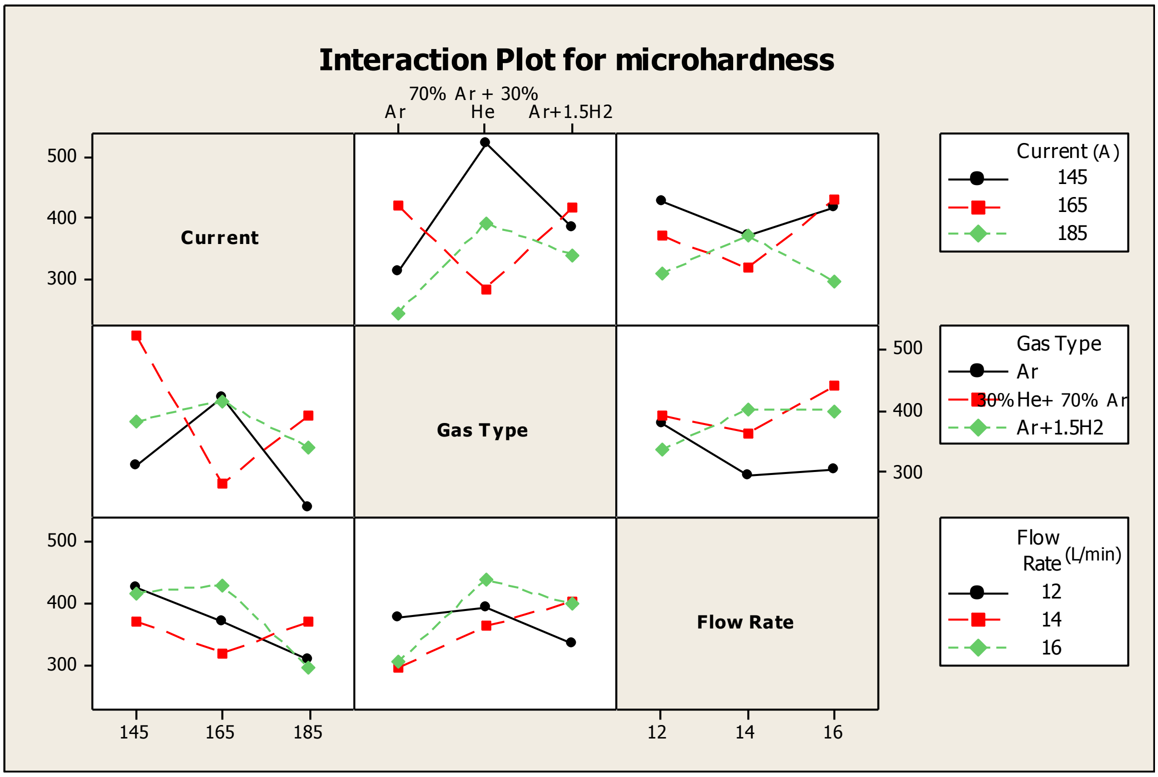


Figure 4.14: Interaction plot of microhardness test for joint AISI 304 with AISI 4340

The various factors are assigned ranks according to their influence on results as shown by ANOVA technique and are listed in Table 4.15. From the response table current is the most influencing factor with rank 1 followed by gas type, post-heating, filler and other factors. Flow rate parameter is seen to be the most insignificant factor with rank 6.

Table 4.15: Response table for microhardness joint between AISI 304 and AISI 4340

| Level | Current | Gas type | Flow rate | Filler | Pre-heating | Post-heating |
|---|---|---|---|---|---|---|
| 1 | 405.7 | 325.3 | 368.9 | 370.4 | 398.4 | 323.2 |
| 2 | 373.7 | 399.3 | 353.8 | 394.9 | 350.6 | 396.9 |
| 3 | 324.9 | 379.9 | 381.7 | 339.1 | 355.3 | 384.3 |
| Delta | 80.8 | 74.1 | 27.8 | 55.7 | 47.8 | 73.6 |
| Rank | 1 | 2 | 6 | 4 | 5 | 3 |

**Optimal Design**

The main effect plot and interaction plot in Fig. 4.13 and Fig. 4.14 respectively are used to estimate the maximum microhardness with optimal design parameter conditions. From Table 4.14 considering higher *F*-value and corresponding percentage contribution for four parameters i.e. current, post-heating and interactions current × gas type and current × flow rate are significantly influencing the microhardness. The level of these factors which gives the maximum microhardness are noted from main effect plot (Fig. 4.13) and the corresponding microhardness for these levels of $\overline{A_2}$, $\overline{F_2}$ are obtained directly from the Table 4.15. For interactions, levels of current × gas type ($A \times B$) and current × flow rate ($A \times C$) is decided from the interaction plot (Fig. 4.14) and maximum microhardness is observed at $\overline{A_1 \times B_2}$ and $\overline{A_1 \times C_1}$. To obtain the best estimate of a mean when an interaction is present, the trials that include that treatment condition should be averaged. Average microhardness for this interaction is obtained by taking the average of three trials (trial 4, 5, 6) for $\overline{A_1 \times B_2}$ and trials (trial 12, 15, 18) $\overline{A_1 \times C_1}$. Maximum value of current and post-heating temperature are selected because microhardness is 'higher the better' type response. Desired mean value in this case is estimated as:

$$\mu_{A_2,F_2,A_1\times B_2,A_1\times C_1} = \overline{A_2} + \overline{F_2} + \overline{A_1 \times B_2} + \overline{A_1 \times C_1} - 3\,\overline{T}$$

$$= 373.7 + 396.9 + 522.56 + 426.52 - 3(368.1414)$$

$$= 615.255 \text{ HRV}$$

Confidence interval

$$CI = \sqrt{\frac{F_{\alpha,v_1,v_2} V_e}{n_{eff}}}$$

Where $F_{\alpha,v_1,v_2}$ = $F$ ratio

α = 0.1 (risk)

Confidence = 1 – α

$v_1$ = DF for mean (always 1)

$v_2$ = Total DF (=26)

$\overline{T}$ = Average of all experimental trials

$n_{eff}$ = Number of tests under that condition using the participating factors

$$n_{eff} = \frac{N}{1+DF_{A,F,A\times B,A\times C}} = \frac{27}{1+12} = 2.07$$

N is the number of trial in the experiment

$V_e$ = Variance (of error)

$$CI = \sqrt{\frac{2.91 \times 12378}{2.07}} = \pm 131.91 \text{ HRV}$$

Thus the optimum value of microhardness is (615.255 ± 131.91)

### 4.4.2 Microhardness of Fusion Zone of welding joint AISI 316 with AISI4340

Results of microhardness of joint AISI 316 and AISI 4340 at fusion zone are shown in Table 4.16. These results are analyzed using analysis of variance ANOVA technique. It helps in identifying the important process parameters affecting the responses.

Table 4.16: Results for microhardness at fusion zone test of joint between AISI 316 and AISI 4340

| Exp. No. | Welding current (A) | Gas type | Flow rate (L/min) | Filler | Pre-heating ($^oC$) | Post-heating ($^oC$) | Microhardness (HVN) |
|---|---|---|---|---|---|---|---|
| 1 | 145 | Ar | 12 | 316 | No | No | 379.065 |
| 2 | 145 | Ar | 14 | EN24 | 175 | 500 | 383.370 |
| 3 | 145 | Ar | 16 | 309 | 250 | 650 | 266.000 |
| 4 | 145 | 70% Ar + 30% He | 12 | EN24 | 175 | 350 | 238.000 |
| 5 | 145 | 70% Ar + 30% He | 14 | 309 | 250 | No | 369.440 |
| 6 | 145 | 70% Ar + 30% He | 16 | 316 | No | 500 | 531.000 |
| 7 | 145 | Ar + 1.5% $H_2$ | 12 | 309 | 250 | 500 | 481.400 |
| 8 | 145 | Ar + 1.5% $H_2$ | 14 | 316 | No | 650 | 335.365 |
| 9 | 145 | Ar + 1.5% $H_2$ | 16 | EN24 | 175 | No | 332.170 |
| 10 | 165 | Ar | 12 | EN24 | 250 | 500 | 477.504 |
| 11 | 165 | Ar | 14 | 309 | No | 650 | 256.000 |
| 12 | 165 | Ar | 16 | 316 | 175 | No | 358.970 |
| 13 | 165 | 70% Ar + 30% He | 12 | 309 | No | No | 345.600 |
| 14 | 165 | 70% Ar + 30% He | 14 | 316 | 175 | 500 | 472.630 |
| 15 | 165 | 70% Ar + 30% He | 16 | EN24 | 250 | 650 | 360.230 |
| 16 | 165 | Ar + 1.5% $H_2$ | 12 | 316 | 175 | 650 | 376.900 |
| 17 | 165 | Ar + 1.5% $H_2$ | 14 | EN24 | 250 | No | 232.064 |
| 18 | 165 | Ar + 1.5% $H_2$ | 16 | 309 | No | 500 | 335.820 |
| 19 | 185 | Ar | 12 | 309 | 175 | 650 | 251.660 |
| 20 | 185 | Ar | 14 | 316 | 250 | No | 353.130 |
| 21 | 185 | Ar | 16 | EN24 | No | 500 | 347.449 |
| 22 | 185 | 70% Ar + 30% He | 12 | 316 | 250 | 500 | 493.950 |
| 23 | 185 | 70% Ar + 30% He | 14 | EN24 | No | 650 | 352.270 |
| 24 | 185 | 70% Ar + 30% He | 16 | 309 | 175 | No | 333.270 |
| 25 | 185 | Ar + 1.5% $H_2$ | 12 | EN24 | No | No | 271.380 |
| 26 | 185 | Ar + 1.5% $H_2$ | 14 | 309 | 175 | 500 | 344.130 |
| 27 | 185 | Ar + 1.5% $H_2$ | 16 | 316 | 250 | 650 | 346.070 |

**Analysis of variance of microhardness**

To find out the significance of various factors like current, gas type, gas flow rate, filler type, pre-heating temperature and post-heating on micro hardness test. ANOVA is performed at measured data with 90% confidence level. *F*-test is utilized for assess relative significance of each input parameter on the response hardness. The principle of *F*-test is that the greater the *F* value for a particular input parameter, the larger is its effect on the output parameter. ANOVA table for micro hardness test of joint between AISI 304 and AISI 4340 is shown in Table 4.14. ANOVA table consists of symbol, sum of squares, variance, *F*- value and percentage contribution for different sources.

Table 4.17: ANOVA table for microhardness test of joint between AISI 316 and AISI 4340

| Sources | Symbol | DF | SS | Variance | *F* - value | PC |
|---|---|---|---|---|---|---|
| Current (A) | *A* | 2 | 2760 | 1380 | 1.04 | 1.6 |
| Gas type | *B* | 2 | 13852 | 6926 | 5.24 | 8.4 |
| Flow rate (L/min) | *C* | 2 | 2619 | 1309 | 0.99 | 1.6 |
| Filler | *D* | 2 | 32098 | 16049 | 12.15 | 19.63 |
| Pre-heating(ºC) | *E* | 2 | 5122 | 2561 | 1.94 | 3.13 |
| Post-heating(ºC) | *F* | 2 | 74435 | 37218 | 28.18 | 45.53 |
| Current × Gas type | *A* × *B* | 4 | 9454 | 2363 | 1.79 | 5.78 |
| Current × Flow rate | *A* × *C* | 4 | 7558 | 1889 | 1.43 | 4.62 |
| Gas Type × Flow rate | *B* × *C* | 4 | 12919 | 3230 | 2.45 | 7.903 |
| Error | | 2 | 2641 | 1321 | | 1.615 |
| Total | | 26 | 163457 | | | 99.08 |

(SS= Sum of square, DF= Degree of freedom, F= F factor, PC = Percent contribution)

Figure 4.15 shows the main effect plot of microhardness test for various parameters. In the plot X-axis shows the process parameters and Y-axis shows the microhardness and center line shows the mean of microhardness. Main plot shows the trend followed by the output parameter with varying different values of parameters *A*, *B*, *C*, *D*, *E* and *F*. There is large influence of gas type, filler, post-heating and interaction between gas type × flow rate on microhardness as compared to other parameters as shown in main effect plot in Fig.4.15, interaction plot in Fig. 4.16 and by observing the *F*- value and percentage contribution from ANOVA Table 4.17. By using different types of gases the penetration increases results in increase in microhardness value as it is seen by using Ar and He mixture the microhardness increases as shown in main effect plot and influencing value of percentage contribution in ANOVA table. By using different type of filler metal the microhardness is found to be very high as seen from main effect plot, the microhardness is highest for AISI 316 reason behind is increases in the nickel content. As shown in Fig. 4.15 the microhardness increases with the increase in post-heating temperature because with the increase in post-heating temperature the residual stresses are reliefied and results in increase in microhardness at some particular value and then start decreasing. There is no influencing percentage contribution of current, flow rate, pre-heating on microhardness as its trend is near to the mean line in main effect plot in Fig. 4.15.

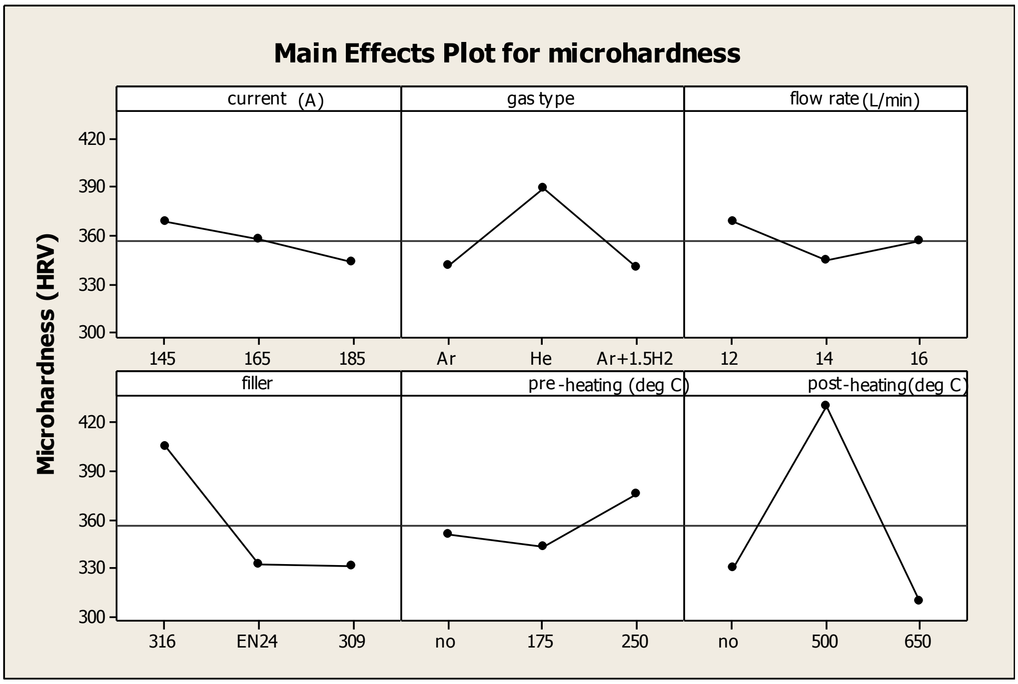


Figure 4.15: Main Effect Plot of microhardness for joint AISI 316 with AISI 4340

Figure 4.16 shows the interaction plots for microhardness correspond to input parameters. Interaction plot tells the combined effect of two parameters which are to be considered. The gas type × flow rate interaction has influencing results for microhardness as seen in ANOVA Table 4.17 and interaction plot in Fig 4.16 as compared to the other parameters. Gas type × flow rate gives the combined effect of increases in penetration and the cooling effect at different gas flow rates. B × C gives the influencing percentage contribution for microhardness.

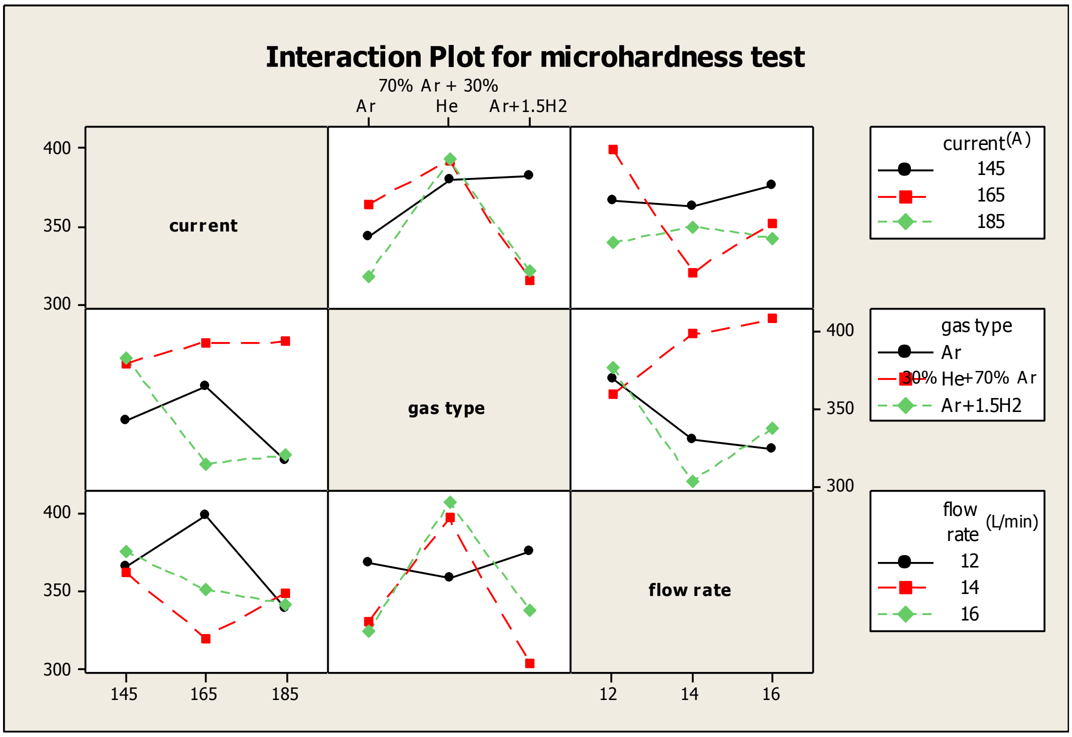


Figure 4.16: Interaction plot of micro hardness test for joint AISI 316 with AISI 4340

The various factors are assigned ranks according to their influence on results as shown by ANOVA technique and are listed in Table 4.18. From the response table post-heating is the most influencing factor with rank 1 followed by filler, gas type, pre-heating and other factors. Flow rate parameter is seen to be the most insignificant factor with rank 6.

Table 4.18: Response table for microhardness joint between AISI 316 and AISI 4340

| Level | Current | Gas type | Flow rate | Filler | Pre-heating | Post-heating |
|---|---|---|---|---|---|---|
| 1 | 368.4 | 341.5 | 368.4 | 405.2 | 350.4 | 330.6 |
| 2 | 357.3 | 388.5 | 344.3 | 332.7 | 343.5 | 429.7 |
| 3 | 343.7 | 339.5 | 356.8 | 331.5 | 375.5 | 309.2 |
| Delta | 24.7 | 49.0 | 24.1 | 73.8 | 32.1 | 120.5 |
| Rank | 5 | 3 | 6 | 2 | 4 | 1 |

**Optimal Design**

The main effect plot and interaction plot in Fig. 4.15 and Fig. 4.16 respectively are used to estimate the maximum microhardness with optimal design parameter conditions. From Table 4.17 considering higher *F*-value and corresponding percentage contribution for four parameters i.e. gas type, filler, post-heating and interaction gas type × flow rate are significantly influencing the microhardness. The level of these factors which gives the maximum microhardness are noted from main effect plot (Fig. 4.15) and the corresponding microhardness for these levels of $\overline{B_2}$,$\overline{D_1}$,$\overline{F_2}$, are obtained directly from the Table 4.18. For interactions, levels of gas type × flow rate (B × C) is decided from the interaction plot (Fig. 4.16) and maximum microhardness is observed at $\overline{B_2 \times C_3}$. To obtain the best estimate of a mean when an interaction is present, the trials that include that treatment condition should be averaged. Average microhardness for this interaction is obtained by taking the average of three trials (trial 6, 15, 24) for $\overline{B_2 \times C_3}$. Maximum value of gas type, filler and post-heating are selected because microhardness is 'higher the better' type response. Desired mean value in this case is estimated as:

$$\mu_{B_2,D_1,F_2,B_2\times C_3} = \overline{B_2} + \overline{D_1} + \overline{F_2} + \overline{B_2 \times C_3} - 3\overline{T}$$

$$= 388.5 + 405.2 + 429.7 + 408.16 - 3(356.4754)$$

$$= 562.133 \text{ HVN}$$

Confidence interval

$$CI = \sqrt{\frac{F_{\alpha,\nu_1,\nu_2} V_e}{n_{eff}}}$$

Where $F_{\alpha,\nu_1,\nu_2}$ = $F$ ratio

$\alpha$ = 0.1 (risk)

Confidence = 1 – $\alpha$

$\nu_1$ = DF for mean (always 1)

$\nu_2$ = Total DF (=26)

$\overline{T}$ = Average of all experimental trials

$n_{eff}$ = Number of tests under that condition using the participating factors

$$n_{eff} = \frac{N}{1+DF_{B,D,F,B\times C}} = \frac{27}{1+10} = 2.45$$

N is the number of trial in the experiment

$V_e$ = Variance (of error)

$$CI = \sqrt{\frac{2.91 \times 1321}{2.45}} = \pm 39.61 \text{ HVN}$$

Thus the optimum value of microhardness is (562.131 $\pm$ 39.61)

## 4.5 Weld Distortion

The effect of current, type of gas, gas flow rate, type of filler, pre-heating temperature and post-heating temperature on dissimilar joining of materials namely AISI 304 with AISI 4340 and AISI 316 with AISI 4340 are analyzed for weld distortion. Following Taguchi experimental design, 27 experiments are conducted as shown in Table 4.19. Weld Distortion is calculated with the help of an apparatus discussed in chapter 3.

$$tan\theta = \frac{\Delta X}{\Delta Z} \tag{4.1}$$

Where $\theta$ = difference in angle between the final and initial (º)

$\Delta X$ = horizontal difference (mm)

$\Delta Z$ = Vertical difference (mm)

### 4.5.1 Distortion of welded joints between AISI 304 and AISI 4340

Results of weld distortion of joint AISI 304 and AISI 4340 calculated by Eq. (4.1) are given in Table 4.19. These results are analyzed using analysis of variance ANOVA technique. It helps in identifying the important process parameters affecting the responses.

Table 4.19: Results for weld distortion of joint between AISI 304 and AISI 4340

| Exp. No. | Welding current (A) | Gas type | Flow rate (L/min) | Filler | Pre-heating ($^oC$) | Post-heating ($^oC$) | Distortion ( $^o$ ) |
|---|---|---|---|---|---|---|---|
| 1 | 145 | Ar | 12 | 304 | No | No | 0.257 |
| 2 | 145 | Ar | 14 | EN24 | 175 | 500 | 2.118 |
| 3 | 145 | Ar | 16 | 308 | 250 | 650 | 1.661 |
| 4 | 145 | 70% Ar + 30% He | 12 | EN24 | 175 | 650 | 0.286 |
| 5 | 145 | 70% Ar + 30% He | 14 | 308 | 250 | No | 0.859 |
| 6 | 145 | 70% Ar +30% He | 16 | 304 | No | 500 | 1.718 |
| 7 | 145 | Ar + 1.5% $H_2$ | 12 | 308 | 250 | 500 | 0.802 |
| 8 | 145 | Ar + 1.5% $H_2$ | 14 | 304 | No | 650 | 0.171 |
| 9 | 145 | Ar + 1.5% $H_2$ | 16 | EN24 | 175 | No | 1.374 |
| 10 | 165 | Ar | 12 | EN24 | 250 | 500 | 1.832 |
| 11 | 165 | Ar | 14 | 308 | No | 650 | 1.203 |
| 12 | 165 | Ar | 16 | 304 | 175 | No | 0.085 |
| 13 | 165 | 70% Ar + 30% He | 12 | 308 | No | No | 0.401 |
| 14 | 165 | 70% Ar + 30% He | 14 | 304 | 175 | 500 | 1.260 |
| 15 | 165 | 70% Ar + 30% He | 16 | EN24 | 250 | 650 | 1.431 |
| 16 | 165 | Ar + 1.5% $H_2$ | 12 | 304 | 175 | 650 | 0.286 |
| 17 | 165 | Ar + 1.5% $H_2$ | 14 | EN24 | 250 | No | 0.315 |
| 18 | 165 | Ar + 1.5% $H_2$ | 16 | 308 | No | 500 | 1.832 |
| 19 | 185 | Ar | 12 | 308 | 175 | 650 | 1.718 |
| 20 | 185 | Ar | 14 | 304 | 250 | No | 1.546 |
| 21 | 185 | Ar | 16 | EN24 | No | 500 | 1.603 |
| 22 | 185 | 70% Ar + 30% He | 12 | 304 | 250 | 500 | 1.059 |
| 23 | 185 | 70% Ar + 30% He | 14 | EN24 | No | 650 | 1.432 |
| 24 | 185 | 70% Ar + 30% He | 16 | 308 | 175 | No | 1.775 |
| 25 | 185 | Ar + 1.5% $H_2$ | 12 | EN24 | No | No | 1.661 |
| 26 | 185 | Ar + 1.5% $H_2$ | 14 | 308 | 175 | 500 | 1.260 |
| 27 | 185 | Ar + 1.5% $H_2$ | 16 | 304 | 250 | 650 | 1.317 |

**Analysis of variance of distortion**

To find out the significance of various factors like current, gas type, gas flow rate, filler type, post-heating temperature and pre-heating on weld distortion ANOVA is performed at measured data with 90% confidence level. *F*-test is utilized for assess relative significance of each input parameter on the response weld distortion. The principle of *F*-test is that the greater the *F* value for a particular input parameter, the larger is its effect on the output parameter. ANOVA table for weld distortion of joint between AISI 304 and AISI 4340 is shown in Table 4.20. ANOVA table consists of symbol, sum of squares, variance, *F*- value and percentage contribution for different sources.

Table 4.20: ANOVA table for weld distortion of joint between AISI 304 and AISI 4340

| Source | Symbol | DF | SS | Variance | *F* - value | PC |
|---|---|---|---|---|---|---|
| Current (A) | *A* | 2 | 1.47081 | 0.73541 | 3.29 | 14.84 |
| Gas type | *B* | 2 | 0.50831 | 0.25416 | 1.14 | 5.132 |
| Flow rate (L/min) | *C* | 2 | 1.13298 | 0.56649 | 2.54 | 11.43 |
| Filler | *D* | 2 | 1.25084 | 0.62542 | 2.80 | 12.62 |
| Pre-heating ($^{o}$C) | *E* | 2 | 0.02759 | 0.01380 | 0.06 | 0.278 |
| Post-heating ($^{o}$C) | *F* | 2 | 1.64833 | 0.82416 | 3.69 | 16.64 |
| Current × Gas type | *A* × *B* | 4 | 0.17608 | 0.04402 | 0.20 | 1.78 |
| Current × Flow rate | *A* × *C* | 4 | 0.95984 | 0.23996 | 1.07 | 9.69 |
| Gas type × Flow rate | *B* × *C* | 4 | 2.28317 | 0.57079 | 2.56 | 23.05 |
| Error | | 2 | 0.44675 | 0.22338 | | 4.51 |
| Total | | 26 | 9.90471 | | | 100 |

(SS= Sum of square, DF= Degree of freedom, F= F factor, PC = Percent contribution)

Figure 4.17 shows the main effect plot of weld distortion for various parameters in which X-axis shows the process parameters and Y-axis shows the distortion and center line shows the mean line. Main plot shows the trend followed by the output parameter with varying different values of parameters *A, B, C, D, E* and *F.* As shown in main effect plot in Fig. 4.17, weld distortion is continuously increasing with the increase in welding current and gas flow rate because with increase in current the heat input increases and large heat input results in increase of temperature leading to weld distortion. Similarly with the increase in gas flow rate the cooling effect increases and more heat is dissipated which increases in weld distortion. Value of percentage contribution for current is 14.84% and gas flow rate is 11.43% as shown in Table 4.20 which has more contribution as compared to other parameters. The value of distortion increases as filler metal AISI 304 is used followed by EN24 and AISI 304 due to its chemical composition. By using different type of gases the distortion first decrease from Ar to 70% Ar + 30% He and then slightly increases at Ar + 1.5 $H_2$ due to its thermal conductivity.

When the metal is been welded the temperature at welded part is high, as the welding is continued the welded metal dissipates the heat to outer metal and results in contraction at the weld part. The heat transferred to the outer metal will results in expanding the metal due to heating effect, this expansion and contraction of the metal results in increase in distortion.

It is seen from main effect plot as shown in Fig. 4.17 that post-heating parameter has significant effect on weld distortion because of residual stress releases as the weld metal is heated at higher temperature (considering above discussed phenomena) results in increase in distortion. As shown in main effect plot Fig. 4.17 the distortion first decreases from no pre-heating temperature to 175 º C and then slightly increases.

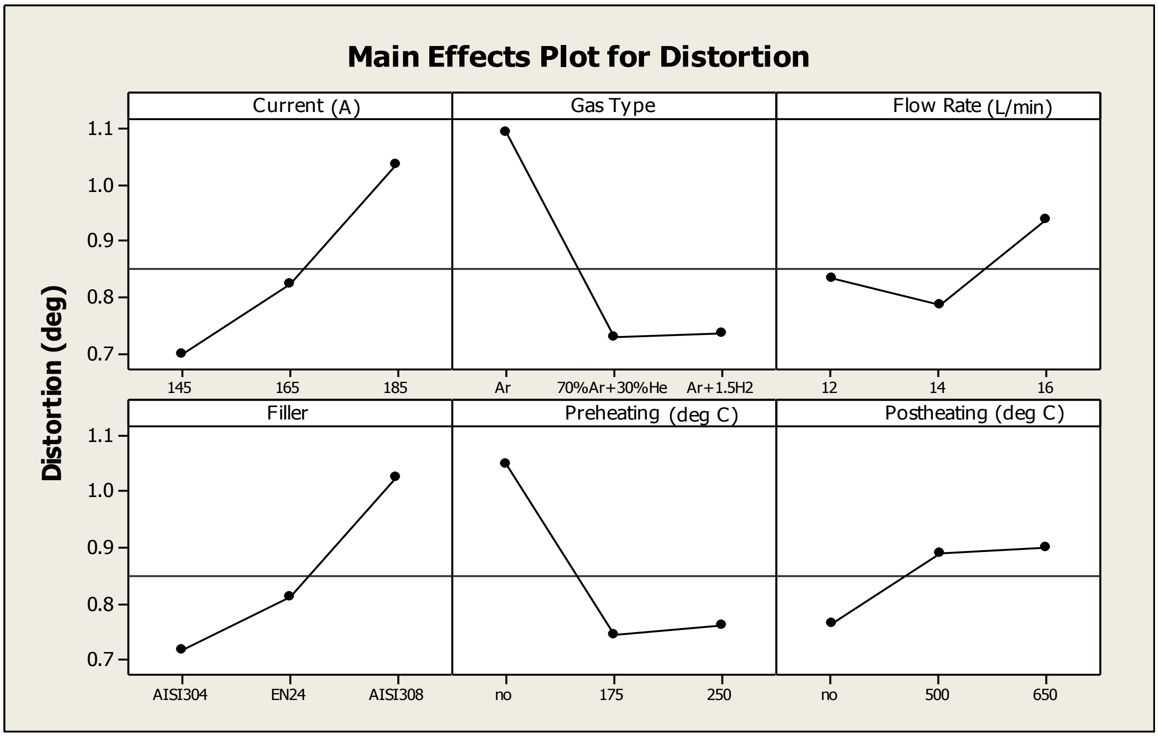


Figure 4.17: Main Effect Plot of weld distortion for joint AISI 304 with AISI 4340

Figure 4.18 shows the interaction plots for weld distortion correspond to input parameters. Interaction plot tells the combined effect of two parameters which are to be considered. From ANOVA Table 4.20 it is seen that the interaction between the gas type × flow rate is significant and the percentage contribution of this interaction is also high as compared to the other interactions. Gas type × gas flow rate gives the combined effect of thermal conductivity and cooling which results in increases in weld distortion.

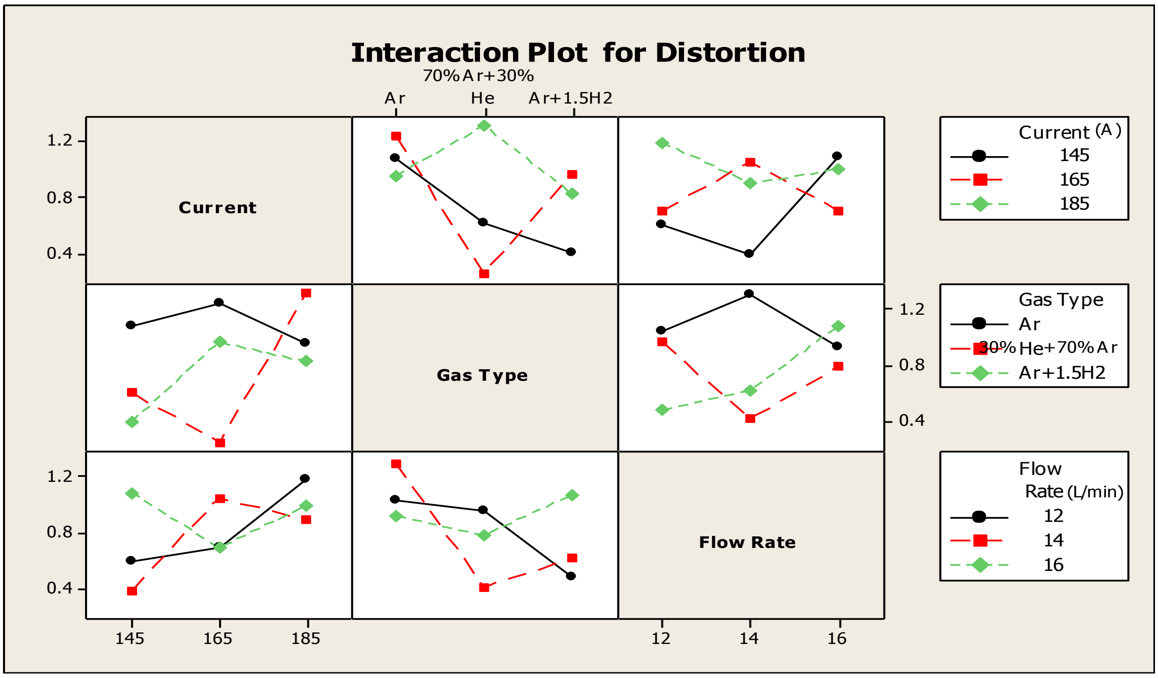


Figure 4.18: Interaction plot of weld distortion for joint AISI 304 with AISI 4340

The various factors are assigned ranks according to their influence on results as shown by ANOVA technique and are listed in Table 4.20. From the response table post-heating is the most influencing factor with rank 1 followed by current, flow rate, filler and other factors. Pre-heating parameter is seen to be the most insignificant factor with rank 6.

Table 4.21: Response table of weld distortion for joint AISI 304 with AISI 4340

| Level | Current | Gas type | Flow rate | Filler | Pre-heating | Post-heating |
|---|---|---|---|---|---|---|
| 1 | 1.0273 | 1.3359 | 0.9224 | 0.8554 | 1.1420 | 0.9192 |
| 2 | 0.9606 | 1.1357 | 1.1293 | 1.3391 | 1.1291 | 1.4982 |
| 3 | 1.4857 | 1.0020 | 1.4218 | 1.2790 | 1.2024 | 1.0561 |
| Delta | 0.5251 | 0.3339 | 0.4993 | 0.4837 | 0.0733 | 0.5790 |
| Rank | 2 | 5 | 3 | 4 | 6 | 1 |

**Optimal design**

In the experimental analysis, the main effect plot for weld distortion Fig. 4.17 is used to estimate the weld distortion with optimal design parameters conditions. Based on the calculated *F*-value and percentage contribution for each factor and the selected interactions (see Table 4.20) factors current, flow rate, filler, post-heating and the interaction gas type × flow rate are observed significantly influencing the weld distortion. $\overline{A_2}, \overline{C_1}, \overline{D_1}, \overline{F_1}$ are obtained directly from the Table 4.21 by selecting the minimum value of current, flow rate, filler and post-heating. $\overline{B_2 \times C_2}$ is obtained by first selecting the gas type and flow rate at minimum distortion from Fig. 4.18 and then taking average of that process parameter conditions. Minimum value of $\overline{A_2}, \overline{C_1}, \overline{D_1}, \overline{F_1}$ and $\overline{B_2 \times C_2}$ are selected because weld distortion is 'lower the better' type response. Desired mean value in this case is estimated as:

$$\mu_{A_2,C_1,D_1,F_1,B_2\times C_2} = \overline{A_2} + \overline{C_1} + \overline{D_1} + \overline{F_1} + \overline{B_2 \times C_2} - 4\,\overline{T}$$

$$= 0.9606 + 0.9224 + 0.8554 + 0.9192 + 1.18 - 4\,(1.157)$$

$$= 0.2096$$

Confidence interval

$$CI = \sqrt{\frac{F_{\alpha,\nu_1,\nu_2} V_e}{n_{eff}}}$$

Where $F_{\alpha,\nu_1,\nu_2}$ = $F$ ratio

$\alpha$ = 0.1 (risk)

Confidence = 1 – $\alpha$

$\nu_1$ = DF for mean (always 1)

$\nu_2$ = DF for total (= 26)

$\overline{T}$ = Average of an experimental trial

$n_{eff}$ = Number of tests under that condition using the participating factors

$$n_{eff} = \frac{N}{1+DF_{A_2,C_1,D_1,F_1,B_2\times C_2}} = \frac{27}{1+12} = 2.076^{o}$$

N is the number of trial in the experiment

$V_e$ = *Variance* (of error)

$$CI = \sqrt{\frac{2.91 \times 0.22338}{2.076}} = \pm\, 0.5595^{o}$$

Thus the optimum value of weld distortion is given by (0.2096 $\pm$ 0.5595) $^{o}$

### 4.5.2 Distortion of welded joints between AISI 316 and AISI 4340

Results of weld distortion of joint AISI 316 and AISI 4340 calculated by Eq. (4.1) are given in Table 4.22. These results are analyzed using analysis of variance ANOVA technique. ANOVA statistical technique helps in identifying the important process parameters affecting the responses.

Table 4.22: Results for weld distortion of joint between AISI 316 and AISI 4340

| Exp. no. | Welding current (A) | Gas type | Flow rate (L/min) | Filler | Pre-heating ($^oC$) | Post-heating ($^oC$) | Distortion ($^o$) |
|---|---|---|---|---|---|---|---|
| 1 | 145 | Ar | 12 | 316 | No | No | 2.147 |
| 2 | 145 | Ar | 14 | EN24 | 175 | 500 | 0.028 |
| 3 | 145 | Ar | 16 | 309 | 250 | 650 | 0.515 |
| 4 | 145 | 70% Ar + 30% He | 12 | EN24 | 175 | 350 | 1.403 |
| 5 | 145 | 70% Ar + 30% He | 14 | 309 | 250 | No | 0.888 |
| 6 | 145 | 70% Ar + 30% He | 16 | 316 | No | 500 | 1.288 |
| 7 | 145 | Ar + 1.5% $H_2$ | 12 | 309 | 250 | 500 | 0.973 |
| 8 | 145 | Ar + 1.5% $H_2$ | 14 | 316 | No | 650 | 0.286 |
| 9 | 145 | Ar + 1.5% $H_2$ | 16 | EN24 | 175 | No | 2.547 |
| 10 | 165 | Ar | 12 | EN24 | 250 | 500 | 0.802 |
| 11 | 165 | Ar | 14 | 309 | No | 650 | 1.203 |
| 12 | 165 | Ar | 16 | 316 | 175 | No | 0.085 |
| 13 | 165 | 70% Ar + 30% He | 12 | 309 | No | No | 0.401 |
| 14 | 165 | 70% Ar + 30% He | 14 | 316 | 175 | 500 | 2.347 |
| 15 | 165 | 70% Ar + 30% He | 16 | EN24 | 250 | 650 | 0.429 |
| 16 | 165 | Ar + 1.5% $H_2$ | 12 | 316 | 175 | 650 | 0.229 |
| 17 | 165 | Ar + 1.5% $H_2$ | 14 | EN24 | 250 | No | 2.433 |
| 18 | 165 | Ar + 1.5% $H_2$ | 16 | 309 | No | 500 | 0.131 |
| 19 | 185 | Ar | 12 | 309 | 175 | 650 | 1.002 |
| 20 | 185 | Ar | 14 | 316 | 250 | No | 0.372 |
| 21 | 185 | Ar | 16 | EN24 | No | 500 | 0.572 |
| 22 | 185 | 70% Ar + 30% He | 12 | 316 | 250 | 500 | 0.859 |
| 23 | 185 | 70% Ar + 30% He | 14 | EN24 | No | 650 | 0.200 |
| 24 | 185 | 70% Ar + 30% He | 16 | 309 | 175 | No | 1.546 |
| 25 | 185 | Ar + 1.5% $H_2$ | 12 | EN24 | No | No | 1.031 |
| 26 | 185 | Ar + 1.5% $H_2$ | 14 | 309 | 175 | 500 | 0.945 |
| 27 | 185 | Ar + 1.5% $H_2$ | 16 | 316 | 250 | 650 | 1.346 |

**Analysis of variance of distortion**

To find out the significance of various factors like current, gas type, gas flow rate, filler type, pre-heating temperature and post-heating temperature on weld distortion ANOVA is performed at measured data with 90% confidence level. *F*-test is utilized for assess relative significance of each input parameter on the response weld distortion. The principle of *F*-test is that the greater the *F* value for a particular input parameter, the larger is its effect on the output parameter. ANOVA table for weld distortion of joint between AISI 316 and AISI 4340 is shown in Table 4.23. ANOVA table consists of symbol, sum of squares, variance, *F*-value and percentage contribution for different sources.

Table 4.23: ANOVA table for weld distortion of joint between AISI 316 and AISI 4340

| Sources | Symbol | DF | SS | Variance | *F* - value | PC |
|---|---|---|---|---|---|---|
| Current | *A* | 2 | 0.3313 | 0.16563 | 1.35 | 2.34 |
| Gas type | *B* | 2 | 0.6468 | 0.32342 | 2.63 | 4.58 |
| Flow rate | *C* | 2 | 0.0085 | 0.00427 | 0.03 | 0.06 |
| Filler | *D* | 2 | 0.2023 | 0.10114 | 0.82 | 1.43 |
| Pre-heating | *E* | 2 | 0.4590 | 0.22951 | 1.87 | 3.25 |
| Post-heating | *F* | 2 | 1.3873 | 0.69363 | 5.64 | 9.83 |
| Current × Gas type | *A* × *B* | 4 | 0.1034 | 0.02585 | 0.21 | 0.733 |
| Current × Flow rate | *A* × *C* | 4 | 8.5251 | 2.13127 | 17.34 | 60.46 |
| Gas type × Flow rate | *B* × *C* | 4 | 2.1906 | 0.54765 | 4.46 | 15.53 |
| Error | | 2 | 0.2458 | 0.12288 | | 1.743 |
| Total | | 26 | 14.1001 | | | 100 |

(SS= Sum of square, DF= Degrees of freedom, F= F factor, PC = Percent contribution)

Figure 4.19 shows the main effect plot of weld distortion for various parameters in which X-axis shows the process parameters and Y-axis shows the distortion and center line shows the mean. Main plot shows the trend followed by the output parameter with varying values of parameters *A, B, C, D, E* and *F*. Post-heating is most varying factors to be considered from Fig. 4.19 whose percentage contribution is also more as compared to other factors as seen in ANOVA table. Post-heating parameter has significant effect as its percentage contribution in Table 4.23 is 9.83% on weld distortion because of release in residual stress. As shown in main effect plot Fig. 4.19 the distortion decreases from no post-heating temperature to 500 º C and then continuously decreases upto 650 ºC. The value of distortion for different type of filler as shown in Fig. 4.19 first increases from AISI 316 to EN 24 and then decreases from EN 24 to AISI 309 due to its chemical composition. By using different type of gases the distortion continuously increases due to its thermal conductivity. The distortion trend in Fig. 4.19 for different gas flow rate is near to the mean line which shows there is no significant effect of gas flow rate on distortion. As seen from Fig 4.19 the value of distortion for current first decreases abruptly and then decreases slowly upto the highest current value. For pre-heating the value of distortion firstly increases and then decreases upto the mean line when the pre-heating temperature increases.

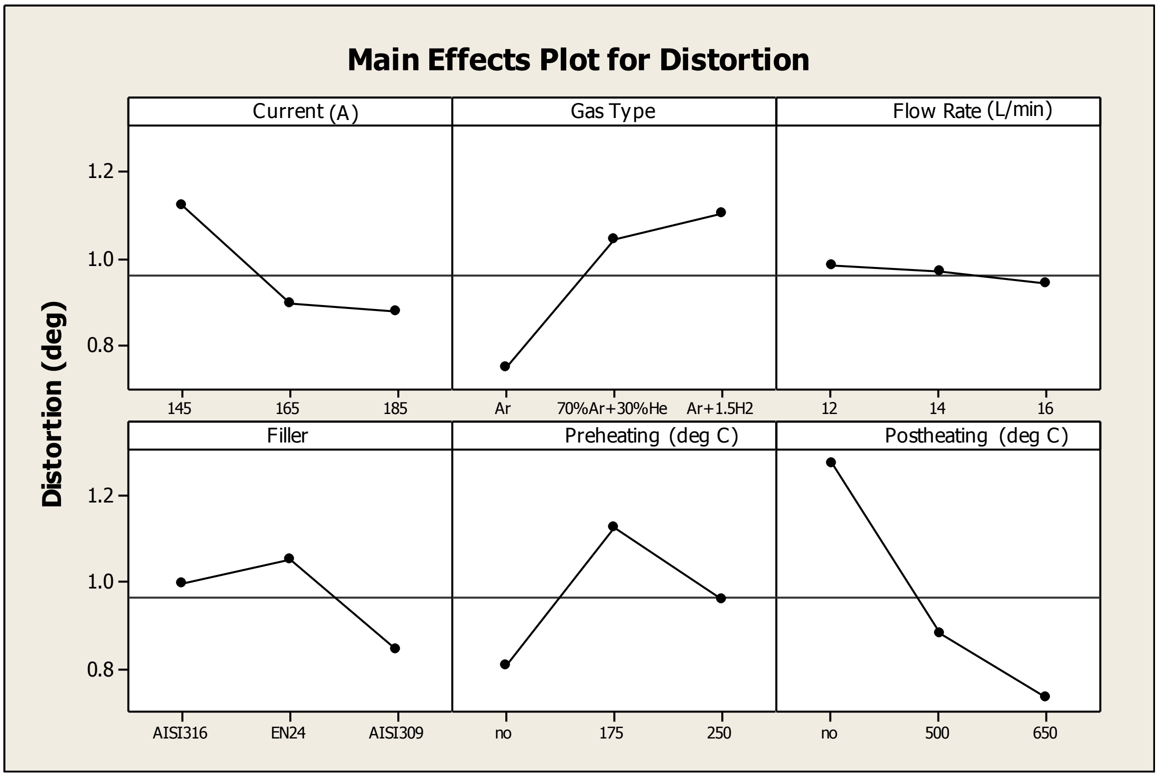


Figure 4.19: Main Effect Plot of weld distortion for joint AISI 316 with AISI 4340

Figure 4.20 shows the interaction plots for weld distortion correspond to input parameters. Interaction plot tells the combined effect of two parameters which are to be considered. From ANOVA Table 4.23 it is seen that the interaction between the current × flow rate is significant having the percentage contribution of 60.46% which is highest of all the parameters. Current × gas flow rate gives the combined effect of heating and cooling simultaneously to the metal and results increase in weld distortion. The interaction between the gas type and gas flow rate has a large value of percentage contribution of 15.53% but its *F- value* is less as compare to other values that's why it is not taken in account of significance.

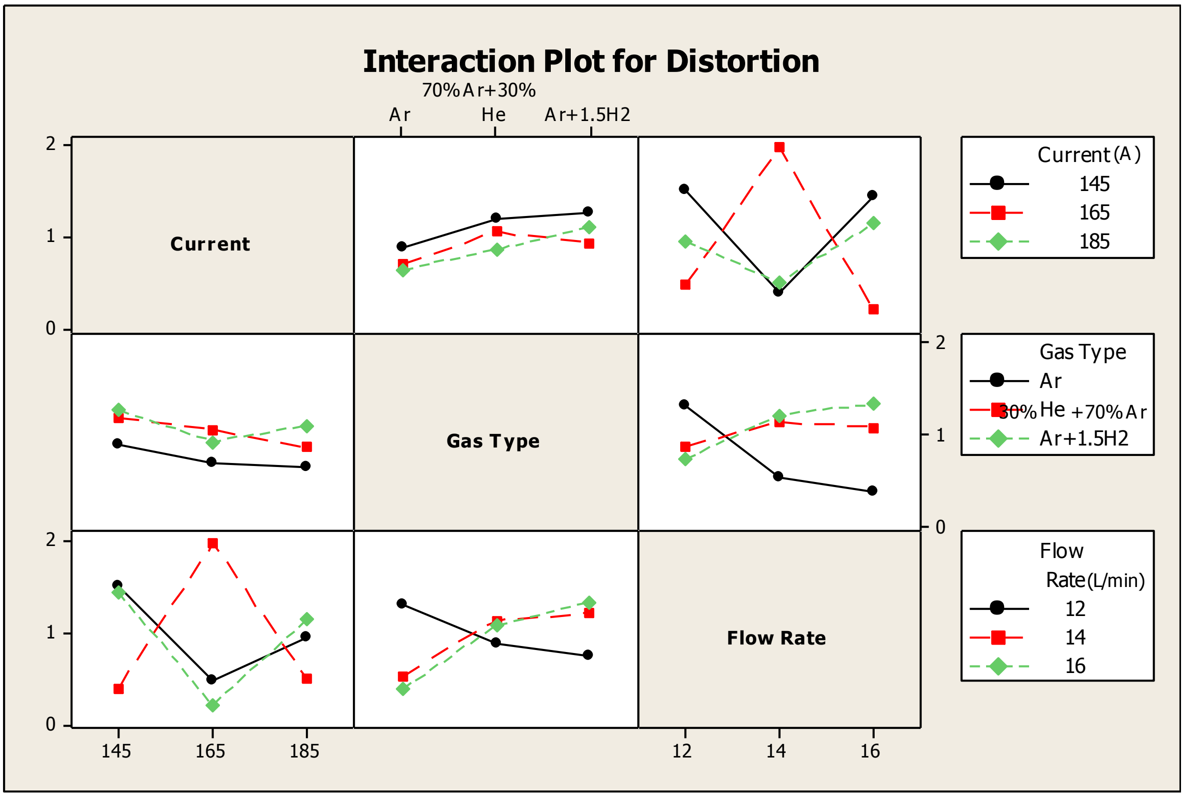


Figure 4.20: Interaction plot of weld distortion for joint AISI 316 with AISI 4340

Table 4.24 shows the response table of weld distortion for joint AISI 316 with AISI 4340. The various factors are assigned ranks according to their influence on results as shown by ANOVA technique and are listed in Table 4.6. From the response table post-heating is the most influencing factor with rank 1 followed by gas type, pre-heating temperature, current and other factors. Gas flow rate parameter is seen to be the most insignificant factor with rank 6 which has least percentage contribution of 0.06% as seen in ANOVA table.

Table 4.24: Response table of weld distortion for joint AISI 316 with AISI 4340

| Level | Current | Gas type | Flow rate | Filler | Pre-heating | Post-heating |
|---|---|---|---|---|---|---|
| 1 | 1.1194 | 0.7473 | 0.9830 | 0.9954 | 0.8066 | 1.2722 |
| 2 | 0.8956 | 1.0401 | 0.9669 | 1.0494 | 1.1258 | 0.8828 |
| 3 | 0.8748 | 0.1023 | 0.9399 | 0.8449 | 0.9574 | 0.7348 |
| Delta | 0.2447 | 0.3550 | 0.0431 | 0.2046 | 0.3192 | 0.5374 |
| Rank | 4 | 2 | 6 | 5 | 3 | 1 |

**Optimal design**

In the experimental analysis, the main effect plot for weld distortion Fig. 4.19 is used to estimate the weld distortion with optimal design parameters conditions. Based on the calculated *F*-value and percentage contribution for each factor and the selected interactions (see Table 4.23) factors post-heating and interaction between current × flow rate are observed significantly influencing the weld distortion. $\overline{F_3}$ is obtained directly from the Table 4.24 by selecting the minimum value of post-heating. $\overline{A_2 \times C_3}$ is obtained by first selecting the current and flow rate at minimum distortion from interaction plot shown in Fig. 4.4 and then taking average of that process parameter conditions. Minimum value of $\overline{F_3}$, and $\overline{A_2 \times C_3}$ are selected because weld distortion is 'lower the better' type response. Desired mean value in this case is estimated as:

$$\mu_{F_3, A_2 \times C_3} = \overline{F_3} + \overline{A_2 \times C_3} - \overline{T}$$

$$= 0.7348 + 0.215 - 0.96325$$

$$= - 0.01345 \equiv 0$$

The optimal calculation for population mean (μ) gives negative value. This situation may appear for responses which are of lower the better (LB) type and where the optimum/ target value is zero. For such cases negative value of μ may not have any physical significance (like responses: surface roughness, distortion, dimension deviation etc.) and to be considered as zero.

Confidence interval

$$CI = \sqrt{\frac{F_{\alpha, v_1, v_2} V_e}{n_{eff}}}$$

Where $F\alpha$, $v_1$, $v_2$ = *F* ratio

$\alpha = 0.1$ (risk)

Confidence = $1 - \alpha$

$v_1$ = DF for mean (always 1)

$v_2$ = DF for total (= 26)

$\overline{T}$ = Average of an experimental trial

$n_{eff}$ = Number of tests under that condition using the participating factors

$$n_{eff} = \frac{N}{1 + DF_{F_3, A_2 \times C_3}} = \frac{27}{1+6} = 3.857^{o}$$

N is the number of trial in the experiment

$V_e$ = *Variance* (of error)

$CI = \sqrt{\frac{2.91 \times 0.12288}{3.857}} = \pm 0.3039^{o}$

Thus the optimum value of weld distortion is given by $(0 \pm 0.3039)^{o} \equiv 0$ to 0.3039

## 4.6 Metallurgical Analysis using Scanning Electron Microscopy

Microstructure analysis was carried out on some selected samples using scanning electron microscope (SEM) machine (Model-JEOL JSM-6480LV) to study change in microstructure after welding with GTAW. SEM is mainly used for imaging the surface and detecting small surface features. Sample preparation was done as per standard requirement. SEM micrographs are taken at 500X for interferences and 1500X for fusion zone magnification. Sample preparation mainly involves cutting the machined samples group in smaller size, so that 4 samples can be accommodated on a slit in a manner to properly accommodate the samples on SEM machine, cleaning of samples by acetone to properly clean the machined surface.

### 4.6.1 Metallurgical Analysis of Joints between AISI 304 and AISI 4340

Table 4.25: SEM images of base metal AISI 304 and AISI 4340

| Base metal of AISI 304 | Base metal of AISI 4340 |
|---|---|
| 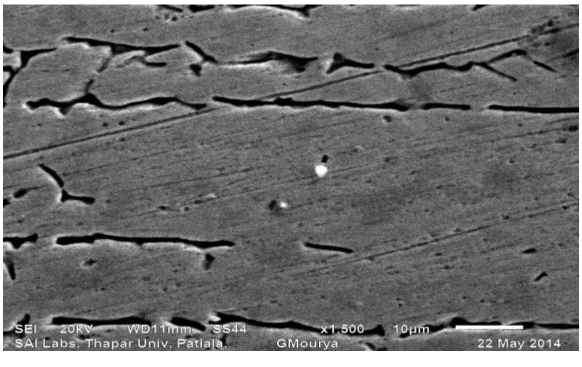 | 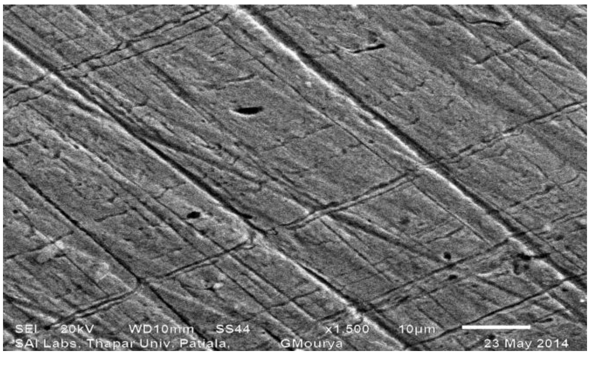 |

Table 4.26: SEM images of different trials of interference of (fusion zone and base metals) and fusion zone

| Trial. No. | Parameters (Current, Gas type, flow rate, filler, pre-heating, post-heating) | Interface of fusion zone and AISI 4340 (Magnification 500X) (a) | Interface of fusion zone and AISI 304 (Magnification 500X) (b) | Fusion zone (Magnification 1500X) (c) |
|---|---|---|---|---|
| 26. | 185 A, Ar + 1.5% $H_2$, 14 L/min, 308, 175 ºC, 500 ºC | 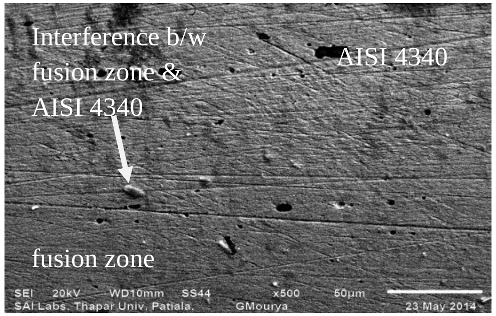 | 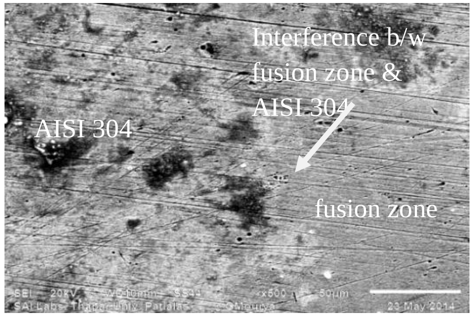 | 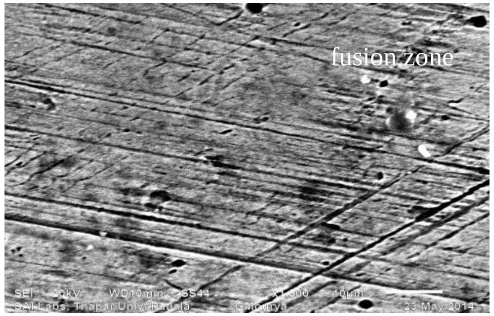 |
| 23. | 185, 70% Ar + 30% He, 14, EN24, No, 650 ºC | 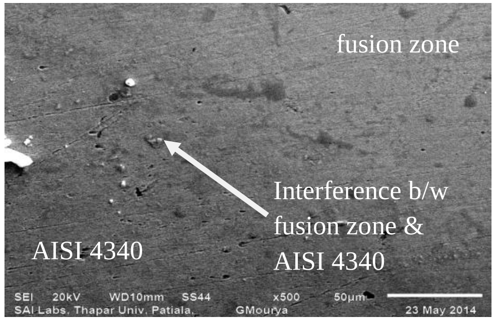 | 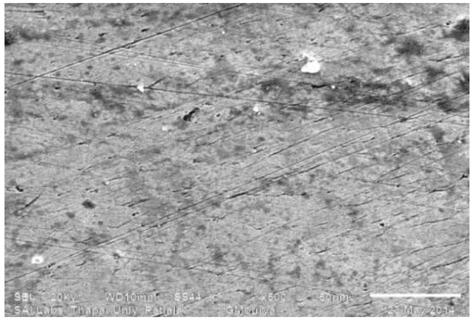 | 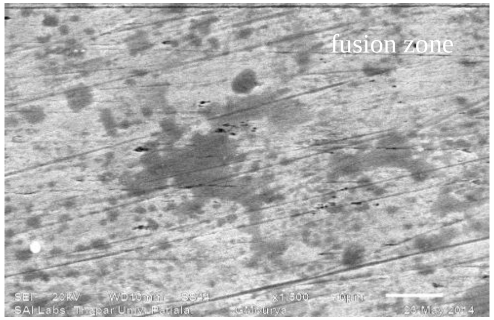 |

| | | | | |
|---|---|---|---|---|
| 19. | 185, Ar, 12, 308, 175 ºC, 650 ºC | 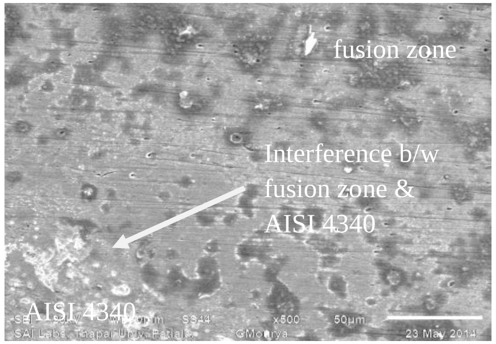 |  | 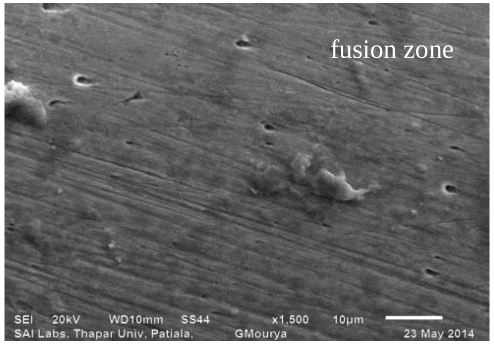 |
| 15. | 165, He, 16, EN24, 250 ºC, 650 ºC | 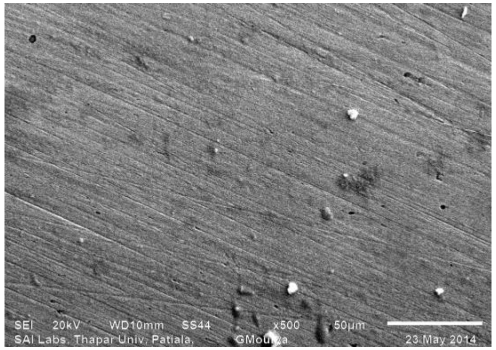 | 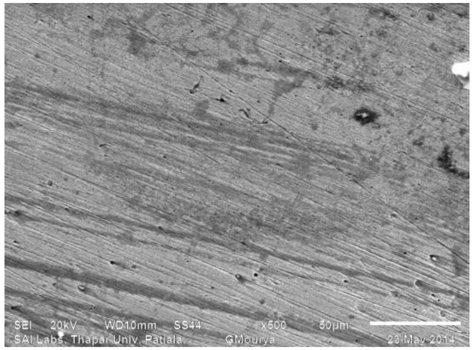 | 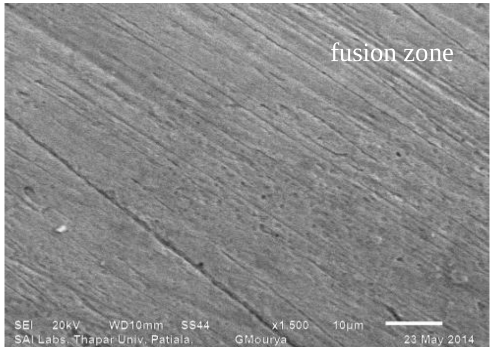 |
| 11. | 165, Ar, 14, 308, No, 650 ºC | 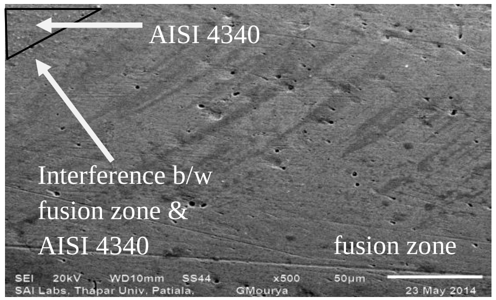 | 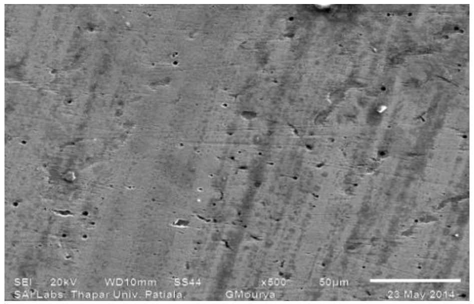 | 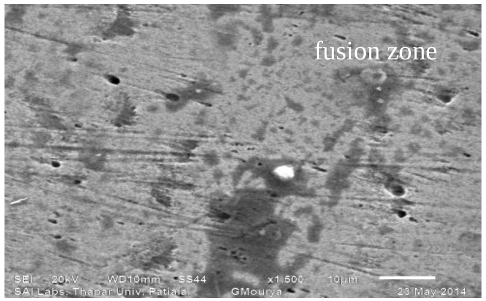 |

| | | | | |
|---|---|---|---|---|
| 10. | 165, Ar, 12, EN24, 250 ºC, 500 ºC | 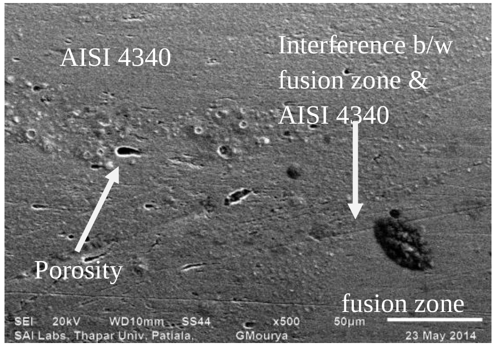 | 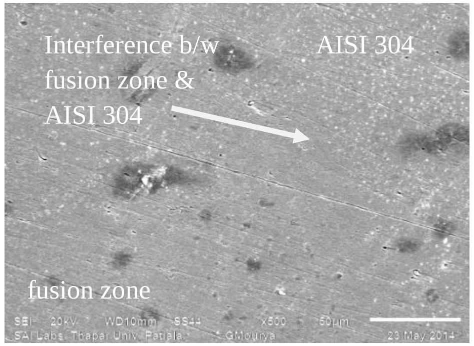 | 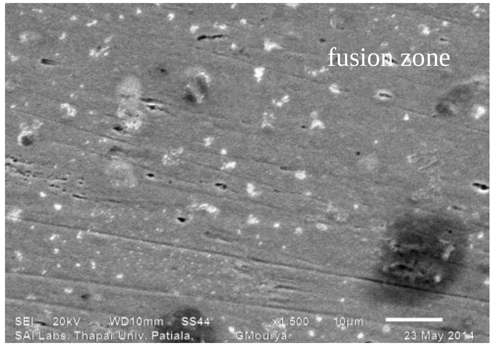 |
| 8. | 145, Ar + 1.5 $H_2$, 14, 304, No, 650 ºC | 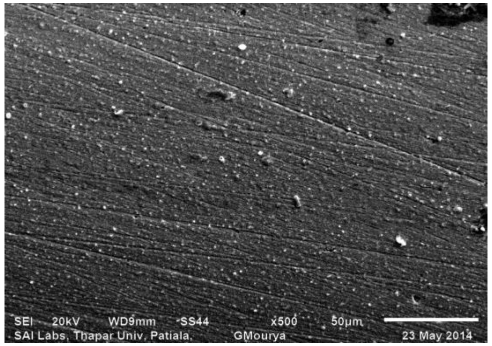 | 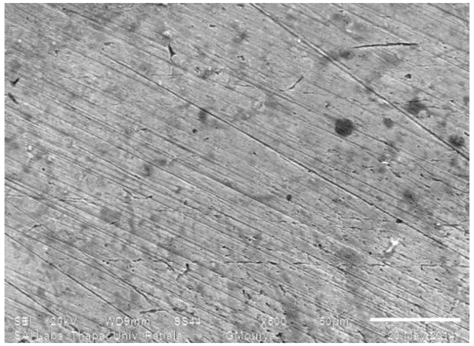 | 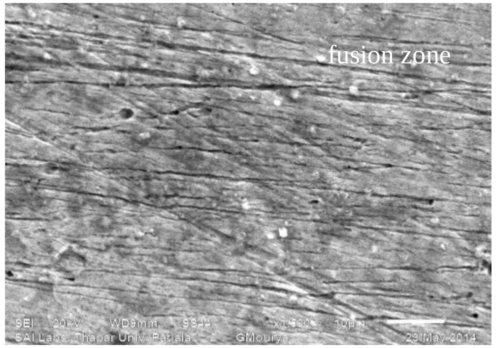 |
| 7. | 145, Ar + 1.5 $H_2$, 12, 308, 250 ºC, 500 | 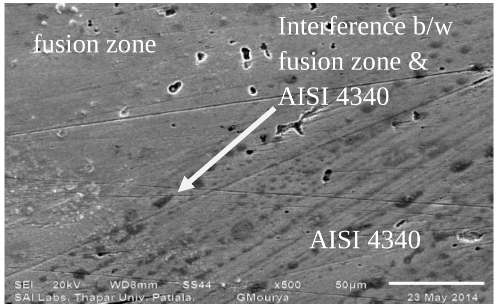 | 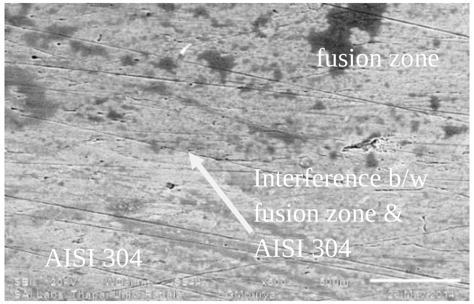 |  |

| | | | | |
|---|---|---|---|---|
| 1. | 145, Ar, 12, 304, No, No | 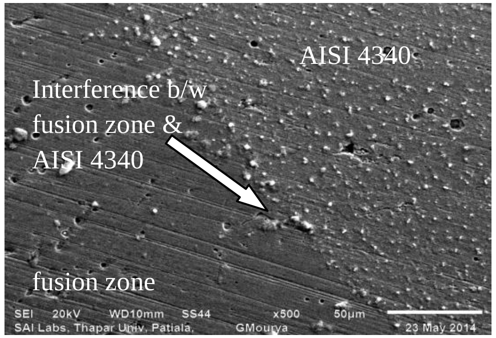 | 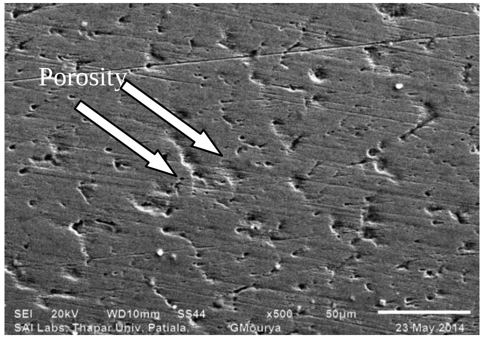 | 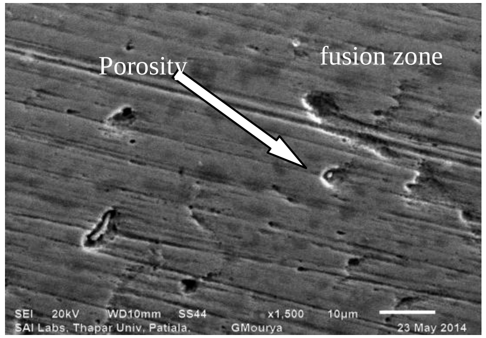 |

Microstructural observations of the weld fusion zone and HAZ of dissimilar joints between AISI 304 and AISI 4340 for some selected welded samples carried out by SEM. Samples are selected based on results having higher and lower values of heat input and toughness. Table 4.25 shows the base metal SEM pictures. Table 4.26 shows the pictorial view at 500X magnification for interferences between the (base metal and fusion zone) and at 1500X for fusion zone by SEM by using different parameters current, gas type, flow rate, filler, pre-heating and post-heating. In the following discussion on the welding metallurgy of austenitic stainless steel, α ferrite describes the low temperature ferrite that forms the austenitic, δ ferrite refers to high temperature ferrite and σ phase denotes low temperature equilibrium phase. From the composition of the present workpiece material, lower Cr/Ni ratio promotes ferrite formation (high temperature δ ferrite). Also lower Cr/Ni ratio promotes austenite formation and higher Cr/Ni ratio promotes ferrite formation. From the composition of the present workpiece material, values of $Cr_{eq}$ (= Cr + 1.5Si + Mo + 0.5Cb) and $Ni_{eq}$ (= Ni + 0.5Mn + 30C + 30N) are obtained as 19.607 and 16.329, respectively. Subsequently observed that there is zero content of the amount of δ ferrite ($\delta = 3(Cr_{eq} – 0.93Ni_{eq} – 6.7)$). Also, the ratio of Cr and Ni percentage is calculated as 1.20 and lower Cr/Ni ratio promotes austenite formation whereas a high value of Cr/Ni ratio promotes ferrite formation. High cooling rate suppresses the formation of austenite and some ferrite will remain in the microstructure. High cooling rate suppresses the formation of austenitic and some ferrite will remain in the temperature. As the weld fusion zone cools through two-phase δ-ferrite and γ-austenite field, the ferrite becomes increasingly unstable and austenitic begin to consume the ferrite via a diffusion controlled reaction. Diffusion across the austenitic-ferrite interface controls the rate and nature of the transformation.

There are four solidification and solid-state transformation possibilities for austenitic stainless steel weld metal. A (fully austenitic) and AF (austenitic + ferrite) solidification modes are associated with primary austenite solidification, whereby austenite is the first phase to form upon solidification. Type FA and F solidification have delta ferrite as the primary phase.

Amount of different heat input rate based on the value of current (145 A, 165 A and 185 A) and gas flow rate (12 L/min, 14 L/min and 16 L/min) concludes the solidification and subsequent solid-state transformation. Nickel and carbon are the austenitic stabilizers form type A and AF solidification and result high toughness and also (Cr and Mo) in A type forms partition to the cells and dendrite boundaries. Mo and Cr are the ferrite stabilizers form F and FA solidification and results in low toughness.

As seen in Table 4.26 (trail 11, 26) due to faster cooling rates with flow rate of 14 L/min, consequently allowing lesser solidification time for the resultant dendritic growth leads to Type A and Type AF solidification and results in high toughness and tensile strength. In (trial 1) heat input applied results in poor toughness. It may be due to porosity in the fusion zone and improper fusion at HAZ with lower gas flow rate of shielding gas i.e. 12 L/min. The explanation holds good for the impact toughness of the heat affected zones of these joints trial 1 i.e. the heat affected zone associated with the low heat input joint possesses less coarseness in the microstructure thus resulting in less impact toughness, whereas the extent of grain coarsening being more in the heat affected zones of the medium trial 15 and trial 23 high input joints, the impact toughness is found to be reduce to 63.765 J and 4.95 J respectively. Fractographs of the impact tested specimens as shown in Table 4.26. trail 8 (b,c) indicate that the fracture morphology was characterized by the presence of dimpled rupture (containing dimples of varying size and shape), the ductile mode prevailed during fracturing of all the specimens. From trail (19, 23 and 26) as shown in Table 4.26 at same heat input, it is seen that in (trial 23) filler EN24 is used which has lower content of nickel and carbon form F and FA solidification results in lower toughness and moderate tensile strength results due to the formation of ferrite as a first primary phase and (trial 19, 26) filler 308 is used which has higher content of nickel and carbon which form type A and AF solidification results in higher toughness and also higher tensile strength due to the formation of austenite as a first phase. Type AF solidification with high heat input can be noticed in Fig. 4.26 (a) trail 26. Relatively high gas flow rate (14 L/min) increases the cooling rate and high rate of solidification in combination with high heat input results in finer grain size. Due to this a significant increases in toughness as well as tensile strength is seen. As trial 1 and 7 are compared at same heat input and fillers, the gas type will gives some significant result for toughness because of the addition of hydrogen (produces more heat) in trial 7 which results in formation of type A solidification as compared to trail 1 in which only argon is used. Mechanical properties may also decreases due to the porosity in the surface in fusion zone as seen in Table 4.26 (c) trail 1. In trial 10, 11 and 15 shown in Table 4.26 having same heat input there is large effect of post-heating temperature at 500 ºC as the residual stresses reliefs results in high toughness value as the value of post-heating temperature increases from 500 ºC it leads to the embrittlement and loss of toughness. In trail 15 as current value is 165 A, gas type of 70% Ar + 30% He, gas flow rate of 16 L/min, filler type of EN24, pre-heating at 250 ºC and post-heating at 650 ºC has less value of toughness compared to other trails because due to gas type addition of helium and very high gas flow rate of 16 L/min may cool down the welded region very rapidly results in formation of martensite which increases the hardness leads in decreases in a toughness.

### 4.6.2 Metallurgical Analysis of Joints between AISI 316 and AISI 4340

Table 4.27: SEM images of base metal AISI 316 and AISI 4340

| Base metal of AISI 316 | Base metal of AISI 4340 |
|---|---|
| 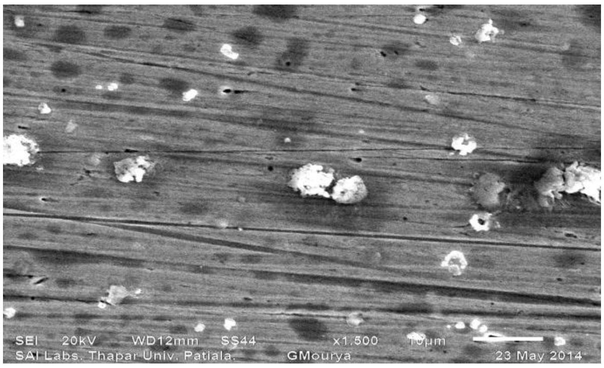 | 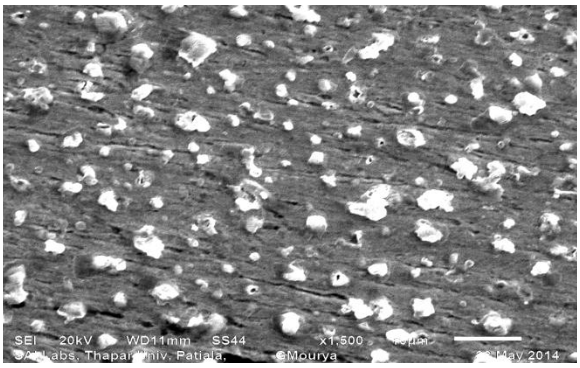 |

Table 4.28: SEM images of different trials of interference of (fusion zone and base metals) and fusion zone

| Trial. No. | Parameters (Current, Gas type, Flow rate, Filler, Pre-heating, Post-heating) | Interface of fusion zone and AISI 4340 (Magnification 500X) (a) | Interface of fusion zone and AISI 316 (Magnification 500X) (b) | Fusion zone (Magnification 1500X) (c) |
|---|---|---|---|---|
| 1. | 145 A, Ar, 12 L/min, AISI 316, No, No | 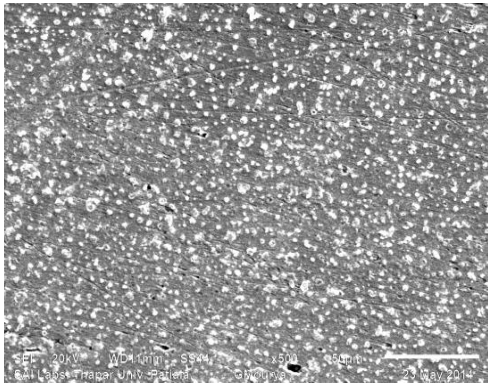 | 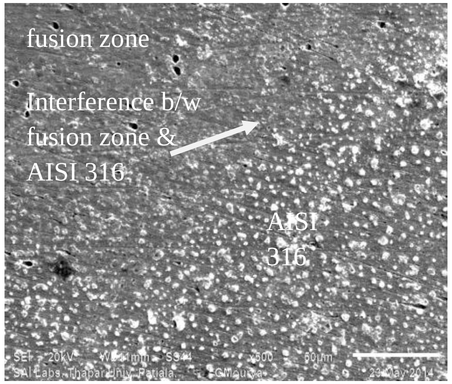 | 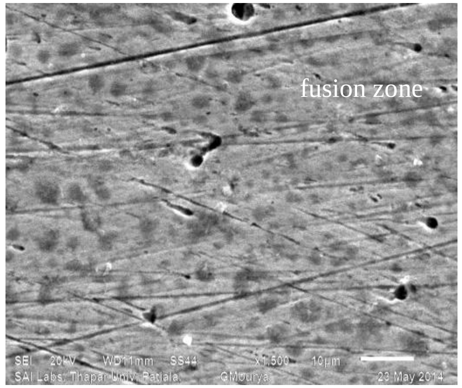 |
| 3. | 145 A, Ar, 16 L/min, AISI 309, 250 ºC, 650 ºC | 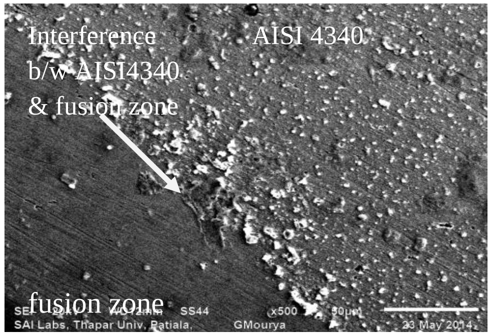 | 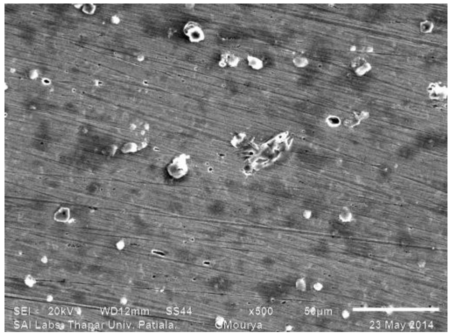 | 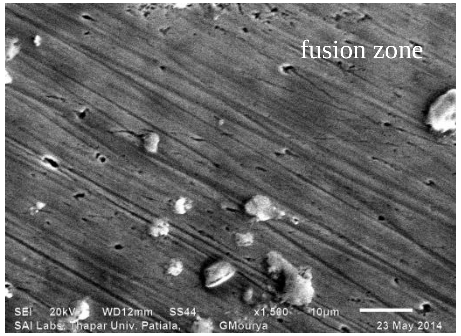 |

| | | | | |
|---|---|---|---|---|
| 7. | 145 A, Ar + 1.5% $H_2$, 12 L/min, AISI 309, 250 ºC, 500 ºC | 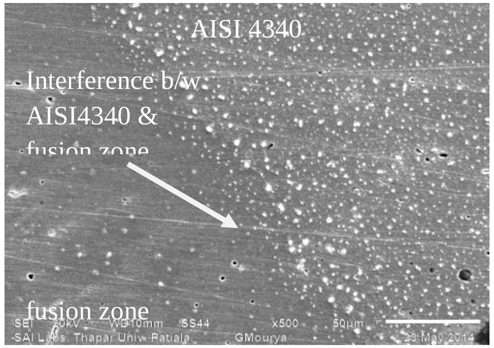 | 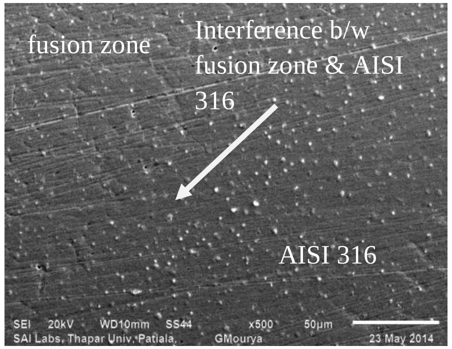 | 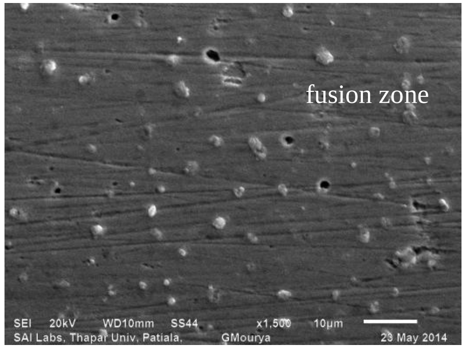 |
| 11. | 165 A, Ar, 14 L/min, AISI 309, No, 650 ºC | 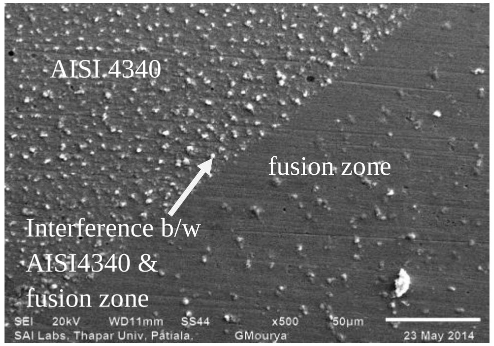 | 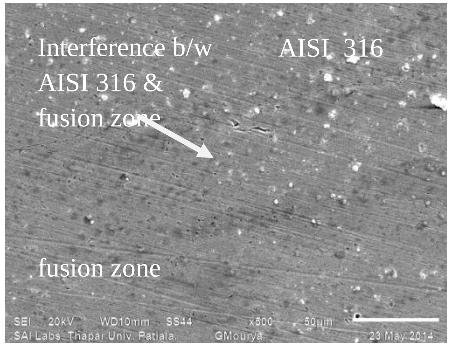 | 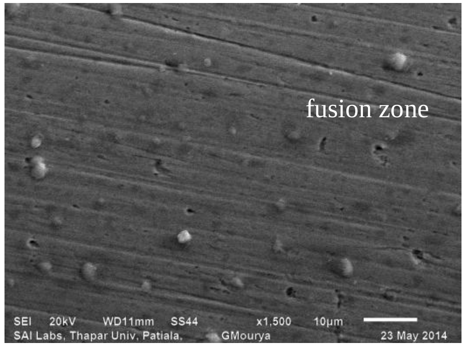 |
| 14. | 165 A, 70% Ar + 30% He , 14 L/min, AISI 316, 175 ºC, 500 ºC | 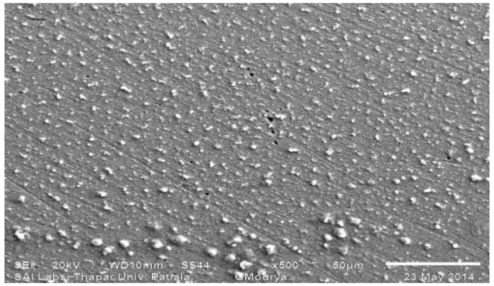 | 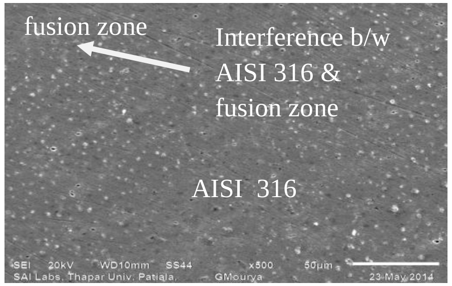 | 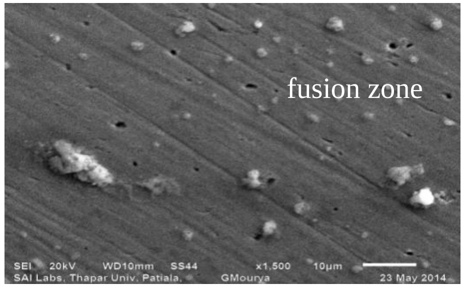 |

| | | | | |
|---|---|---|---|---|
| 18. | 165 A, Ar + 1.5% $H_2$, 16 L/min, SS309, No, 500 ºC | 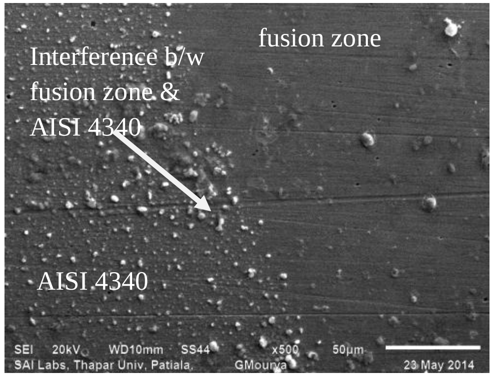  | 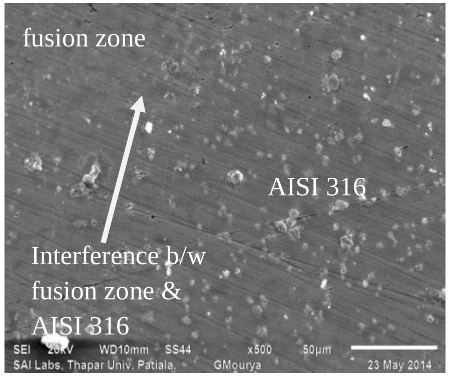  | 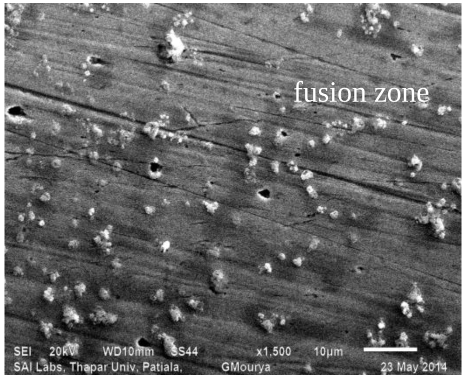  |
| 26. | 185 A, 70%Ar + 30%He, 14 L/min, EN24, No, 650 ºC | 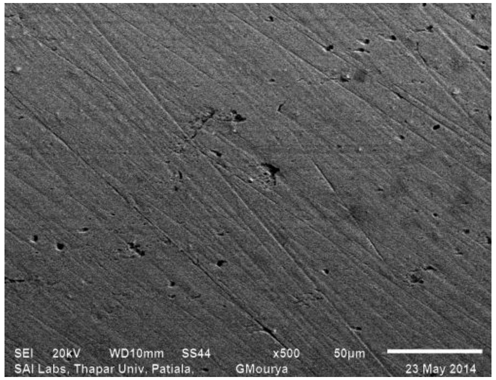 | 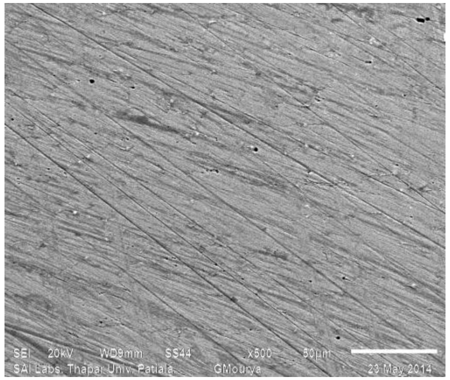 | 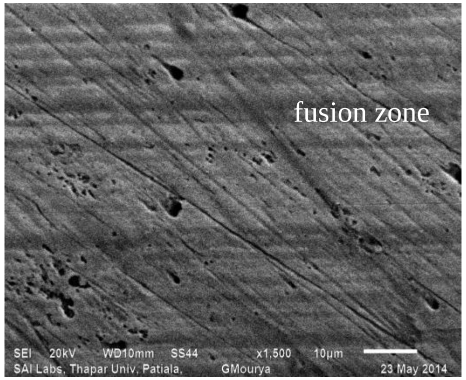  |

Microstructural observations of the weld fusion zone and HAZ of dissimilar joints between AISI 316 and AISI 4340 for some selected welded samples carried out by SEM. Samples are selected based on results having higher and lower values of heat input and toughness. SEM images for base metals are shown in Table 4.27. Table 4.28 shows the pictorial view at 500X magnification for interferences between the (base metal and fusion zone) and at 1500X for fusion zone by SEM by using different parameters current, gas type, flow rate, filler, pre-heating and post-heating. In the following discussion on the welding metallurgy of austenitic stainless steel, α ferrite describes the low temperature ferrite that forms the austenitic, δ ferrite refers to high temperature ferrite and σ phase denotes low temperature equilibrium phase. From the composition of the present workpiece material, lower Cr/Ni ratio promotes ferrite formation (high temperature δ ferrite). Also lower Cr/Ni ratio promotes austenite formation and higher Cr/Ni ratio promotes ferrite formation. From the composition of the present workpiece material, values of $Cr_{eq}$ (= Cr + 1.5Si + Mo + 0.5Cb) and $Ni_{eq}$ (= Ni + 0.5Mn + 30C + 30N) are obtained as 19.307 and 16.596, respectively. Subsequently observed that there is zero content of the amount of δ ferrite ($\delta = 3(Cr_{eq} - 0.93Ni_{eq} - 6.7)$). Also, the ratio of Cr and Ni percentage is calculated as 1.16 and lower Cr/Ni ratio promotes austenite formation whereas a high value of Cr/Ni ratio promotes ferrite formation. High cooling rate suppresses the formation of austenitic and some ferrite will remain in the temperature. As the weld fusion zone cools through two-phase δ-ferrite and γ-austenite field, the ferrite becomes increasingly unstable and austenitic begin to consume the ferrite via a diffusion controlled reaction. Diffusion across the austenitic-ferrite interface controls the rate and nature of the transformation.

There are four solidification and solid-state transformation possibilities for austenitic stainless steel weld metals. These reactions are and related to the Fe-Cr-Ni phase diagram. AF solidification modes are associated with primary austenite solidification, whereby austenite is the first phase to form upon solidification. The solidification if some ferrite forms at the end of the primary austenite solidification process via a eutectic reaction, solidification is termed Type AF. This occurs if sufficient ferrite-promoting elements (primarily Cr and Mo) partition to the solidification sub grain boundaries during solidification to promote the formation of ferrite as a terminal solidification product. This is thought to occur by a eutectic reaction and is represented by the three-phase triangular region of the phase. The ferrite that forms along the boundary is relatively stable and resists transformation to austenite during weld cooling since it is already enriched in ferrite-promoting elements.

Amount of different heat input rate based on the value of current (145 A, 165 A and 185 A) and gas flow rate (12 L/min, 14 L/min and 16 L/min) concludes the solidification and subsequent solid-state transformation. Nickel and carbon are the austenitic stabilizers form type A and AF solidification and result high toughness and also (Cr and Mo) in A type forms partition to the cells and dendrite boundaries. Mo and Cr are the ferrite stabilizers form F and FA solidification and results in low toughness.

Table 4.28 shows the SEM of weld fusion zone and heat affected zone for 12 L/min, 14 L/min and 16 L/min flow rate of shielding gas of Ar, 70% Ar + 30% He, and Ar + 1.5% H2. SEM of some experimental trials with different value of process parameters such as current with constant speed and constant voltage are converted to heat input rate. This heat input rate at each of three gas flow rate with effect of shielding is observed and analysed. Heat input rate in trial 18 results in fast cooling rate. Due to faster cooling rate fine grains are formed. In this solidification cells and dendritic structure can be observed and results in good toughness and tensile strength is achieved. . Whereas in trial no. 26 rate of heat input is more leads to formation of coarse grain size in fusion zone results in poor toughness as shown in Table 4.28. This observation is based upon the theory of solidification which states that high welding heat input into the joint would result into high heat accumulation, thus resulting into low temperature gradient and slow growth rate, consequently leading to a significant increase in the dendrite arm spacing. Conversely low heat input combination into the joint would tend to make steep temperature gradient in combination with rapid growth rate thus resulting in small dendrite arm spacing. As observed from the photomicrographs of the heat affected zones (HAZs) of these weldments shown in (trial no. 26) from Table 4.28, grain coarsening effect is induced which tends to weaken this part of the joint and, thus could affect the functional performance of the weld joint in actual service. It is seen that with higher heat input the extent of grain coarsening in this zone is relatively higher, whereas low heat input, by virtue of subjecting this zone to steeper thermal gradients, helps in inhibiting the grain growth. In trial 14 and 11 it is seen at same temperature toughness vary due to the filler metal composition. Least toughness is therefore seen in trial no 7 due to the current or the heat input is lower than others. In (trial 1, 26, 11) (c) porosity is found to be seen due to the fast cooling rate after the welding.

## 4.7 Dye Penetration Test

Dye penetration method is used for inspecting weld bead when attempting to locate flaws open to the surface of non-porous materials. Basic steps that are performed on the material during inspection, based on the particular technique being used.

DPT is based upon the principle of capillary, where surface tension fluid i.e. red dye penetration low penetrates into clean and dry surface-breaking discontinuities. Penetrant is applied to the test material by spraying. After dwell time has been allowed, the excess penetrant is removed and a developer is applied. The developer helps to draw penetrant out of the flaw so that an invisible indication becomes visible to the inspector. Inspection is performed under ultraviolet or white light, depending on the type of dye used - fluorescent or non-fluorescent (visible).

- Clean the material to be inspected
- Apply penetrant to test part
- Allow correct dwell time to elapse
- Remove excess penetrant from part surface
- Dry, if applicable
- Apply developer and allow to dwell
- Inspect component
- Post-clean part

### 4.7.1 Dye Penetration Test of AISI 304 and AISI 4340

Dye penetration is carried out on joints performed as per L27 orthogonal array on the welding of materials AISI 304 and AISI 4340 as shown in Table 4.29.

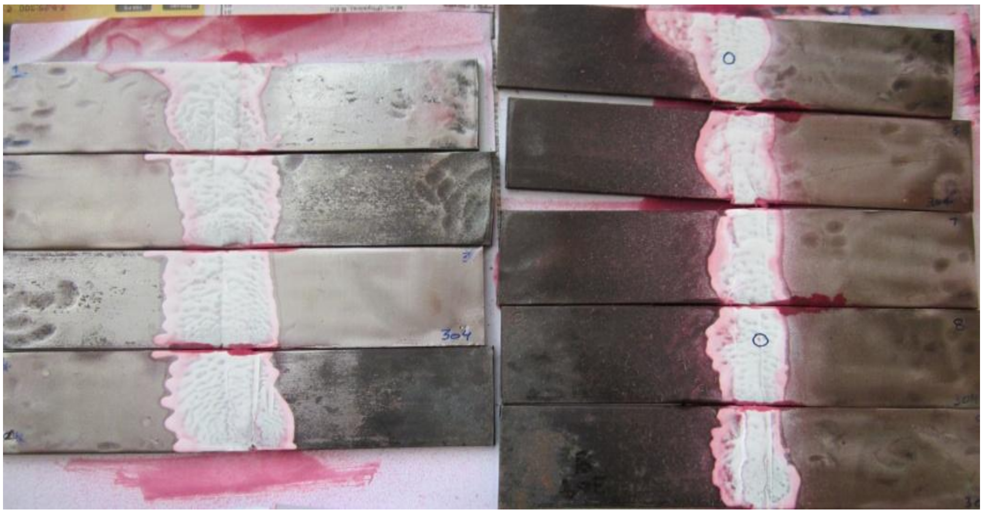

(a)

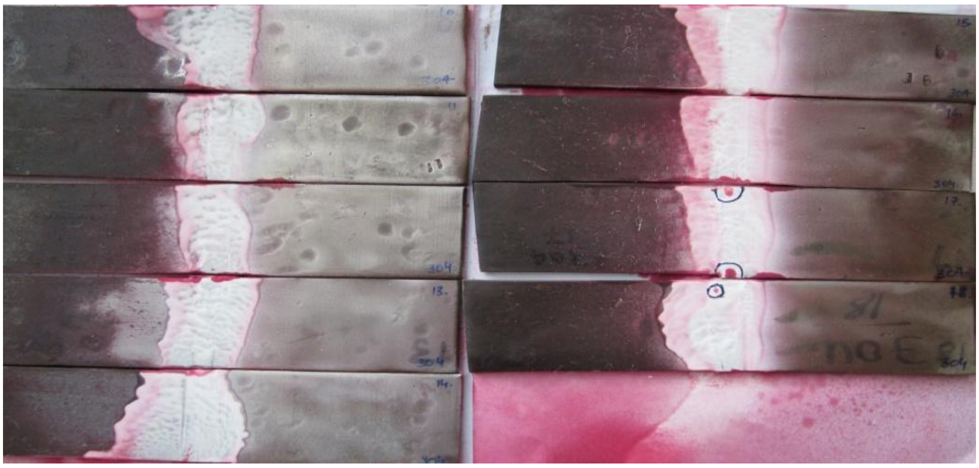

(b)

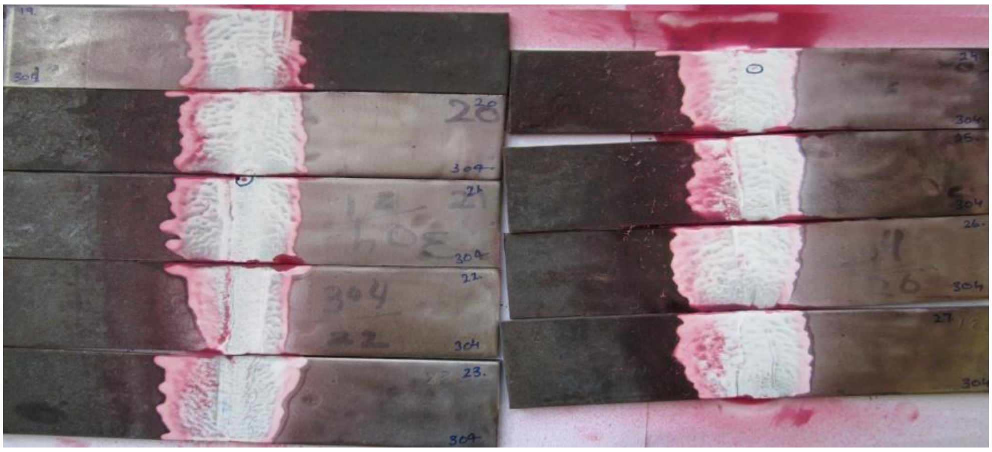

(c)

Figure 4.21: Results of dye penetrant test (DPT) carried on AISI 304 and AISI 4340

Above Figure 4.21 shows that welded joints have no surface defect except specimen no. 5, 8, 17, 18, 21, 24 which is having a minor surface defect at the extreme end of the plates. Last end of plate (nearly 3 – 5 mm) would be rejected while cutting the plates for various mechanical testing. In overall we can conclude that welded region have no surface cracks and porosity for the effective portion of the welded plates. The workpieces are marked in circle which has surface defect by dye penetration are as shown in Fig. 4.21.

After the visual inspection of cracks using dye penetration, optical microscope is used to find out the surface cracks on weld surface. By using optical microscope, weld surface is examined for cracks measurements. After taking all the measured values, average length of crack is calculated for each trial by dividing the total cracks length to the number of cracks. Based on the average value cracks are assigned with different rank. The crack with minimum average length is assigned with rank 1 and crack with higher average length are assigned with rank last. Table 4.28 shows the average value of surface crack at each trial.

Table 4.29: Results of surface cracks for joints between AISI 304 and AISI 4340

| Exp. No. | Welding current (A) | Gas type | Flow rate (L/min) | Filler | Pre-heating ($^oC$) | Post-heating ($^oC$) | Average Crack Length (mm) |
|---|---|---|---|---|---|---|---|
| 1 | 145 | Ar | 12 | 304 | No | No | No cracks |
| 2 | 145 | Ar | 14 | EN24 | 175 | 500 | No cracks |
| 3 | 145 | Ar | 16 | 308 | 250 | 650 | 1.795 |
| 4 | 145 | 70% Ar + 30% He | 12 | EN24 | 175 | 650 | 0.503 |
| 5 | 145 | 70% Ar + 30% He | 14 | 308 | 250 | No | No cracks |
| 6 | 145 | 70% Ar + 30% He | 16 | 304 | No | 500 | 0.42 |
| 7 | 145 | Ar + 1.5% $H_2$ | 12 | 308 | 250 | 500 | 0.576 |
| 8 | 145 | Ar + 1.5% $H_2$ | 14 | 304 | No | 650 | No cracks |
| 9 | 145 | Ar + 1.5% $H_2$ | 16 | EN24 | 175 | No | No cracks |
| 10 | 165 | Ar | 12 | EN24 | 250 | 500 | No cracks |
| 11 | 165 | Ar | 14 | 308 | No | 650 | No cracks |
| 12 | 165 | Ar | 16 | 304 | 175 | No | 0.825 |
| 13 | 165 | 70% Ar + 30% He | 12 | 308 | No | No | 0.382 |
| 14 | 165 | 70% Ar + 30% He | 14 | 304 | 175 | 500 | No cracks |
| 15 | 165 | 70% Ar + 30% He | 16 | EN24 | 250 | 650 | No cracks |
| 16 | 165 | Ar + 1.5% $H_2$ | 12 | 304 | 175 | 650 | No cracks |
| 17 | 165 | Ar + 1.5% $H_2$ | 14 | EN24 | 250 | No | No cracks |
| 18 | 165 | Ar + 1.5% $H_2$ | 16 | 308 | No | 500 | 0.400 |
| 19 | 185 | Ar | 12 | 308 | 175 | 650 | 0.994 |
| 20 | 185 | Ar | 14 | 304 | 250 | No | 0.141 |
| 21 | 185 | Ar | 16 | EN24 | No | 500 | 0.217 |
| 22 | 185 | 70% Ar + 30% He | 12 | 304 | 250 | 500 | No cracks |
| 23 | 185 | 70% Ar + 30% He | 14 | EN24 | No | 650 | 0.427 |
| 24 | 185 | 70% Ar + 30% He | 16 | 308 | 175 | No | 0.690 |
| 25 | 185 | Ar + 1.5% $H_2$ | 12 | EN24 | No | No | 0.154 |
| 26 | 185 | Ar + 1.5% $H_2$ | 14 | 308 | 175 | 500 | No cracks |
| 27 | 185 | Ar + 1.5% $H_2$ | 16 | 304 | 250 | 650 | No cracks |

Table 4.30: Response of cracks at different Process parameters for AISI 304 and AISI 4340

| Average crack length (mm) | Trial no. | Total number of experiments |
|---|---|---|
| $\leq 1$ | 4, 6, 7, 12, 13, 18, 19, 20, 21, 23, 24, 25. | 12 |
| $1 \leq 2$ | 3 | 1 |
| $2 \leq 3$ | - | 0 |

### 4.7.2 Dye Penetration Test of AISI 316 and AISI 4340

The visual inspection of dye penetration carried out on joints performed as per L27 orthogonal array on the welding of materials AISI 316 and AISI 4340 as shown in Table 4.31.

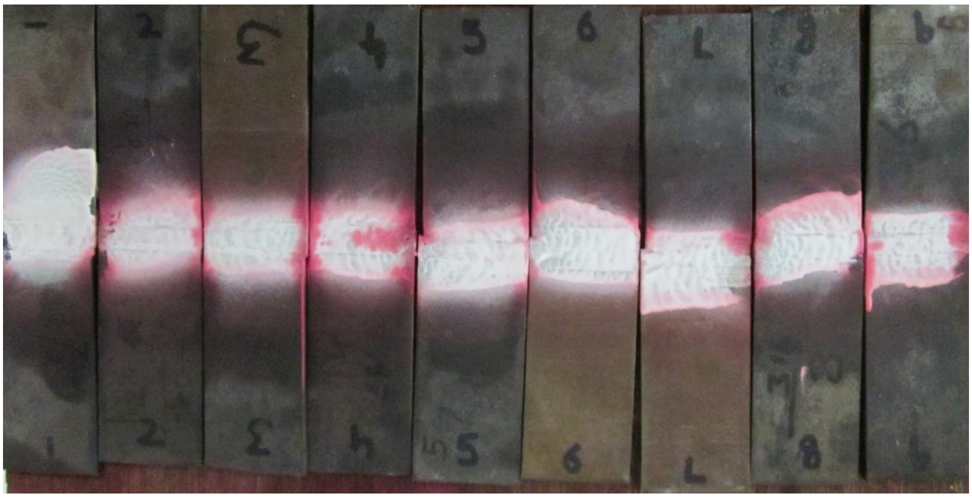

(a)

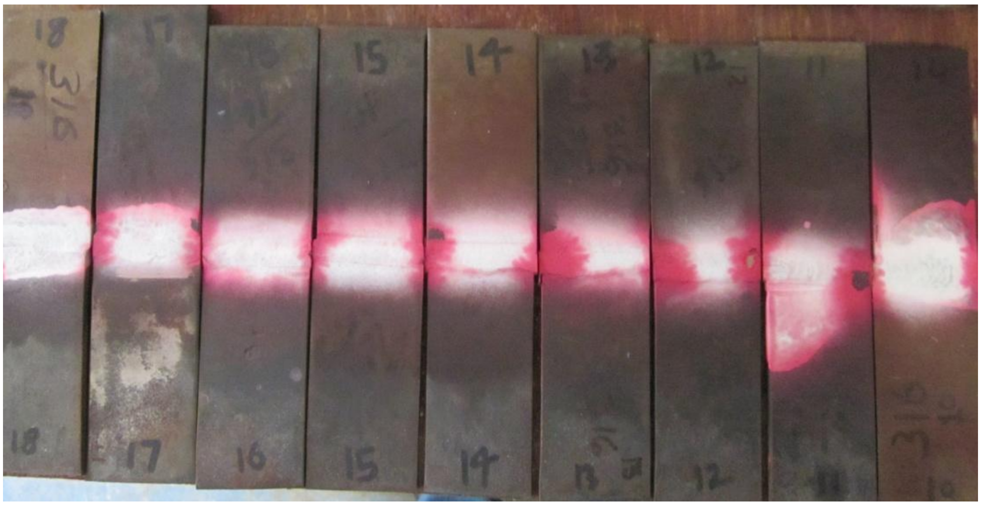

(b)

(c)

Figure 4.22: Results of dye penetrant test (DPT) carried on AISI 316 and AISI 4340

Above Figure 4.22 shows that welded joints have no surface defect except specimen no. 4, 25 which is having a minor surface defect at the extreme end of the plates. In specimen 23porosity is found due to the addition of He as a shielding gas. Last end of plate (nearly 3 – 5 mm) would be rejected while cutting the plates for various mechanical testing. In overall it can conclude that welded region have no surface cracks and porosity for the effective portion of the welded plates. The workpieces are marked in circle which has surface defect by dye penetration are as shown in Fig. 4.22.

After the visual inspection of cracks using dye penetration, optical microscope is used to find out the surface cracks on weld surface. By using optical microscope, weld surface is examined for cracks measurements. After taking all the measured values, average length of crack is calculated for each trial by dividing the total cracks length to the number of cracks. Based on the average value cracks are assigned with different rank. The crack with minimum average length is assigned with rank 1 and crack with higher average length are assigned with rank last. Table 4.28 shows the average value of surface crack at each trial.

Table 4.31: Results of surface cracks for joints between AISI 316 and AISI 4340

| Exp. no. | Welding current (A) | Gas type | Flow rate (L/min) | Filler | Pre-heating ($^oC$) | Post-heating ($^oC$) | Average Crack Length (mm) |
|---|---|---|---|---|---|---|---|
| 1 | 145 | Ar | 12 | 316 | No | No | 1.37 |
| 2 | 145 | Ar | 14 | EN24 | 175 | 500 | 0.303 |
| 3 | 145 | Ar | 16 | 309 | 250 | 650 | No cracks |
| 4 | 145 | 70% Ar + 30% He | 12 | EN24 | 175 | 350 | No cracks |
| 5 | 145 | 70% Ar + 30% He | 14 | 309 | 250 | No | No cracks |
| 6 | 145 | 70% Ar + 30% He | 16 | 316 | No | 500 | No cracks |
| 7 | 145 | Ar + 1.5% $H_2$ | 12 | 309 | 250 | 500 | 0.964 |
| 8 | 145 | Ar + 1.5% $H_2$ | 14 | 316 | No | 650 | 1.318 |
| 9 | 145 | Ar + 1.5% $H_2$ | 16 | EN24 | 175 | No | 0.908 |
| 10 | 165 | Ar | 12 | EN24 | 250 | 500 | 0.724 |
| 11 | 165 | Ar | 14 | 309 | No | 650 | 1.062 |
| 12 | 165 | Ar | 16 | 316 | 175 | No | 0.471 |
| 13 | 165 | 70% Ar + 30% He | 12 | 309 | No | No | 0.3215 |
| 14 | 165 | 70% Ar + 30% He | 14 | 316 | 175 | 500 | 1.280 |
| 15 | 165 | 70% Ar + 30% He | 16 | EN24 | 250 | 650 | 2.61 |
| 16 | 165 | Ar + 1.5% $H_2$ | 12 | 316 | 175 | 650 | 1.221 |
| 17 | 165 | Ar + 1.5% $H_2$ | 14 | EN24 | 250 | No | 1.3 |
| 18 | 165 | Ar + 1.5% $H_2$ | 16 | 309 | No | 500 | No cracks |
| 19 | 185 | Ar | 12 | 309 | 175 | 650 | 0.790 |
| 20 | 185 | Ar | 14 | 316 | 250 | No | No cracks |
| 21 | 185 | Ar | 16 | EN24 | No | 500 | 0.695 |
| 22 | 185 | 70% Ar + 30% He | 12 | 316 | 250 | 500 | 1.15 |
| 23 | 185 | 70% Ar + 30% He | 14 | EN24 | No | 650 | 0.7365 |
| 24 | 185 | 70% Ar + 30% He | 16 | 309 | 175 | No | No cracks |
| 25 | 185 | Ar + 1.5% $H_2$ | 12 | EN24 | No | No | No cracks |
| 26 | 185 | Ar + 1.5% $H_2$ | 14 | 309 | 175 | 500 | 1.106 |
| 27 | 185 | Ar + 1.5% $H_2$ | 16 | 316 | 250 | 650 | 0.981 |

Table 4.32: Response of cracks at different Process parameters for AISI 316 and AISI 4340

| Average crack length (mm) | Trial no. | Total number of experiments |
|---|---|---|
| $\leq 1$ | 2, 7, 9, 12, 13, 19, 21, 23, 27 | 9 |
| $1 \leq 2$ | 1, 8, 11, 14, 16, 17, 22, 26 | 8 |
| $2 \leq 3$ | 15 | 1 |

# Chapter 5
# Conclusion and Scope for Future Work

## 5.1 Conclusion

This study was mainly aimed at finding the most significant process parameters and optimal solution for joining of dissimilar materials between (AISI 304 and AISI 4340) and (AISI 316 and AISI 4340). Different process parameters like current (145A, 165A, 185A), gas type (Ar, 70% Ar + 30% He, Ar + 1.5% $H_2$), gas flow rate (12, 14, 16 L/min.), filler wire (AISI 304, AISI 316, EN24, AISI 308, AISI 309), pre-heating temperature of (No, 175, 250 ºC), post-heating temperature of (No, 500, 650 ºC) varied at three levels of each parameter. Different response characteristics considered are tensile strength, toughness, microhardness, weld distortion, metallurgical analysis (SEM) and visual inspection of cracks of some selected samples. Based on detailed experimental study and analysis of results the following conclusions are drawn:

- Tensile strength results for joining AISI 304 and AISI 4340 mainly depends on current, gas type and gas flow rate. Because with increase in current voltage and gas flow rate tensile strength increases. By using different gases due to cooling rates and filler wires more tensile strength is obtained.
- In case of AISI 316 and AISI 4340 more tensile strength is obtained as current is increased. More tensile strength is achieved with filler wire of AISI 309. As post-heating temperature increases the tensile strength decreases.
- Charpy impact test results for AISI 304 and AISI 4340 shows that toughness mainly depends on gas type, gas flow rate and type of filler used. There is no effect of current on toughness value. Toughness is seen to be maximum by using AISI 308 filler wire.
- Charpy impact test results for AISI 316 and AISI 4340 shows that toughness depends on gas type, gas flow rate and filler. Toughness value is seen to be maximum at post-heating temperature of 500ºC. When filler wire of AISI 309 is used than toughness increases.
- Microhardness results for joining of AISI 304 and AISI 4340 mainly depends upon current, gas type, gas flow rate and type of filler used. Microhardness is find to be maximum while using filler wire of EN24 and it also increases when post-heated at 500ºC. Microhardness is seen to be the maximum at maximum gas flow rate of 16L/min.

- Microhardness results for joining of AISI 316 and AISI 4340 mainly depends upon gas type, post-heating temperature. As AISI 316 is used as filler wire microharness is find to be the more as compared to the other filler wires. At 500ºC of post-heatig temperature the micro hardness is maximum. There is no much effect of current on micro hardness while joining AISI 316 and AISI 4340.
- Weld distortion for joining of AISI 304 and AISI 4340 shows that with increase in rate of heat input weld distortion increases which is obtained by the product of current and voltage. Weld distortion also depends upon the filler and gas type. Weld distortion is seen to be more when pure argon is used in the experiments. As comared to the other mixture of gases.
- Weld distortion for joining of AISI 316 and AISI 4340 depends upon the current, gas type and post-heating. As the value of current increases weld distortion seen to be decreasing and also as the temperature of the post-heating increases the distortion decreases. Weld distortion is seen to be more when EN24 as a filler wire is used. There is no much effect of gas flow rate over weld distortion.
- Dye penetrant test (DPT) results for joining of dissimilar material (AISI 304 with AISI 4340 and AISI 316 with AISI 4340) material shows that there is no surface crack in the welded region. In general the results show that quality of welding is very good.
- Scanned electron microscopy of (AISI 304 and AISI 4340) and (AISI 316 and AISI 4340) shows that with increase in rate of heat input ferrite structure is obtained and there is a tendency of formation of sigma phase in AISI 4340 which will reduce the toughness and tensile strength. If the rate of heat input is less than desired value then proper fusion of weld metal is not taken place and results in cracks at the interference. Effect of shielding gas flow rate is that if flow rate is more than faster cooling of weld metal takes place and leads to austenitic and (austenitic + ferrite) solidification.

## 5.2 Scope for Future Work

Following are the some of the future recommendations:

- Effect of pure helium and nitrogen has been studied by many researchers on various grades of steels. Same may also be carried out for dissimilar material joining of AISI 304 and AISI 316 with AISI 4340.
- Effect of voltage and arc force parameter has been studied by many researchers for various grades of steels. Same may also be carried for these materials.

- Bending and reverse bending test etc. may also be carried along with other non-destructive tests like radiography, ultrasonic testing etc.
- Welding speed may be an important parameter in GTAW process and may be studied in automatic GTAW welding machines.
- Microstructure analysis may be carried on the welded joints by using XRD to study the various grains.
- Study the effect of metal powder addition in order to increase the mechanical properties.
- Modeling of gas tungsten arc welding processes can be carried out by using finite elements analysis.
- Different type of welding electrodes (Zirconiated electrode) and different diameters may also be used.

# References

Ahmad, M.; Akhter, J.I.; Akhtar, M.; Iqbal, M. (2007) Microstructure and characterization of phases in TIG welded joints of Zircaloy-4 and stainless steel 304L. *Journals of Material Science*, 42: 328 – 331.

Ahmad, R.; Bakar, M.A. (2011) Effect of a post-weld heat treatment on the mechanical and microstructure properties of AA6061 joints welded by the gas metal arc welding cold metal transfer method. *Material and Design*, 32: 5120 – 5126.

Arivazhagan, N.; Singh, S.; Prakash, S.; Reddy, G.M. (2011) Investigation on AISI 304 austenitic stainless steel to AISI 4140 low alloy steel dissimilar joints by gas tungsten arc, electron beam and friction welding. *Materials and Design*, 32: 3036 – 3050.

Barnett, O.T. (1959) Filler Metals For Joining. Reinhold Publishing Corporation, New York

Blondeau, R. (2008) Metallurgy and Mechanics of Welding. John Wiley & Sons, Inc 111 River Street Hoboken, NJ 07030, USA, 1st Edn.

Dewan, M.W.; Liang, J.; Wahab, M.A.; Okeil, A.M. (2014) Effect of post-weld heat treatment and electrolytic plasma processing on Tungsten inert gas welded AISI 4140 alloy steel, *Materials and Design,* 54: 6 – 13.

Durgutlu, A. (2004) Experimental investigation of the effect of hydrogen in argon as a shielding gas on TIG welding of austenitic stainless steel. *Material and Design*, 25: 19 – 23 .

Fahimpour, V.; Sadrnezhaad, S.K.; Karimzadeh, F. (2012) Corrosion behavior of aluminum 6061 alloy joined by friction stir welding and gas tungsten arc welding methods. *Materials and Design*, 39: 329 – 33 .

Gharibshahiyan, E.; Raouf, A.H.; Parvin, N.; Rahimian, M. (2011) The effect of microstructure on hardness and toughness of low carbon welded steel using inert gas welding. *Material and Design*, 32: 2042 – 2048.

Hajiannia, I.; Shamanian, M.; Kasiri, M. (2013) Microstructure and mechanical properties of AISI 347 stainless steel or A335 low alloy steel dissimilar joint produced by gas tungsten arc welding. *Materials and Design*, 50: 566 – 573 .

Hsieh, R.I.; Pan, Y.T.; Liou; H.Y. (1999) The Study of Minor Elements and Shielding Gas on Penetration in TIG Welding of Type 304 Stainless Steel. *The Journal of Materials Engineering and Performance* 8: 68 – 74.

Khanna, O.P. (2011) A Text book of Welding Technology, Dhanpat Rai Publications New Delhi. 2nd Edn.

Lakshminarayanan, A. K.; Balasubramanian, V.; Elangovan, K. (2009) Effect of welding processes on tensile properties of AA6061 aluminum alloy joints. *International Journal of Advanced Manufacturing Technology*, 40: 286 – 296.

Lin, S.B.; Song, J.L.; Yang, C.L.; Fan, C.L.; Zhang, D.W. (2010) Brazability of dissimilar metals tungsten inert gas butt welding–brazing between aluminium alloy and stainless steel with Al-Cu filler metal. *Material and Design*, 31: 2637 – 2642.

Liu, F.; Ren, D.; Liu, L. (2013) Effect of Al foils interlayer on microstructures and mechanical properties of Mg-Al butt joints welded by gas tungsten arc welding filling with Zn filler metal. *Material and Design*, 46: 419 – 425.

Lu, S.P.; Qin, M.P.; Dong, W.C. (2013) Highly efficient TIG welding of Cr13Ni5Mo martensitic stainless steel. *Journals of Materials Processing Technology*, 213: 229 – 237.

Norrish, J. (2006) Advance welding processes, Woodhead Publishing Limited, Abington Hall. Abington, Cambridge CB1 6AH, England, 1st Edn : 74 – 99.

Ozdemir, N.; Sarsilmaz, F.; Hascalik, A. (2007) Effect of rotational speed on the interface properties of friction-welding AISI 304L to 4340 steel. *Material and Design*, 28: 301 – 307 .

Parmar, R.S. (2011) Welding processes and technology. Khanna Publishers New Delhi, 3rd Edn.

Peasura, P.; Watanapa, A. (2012) Influence of Shielding Gas on Aluminum Alloy 5083 in Gas Tungsten Arc Welding, *Procedia Engineering*, 29: 2465 – 2469.

Ramkumar, D.K.; Arivazhagan, N.; Narayanan, S. (2012) Effect of filler materials on the performance of gas tungsten arc welded AISI 304 and Monel 400. *Materials and Design*, 40: 70 – 79.

Shen, J.; Xu, N. (2012) Effect of preheat on TIG welding of AZ61 magnesium alloy, *International Journal of Minerals, Metallurgy and Materials*, 19(4): 360.

Sivashanmugam, M.; Shanmugam, C.; Kuma, .T.; Kumar, M. (2010) Investigation of Microstructure and Mechanical properties of GTAW and GMAW joints on AA7075 Aluminum Alloy. *IEEE* (978-1-4244-9082-0): 241 – 246.

Temmar, M.; Hadji, M.; Sahraoui, T. (2011) Effect of post-weld aging treatment on mechanical properties of Tungsten Inert Gas welding low thickness 7075 aluminium alloy joints. *Materials and Design*, 32: 2532 – 3536.

Yan, J.; Gao, M.; Zeng, X. (2010) Study on microstructure and mechanical properties of 304 stainless steel joints by TIG hybrid welding. *Optics and Lasers in Engineering*, 48: 512 – 517.

Yuri, T.; Ogata, T.; Saito, M.; Hirayama, Y. (2000) Effect of welding structure and δ-ferrite on fatigue properties for TIG welded austenitic stainless steels at cryogenic temperatures., *Cryogenics*, 40: 251 – 259.

Zhu, Q.; Lie, Y.C.; Chen, X.; Ren, W.; Ju, X.; Ye Y. (2011) Microstructure and mechanical properties in TIG welding of CLAM steel, *Fusion Engineering and Design*, 86: 407 – 411.

# Web Reference

http://www.weldguru.com/saw.html downloaded on dated Dec 08, 2013

http://www.mechanicalengineeringblog.com/tag/tig-welding downloaded on dated Dec 08, 2013

http://vivesoldando-camilo.blogspot.in/2010/06/proceso-gmaw-mig-mag.html downloaded on dated Dec 08, 2013

http://just122.justhost.com/suspended.page/disabled.cgi/gadgetflash.com downloaded on dated Dec 08, 2013

http://www.hotrodders.com/forum/welder-reccomendations-51105-2.html downloaded on dated Dec 08, 2013

http://www.classictrucks.com/tech/1110clt_basic_tig_welding_101_with_inverter_machines/photo_13.html downloaded on dated Dec 08, 2013

http://www.cartech.com/techarticles.aspx?id=1600 downloaded on dated Dec 08, 2013